

CYBER-PHYSICAL MODELING, ANALYSIS, AND
OPTIMIZATION - A SHIPBOARD SMARTGRID
RECONFIGURATION CASE STUDY

by

SAYAK BOSE

B.Tech, University of Kalyani, 2003

M.S., University of Kansas, 2009

AN ABSTRACT OF A DISSERTATION

submitted in partial fulfillment of the
requirements for the degree

DOCTOR OF PHILOSOPHY

Department of Electrical and Computer Engineering

College of Engineering

KANSAS STATE UNIVERSITY

Manhattan, Kansas

2012

Abstract

Many physical and engineered systems (e.g., smart grid, transportation and biomedical systems) are increasingly being monitored and controlled over a communication network. These systems where sensing, communication, computation and real time control are closely integrated are referred to as cyber physical systems (CPS). Cyber physical systems present a plethora of challenges related to their design, analysis, optimization and control. In this dissertation, we present some fundamental methodologies to analyze the optimization of physical systems over a communication network. Specifically, we consider a medium voltage DC shipboard smart grid (SSG) reconfiguration problem as a test case to demonstrate our approach.

The main goal of SSG reconfiguration is to change the topology of the physical power system by switching circuit breakers, switches, and other devices in the system in order to route power effectively to loads especially in the event of faults/failures. A majority of the prior work has focused on centralized approaches to optimize the switch configuration to maximize specific objectives. These methods are prohibitively complex and not suited for agile reconfiguration in mission critical situations. Decentralized solutions proposed do reduce complexity and implementation time at the cost of optimality. Unfortunately, none of the prior efforts in this arena address the cyber physical aspects of an SSG. This dissertation aims to bridge this gap by proposing a suite of methods to analyze both centralized and decentralized SSG reconfigurations that incorporate the effect of the underlying cyber infrastructure.

The SSG reconfiguration problem is a mixed integer non convex optimization problem for which branch and bound based solutions have been proposed earlier. Here, optimal reconfiguration strategies prioritize the power delivered to vital loads over semi-vital and non vital

loads. In this work, we propose a convex approximation to the original non convex problem that significantly reduces complexity of the SSG reconfiguration. Tradeoff between power delivered and number of switching operations after reconfiguration is discussed at steady state. Second, the distribution of end-to-end delay associated with fault diagnosis and reconfiguration in SSG is investigated from a cyber-physical system perspective. Specifically, a cross-layer total (end-to-end) delay analysis framework is introduced for SSG reconfiguration. The proposed framework stochastically models the heterogeneity of actions of various sub-systems viz., the reconfiguration of power systems, generation of fault information by sensor nodes associated to the power system, processing actions at control center to resolve fault locations and reconfiguration, and information flow through communication network to:(1) analyze the distribution of total delay in SSG reconfiguration after the occurrence of faults; and (2) propose design options for real-time reconfiguration solutions for shipboard CPS, that meet total delay requirements.

Finally, the dissertation focuses on the quality of SSG reconfiguration solution with incomplete knowledge of the overall system state, and communication costs that may affect the quality (optimality) of the resulting reconfiguration. A dual decomposition based decentralized optimization in which the shipboard system is decomposed into multiple separable subsystems with agents is proposed. Specifically, agents monitoring each subsystem solve a local concave dual function of the original objective while neighboring agents share information over a communication network to obtain a global solution. The convergence of the proposed approach under varying network delays and quantization noise is analyzed and comparisons with centralized approaches are presented. Results demonstrate the effectiveness as well as tradeoffs involved in centralized and decentralized SSG reconfiguration approaches.

CYBER-PHYSICAL MODELING, ANALYSIS, AND
OPTIMIZATION - A SHIPBOARD SMARTGRID
RECONFIGURATION CASE STUDY

by

SAYAK BOSE

B.Tech, University of Kalyani, 2003

M.S., University of Kansas, 2009

A DISSERTATION

submitted in partial fulfillment of the
requirements for the degree

DOCTOR OF PHILOSOPHY

Department of Electrical and Computer Engineering
College of Engineering

KANSAS STATE UNIVERSITY

Manhattan, Kansas

2012

Approved by:

Co-Major Professor

Dr. Balasubramaniam Natarajan

Approved by:

Co-Major Professor

Dr. Caterina Scoglio

Copyright

Sayak Bose

2012

Abstract

Many physical and engineered systems (e.g., smart grid, transportation and biomedical systems) are increasingly being monitored and controlled over a communication network. These systems where sensing, communication, computation and real time control are closely integrated are referred to as cyber physical systems (CPS). Cyber physical systems present a plethora of challenges related to their design, analysis, optimization and control. In this dissertation, we present some fundamental methodologies to analyze the optimization of physical systems over a communication network. Specifically, we consider a medium voltage DC shipboard smart grid (SSG) reconfiguration problem as a test case to demonstrate our approach.

The main goal of SSG reconfiguration is to change the topology of the physical power system by switching circuit breakers, switches, and other devices in the system in order to route power effectively to loads especially in the event of faults/failures. A majority of the prior work has focused on centralized approaches to optimize the switch configuration to maximize specific objectives. These methods are prohibitively complex and not suited for agile reconfiguration in mission critical situations. Decentralized solutions proposed do reduce complexity and implementation time at the cost of optimality. Unfortunately, none of the prior efforts in this arena address the cyber physical aspects of an SSG. This dissertation aims to bridge this gap by proposing a suite of methods to analyze both centralized and decentralized SSG reconfigurations that incorporate the effect of the underlying cyber infrastructure.

The SSG reconfiguration problem is a mixed integer non convex optimization problem for which branch and bound based solutions have been proposed earlier. Here, optimal reconfiguration strategies prioritize the power delivered to vital loads over semi-vital and non vital

loads. In this work, we propose a convex approximation to the original non convex problem that significantly reduces complexity of the SSG reconfiguration. Tradeoff between power delivered and number of switching operations after reconfiguration is discussed at steady state. Second, the distribution of end-to-end delay associated with fault diagnosis and reconfiguration in SSG is investigated from a cyber-physical system perspective. Specifically, a cross-layer total (end-to-end) delay analysis framework is introduced for SSG reconfiguration. The proposed framework stochastically models the heterogeneity of actions of various sub-systems viz., the reconfiguration of power systems, generation of fault information by sensor nodes associated to the power system, processing actions at control center to resolve fault locations and reconfiguration, and information flow through communication network to:(1) analyze the distribution of total delay in SSG reconfiguration after the occurrence of faults; and (2) propose design options for real-time reconfiguration solutions for shipboard CPS, that meet total delay requirements.

Finally, the dissertation focuses on the quality of SSG reconfiguration solution with incomplete knowledge of the overall system state, and communication costs that may affect the quality (optimality) of the resulting reconfiguration. A dual decomposition based decentralized optimization in which the shipboard system is decomposed into multiple separable subsystems with agents is proposed. Specifically, agents monitoring each subsystem solve a local concave dual function of the original objective while neighboring agents share information over a communication network to obtain a global solution. The convergence of the proposed approach under varying network delays and quantization noise is analyzed and comparisons with centralized approaches are presented. Results demonstrate the effectiveness as well as tradeoffs involved in centralized and decentralized SSG reconfiguration approaches.

Table of Contents

Table of Contents	viii
List of Figures	xi
List of Tables	xiii
Acknowledgements	xiv
Dedication	xv
Preface	xv
1 Introduction	1
1.1 Optimization of CPS - Challenges	3
1.2 MVDC Shipboard System Overview	5
1.3 MVDC Shipboard Reconfiguration	10
1.4 Prior Work on SSG Reconfiguration	11
1.4.1 Centralized Approaches	13
1.4.2 Centralized Cyber-Physical Modeling and Delay Analysis	14
1.4.3 Decentralized Reconfiguration	15
1.5 Motivation of Research	16
1.6 Contributions	17
1.7 Organization of the Thesis	20
2 Centralized Reconfiguration of Shipboard Smartgrid	22
2.1 Introduction	22
2.2 Reconfiguration formulation	25
2.2.1 Mixed-Integer Non-Convex formulation ($P1$)	25
2.2.2 Relaxed-Integer Non-convex Formulation ($P2$)	27
2.2.3 Relaxed-Integer Convex Formulation ($P3$)	27
2.2.4 Dual-objective Formulation	28
2.3 Analysis Of Results	30
2.4 Computational Complexity	39
2.5 Summary	41
3 Centralized Reconfiguration-Response Time Analysis	43
3.1 Introduction	43
3.2 Problem Statement	45

3.3	General Framework for End-to-end Response Time Distribution	46
3.4	End-to-end response time for SSG reconfiguration	48
3.4.1	Delay distribution of power electronics network	49
3.4.2	Delay distribution of communications network	50
3.4.3	Delay distribution of sensor network	52
3.4.4	Delay distribution for fault diagnosis	55
3.5	Analysis and Validation of Proposed Framework	55
3.5.1	Analysis Procedure for Proposed Framework	56
3.5.2	Validation of RTA Framework	57
3.6	Summary	62
4	Decentralized Reconfiguration of Shipboard SmartGrid	64
4.1	Introduction	64
4.2	Dual Decomposition Based Shipboard Smartgrid Reconfiguration	66
4.3	Simulation Results	71
4.4	Summary	74
5	Decentralized Reconfiguration Under Imperfect Communications	75
5.1	Introduction	75
5.2	Impact of Communication Network	76
5.2.1	Convergence Rate With No Packet Loss:	76
5.2.2	Convergence Rate With Packet Loss:	79
5.3	Simulation Results	83
5.4	Summary	87
6	Comparative Analysis	88
6.1	Optimal Centralized Vs. Decentralized Reconfiguration	88
6.2	Total Delay for Centralized Vs. Decentralized Reconfiguration of SSG	90
6.3	Convergence Under Lossy Network for Decentralized Reconfiguration	93
6.4	Summary	94
7	Conclusions and Future Work	95
7.1	Conclusions	95
7.1.1	Centralized Reconfiguration	96
7.1.2	Decentralized Reconfiguration	97
7.2	Future Work	98
	Bibliography	105
	Bibliography	115
	A Proof of Theorem 1	116

B FDDI Backbone Network Delay **118**
B.1 Derivation of FDDI Backbone Network Delay Distribution **118**

List of Figures

1.1	Components of a Cyber physical Systems	2
1.2	Infrastructure of a CPS based personal health care [cf [1]]	3
1.3	Hierarchical structure of a CPS based industrial motor control [cf [2]]	4
1.4	Zonal architecture of shipboard power system (From [3])	6
1.5	Shipboard Model [Ref: Model provided to Electric Ship Research and Development Consortium, Keith Corzine, Missouri University of Science and Technology, 2010.]	7
1.6	Shipboard model [Ref: Model provided to Electric Ship Research and Development Consortium, Keith Corzine, Missouri University of Science and Technology, 2010.]	8
1.7	Overview of Shipboard Smartgrid Research Areas	10
1.8	Overview of Shipboard Prior Work on Smartgrid Research	12
2.1	Methods to analyze optimal solutions to SPS reconfiguration problem	24
2.2	Schematic view of SPS under normal condition (pre-fault)	32
2.3	Schematic view of SPS under faults occurring at 1 – 3, 3 – 35, and 35 – 5	33
2.4	Schematic view of SPS under faults occurring at 3 – 35, 35 – 5, 2 – 4 and 6 – 8	34
2.5	Schematic view of SPS under normal condition (pre-fault)	35
2.6	CDF of power delivered (MW)	37
2.7	Power delivered for faults between 12 – 4 and 7 – 1	37
2.8	Number of switching performed for faults between 12 – 4 and 7 – 1	38
3.1	General Framework for End-to-end Response Time	46
3.2	Process Overview of Shipboard Power System Reconfiguration	48
3.3	Communication Network Infrastructure for Shipboard LAN	50
3.4	Centralized Network Control for Shipboard LAN	53
3.5	Centralized Network Control with Backbone for Shipboard LAN	53
3.6	Centralized-Cluster Network Control for Shipboard LAN	54
3.7	Response Time Distribution of Power Network with Uniform Fault Occurrence, and $c_{ij}(x)$ Uniform and Exponential	56
3.8	Response Time Distribution of Communication Network with Slotted Non-persistent CSMA, $w = 32$, $p_s = 0.7$	57
3.9	Simulation process for validation of the proposed framework. The validation uses shipboard system reconfiguration as the VTB process	58
3.10	OPNET model for Architecture-I with 14 sensor nodes connected by Ethernet 100-BASE-T Duplex links in a switched LAN topology	59

3.11	OPNET model for Architecture-II with total 14 sensor nodes in 3 subnets connected by Ethernet 100-BASE-T Duplex Backbone in a switched LAN topology	60
3.12	OPNET model for Architecture-III with 14 sensor nodes in 3 subnets with 3 cluster heads connected by Ethernet 100-BASE-T Duplex links in a switched LAN topology	61
3.13	Comparison of End-to-end Response Time Distribution for Different Architectures with Switched Ethernet, and 14 Sensors	61
3.14	Comparison of End-to-end Response Time Distribution for Architecture-II With Ethernet, Gigabit Ethernet, and FDDI Token Ring Backbone	62
4.1	Subsystem formation for dual decomposition. Agents are represented by S_1, S_2, \dots, S_{15}	68
4.2	Equivalent model for decomposed subsystems with private variable \mathbf{x}_k and public variables \mathbf{y}_k for all $k \in K$	68
4.3	Shipboard microgrid with 4 simultaneous faults	72
4.4	Shipboard microgrid reconfiguration with 4 simultaneous faults	73
5.1	Shipboard microgrid reconfiguration with 4 simultaneous faults	83
5.2	Comparison of delay distribution between decentralized and centralized-cluster	84
5.3	Comparison of delay distribution between decentralized and centralized-backbone	85
5.4	Comparison of delay distribution between decentralized and centralized	85
5.5	Decentralized dual decomposition convergence rate with K_p packet loss'	86
6.1	Shipboard microgrid with 4 simultaneous faults	90
6.2	Comparison of delay distribution between decentralized and centralized	91
6.3	Comparison of delay distribution between decentralized and centralized-backbone	92
6.4	Comparison of delay distribution between decentralized and centralized-cluster	92
6.5	Decentralized dual decomposition convergence rate with K_p packet loss'	93
7.1	An example of a factor graph for (7.5)	100
7.2	Min-sum update for variable node v_1	100
7.3	Subsystem formation for belief propagation with different types of agents	102
7.4	Factor graph constructed from the graphical shipboard model $G \in (V, C)$ with variable nodes $v \in V$ as agents and factor nodes $C \in C$ as constraints	102

List of Tables

2.1	Simulation parameters	32
2.2	Power delivered to loads under faults occurring at 1 – 3, 3 – 35, and 35 – 5 .	33
2.3	Power delivered to loads under faults occurring at 3 – 35, 35 – 5, 2 – 4 and 6 – 8	34
2.4	Power delivered as a function of faults	36
2.5	Power delivered and switch transition to faults occurring at 2 – 10 and 12 – 4	39
2.6	Execution time efficiency (ETE) for original nonconvex and transformed con- vex methods. Reference execution time for original nonconvex method = 1 second	40
4.1	Shipboard smartgrid reconfiguration with 4 faults	72
6.1	Simulation parameters	89
6.2	Shipboard smartgrid reconfiguration with 4 faults	89

Acknowledgments

I would like to give my thanks for all people that helped me in the past three years while I pursued my Ph.D study and research. First of all, I would like to express my sincere thanks to my advisors, Dr. Bala Natarajan, and Dr. Caterina Scoglio, for giving me an opportunity to pursue my Ph.D degree in Kansas State University, for their inspiration, patience, and encouragement on my research work. It was their guidance and encouragement that helped me to conquer the difficulties and led me to the success of my PhD study. I would like to thank Dr. Bala Natarajan, Dr. Caterina Scoglio, Dr. Noel Schulz, and Dr. Sanjoy Das, for their serving on my committee, and for the valuable guidance they have given to me. I also would like to thank Dr. Gurdip Singh for providing me guidance in my prospectus defense. In the past four years, Dr. Bala Natarajan and Dr. Caterina Scoglio gave me much support in both my research and writing publications. I would like to give my appreciation to them for the inspiration they provided me, and for the academic discussions and research group meetings we had that truly motivated my research. I also would like to thank Dr. Schulz for sharing her vast experience in research, and being encouraging to explore research ideas. I also would like to thank Dr. Sanjoy Das for providing valuable inputs to improve the quality of my research, discussion on algorithm development. Their great work and support expedited my research work and helped me to validate my algorithm. Additionally, I would like to thank my research colleagues, Joseph Diecker, and Amanuel Kesete, and members of the WiCom and Sunflower Network group for sharing their research experiences, skills, and also for making the workplace a friendly and fun-filled environment. Finally, I would like to thank my mother, Khela, my loving wife, Priyanka, and all my family members in USA and in India for their emotional support, understanding, encouragement, trust, and love.

Dedication

Dedicated to my mother

Chapter 1

Introduction

Cyber-physical systems (CPS) essentially enable seamless interaction between physical systems and cyber or computational resources, making physical systems intelligent. The primary focus of CPS is therefore, effective integration of the system computation resources and physical systems as shown in Fig. 1.1. With advances in CPS, many systems in the areas of automotive, health care, and transportation will be enhanced in term of reliability, integrity, and adaptability. Recent advances in cyber-physical systems could provide pathways to transform systems that respond quicker (viz., autonomous collision avoidance systems), are more accurate (viz., robot assisted medical functions and nano-tolerance manufacturing), work in hazardous environments (e.g., autonomous systems for fire-fighting), provide scalable, distributed coordination (viz., automated traffic control), enhance human capabilities, and societal wellbeing (viz., assisting technologies and ubiquitous health care monitoring and delivery) [4, 5].

An example of CPS is shown in Fig. 1.2. Portable, wearable sensors and medical measurement can be used to collect health information and take health-promoting actions. A powerful mobile system, e.g., a smartphone or a handheld device, is often used to collect and store data from them. It then relays the data to the Cyber-infrastructure where the necessary assessment related to patient health is taken and the resolution information is fed back to the devices for appropriate actions.

Fig. 1.3 shows another example of the cyber-physical systems (CPS) framework to model

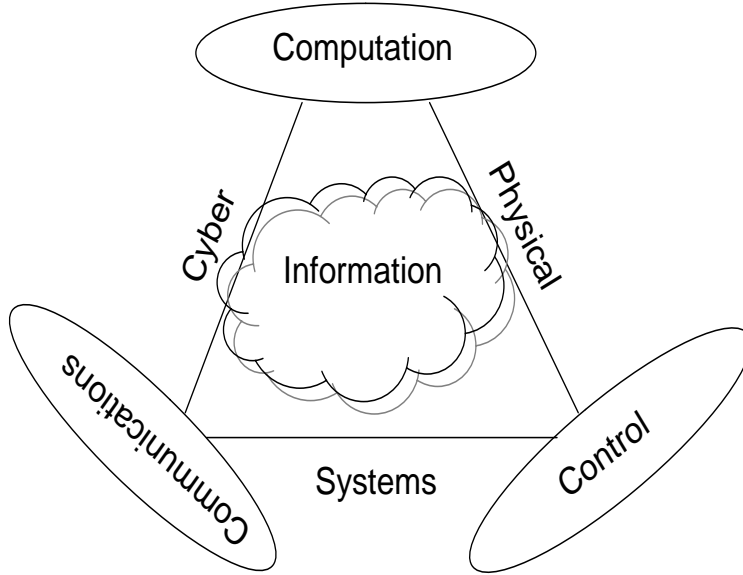


Figure 1.1: *Components of a Cyber physical Systems*

the intelligent adaptation behaviors in complex network systems. The CPS framework performs the core communication activities while adapting its behavior to the changing network conditions and user inputs. In this example, $g(I;O)$ is the motor in an industrial control system, with I and O denoting the electrical signal and rotational speed respectively. The idea of CPS modeling is to extend $g(I;O)$ into a coherent intelligent physical entity A_p that is self-aware and can reconfigure itself from the damages caused by environment conditions through interaction with computation and communication resources.

Another important example of CPS infrastructure that is of primary interest in this dissertation is the shipboard smart grid (SSG) system. In this infrastructure, the physical system is the power system which is connected to cyber resources such as sensors, communications network, and control centers. Through continuous interactions between the power system and computing resources via the communication networks, the SSG is transformed into a self-aware, reconfigurable system that can adapt to environmental/situational changes. For instance, after occurrence of faults, SSG can generate signals that carry in-

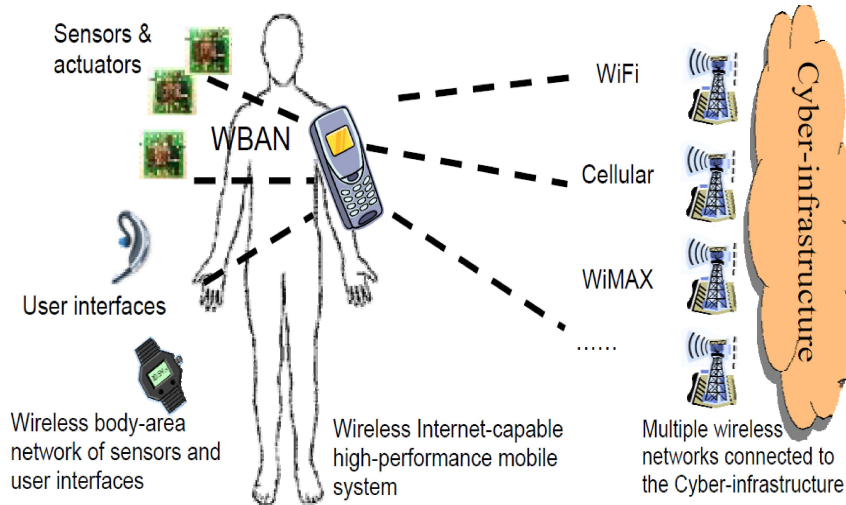


Figure 1.2: *Infrastructure of a CPS based personal health care [cf [1]]*

formation about locations and nature of faults and the control center can take appropriate remedial actions. The logical action sequences are then translated to the physical action sequences on the power system components (actuators, switches etc.) to complete the process.

1.1 Optimization of CPS - Challenges

The design and implementation of CPS based infrastructure present several challenges related to time- and event-driven computing, software, variable time delays, failures, reconfiguration, and distributed decision and control. Protocol design for real-time quality-of-service guarantees over wired and wireless networks, tradeoffs between control design and real-time-implementation complexity, matching performances between continuous and discrete-time systems, and guaranteeing robustness to failure are some of the key areas for CPS research. To this end, a suite of algorithms, software and hardware solutions are needed to meet the reliability and security requirements in cooperating cyber components that interact through a complex, coupled, physical environment.

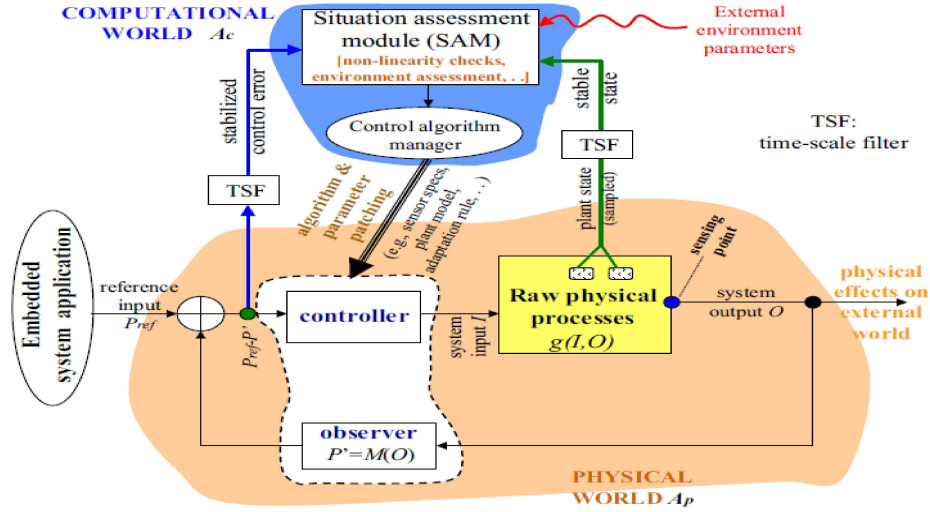


Figure 1.3: Hierarchical structure of a CPS based industrial motor control [cf [2]]

Some engineered CPS systems such as the SSG allow for physical system components to be reconfigured in response to emergency situations as well as to maintain optimality of operation. In a CPS system capable of performing automatic reconfiguration, command and control centers automatically recalculate corrective actions in response to failures and additions of network components. This allows the network to continue normal operation without need of human intervention. Reconfiguration is quick enough not to ensure that the higher-level protocols are not disrupted. Fault monitoring, fault isolation, communications network topologies, and total delay are extremely critical to automatic reconfiguration. Therefore, for a CPS, optimization of its reconfigurability creates a major challenge and needs much attention.

In this dissertation, we address challenges related to CPS optimization. We propose and analyze optimization methodologies with a case-study of reconfiguration of shipboard smart grid (SSG) system.

In an SSG, reconfiguration is a process to change the topology of the power system by switching the circuit breakers (CBs), switches, and other devices in the system in order to route power effectively to loads. Specifically, the reconfiguration is performed in

power systems to achieve certain objectives, such as restoring the connectivity, minimizing the power loss, maintaining the stability, or maximizing the loads. Since there are many possible switching combinations in a power system, the reconfiguration can be viewed as a combinatorial, non differentiable constrained optimization problem [6]. In recent years, several reconfiguration methodologies have been proposed for power systems [7, 8, 9, 10, 11, 12, 13, 14, 15, 16].

With a push to implement effective reconfiguration strategies in shipboard power systems, there arises requirements for a fairly new look at solving the reconfiguration problem, especially due to the shipboard's unique characteristics. Like their terrestrial counterparts, shipboard power systems are seeing a revolution related to "smart grid" applications. There are new opportunities for the integration of advanced power electronic, computer, controls and communications technologies into the all electric ship platform. The Office of Naval Research (ONR) have recently started proof of concept studies related to the design, operation and control of medium voltage DC (MVDC) distribution systems. The MVDC distribution systems will have new technical challenges in providing flexibility and survivability for the next generation ship power system. The MVDC system will also have additional power electronic devices that allow for innovative solutions related to control and communications. Therefore, new reconfiguration methodologies need to be researched and developed for smart grid with medium scale and integrated topologies. Automated reconfiguration is preferred to manual switching under more severe circumstances (cf. [17]). This necessitates the use of a Cyber physical systems based design for reconfigurability strategies to surface, especially in systems that has tightly coupled subsystems such a as shipboard power system.

1.2 MVDC Shipboard System Overview

Traditionally, SPS systems are self-contained and have radial distribution architectures. The space and weight constraints limit the amount of redundancy that can be incorporated

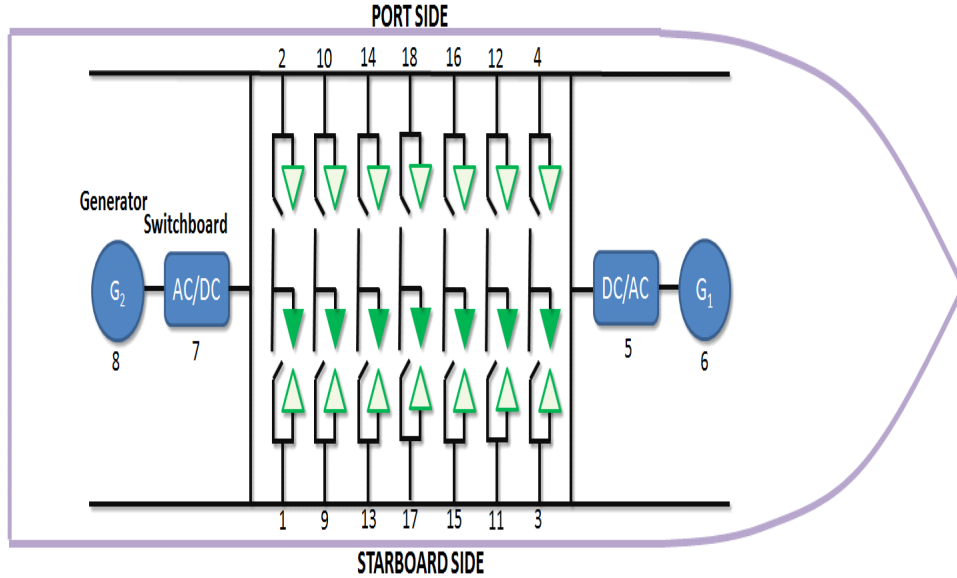


Figure 1.4: *Zonal architecture of shipboard power system (From [3])*

into the system for reconfiguration and restoration purposes. The SPS distribution network is tightly coupled, and therefore resistive losses are negligible. In the recent past, some researchers have proposed a radial distribution architecture with a zonal approach that employs a starboard bus (SB) and a port bus (PB), thus partitioning the ship into a number of electric zones [3]. Each DC zone has load centers driven by generator switchboards radially from port bus and star side bus. Each load center is divided into three categories based on priority of service; vital (VL), semi-vital (SVL), and non-vital (NVL) loads. Vital loads, and semi-vital loads are required for combat operations, while non-vital loads are dedicated to general purposes on the shipboard. It is assumed that non-vital loads can be shed to maintain power in the vital and semi-vital loads in case of emergencies.

The actual physical model considered in this dissertation for an all electric medium voltage DC (MVDC) shipboard system with all the loads and generators are shown in Fig. 1.5. Throughout this dissertation, we consider a DC zone electric distribution system as described in Fig. 1.4, and adopted in a new model in Fig. 1.5. Both models have 4 generators and 7 load centers. Load priorities and other constraints for the new model in Fig. 1.5 are similar to the model in Fig. 1.4. The power from the output of the generators

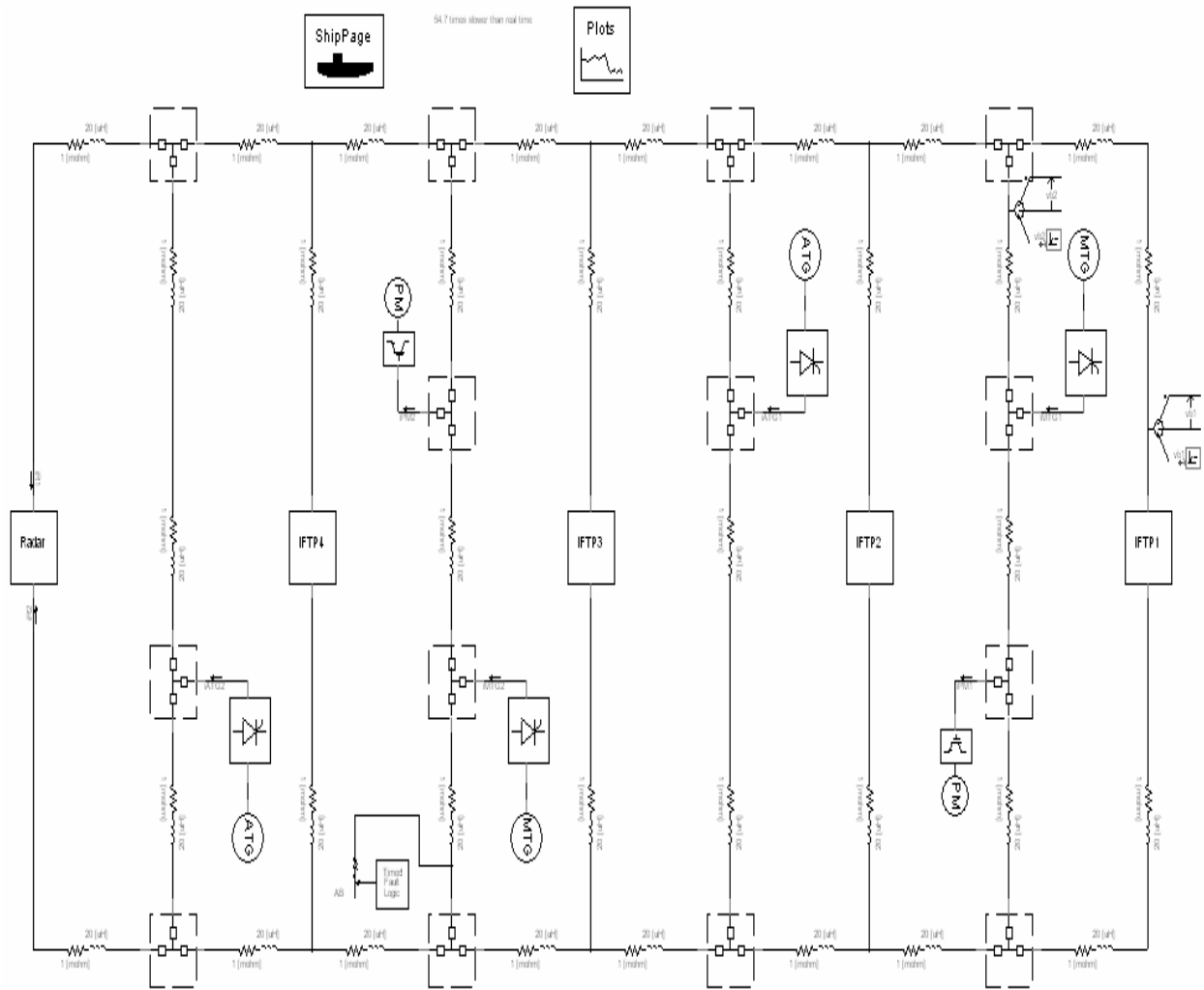


Figure 1.5: Shipboard Model [Ref: Model provided to Electric Ship Research and Development Consortium, Keith Corzine, Missouri University of Science and Technology, 2010.]

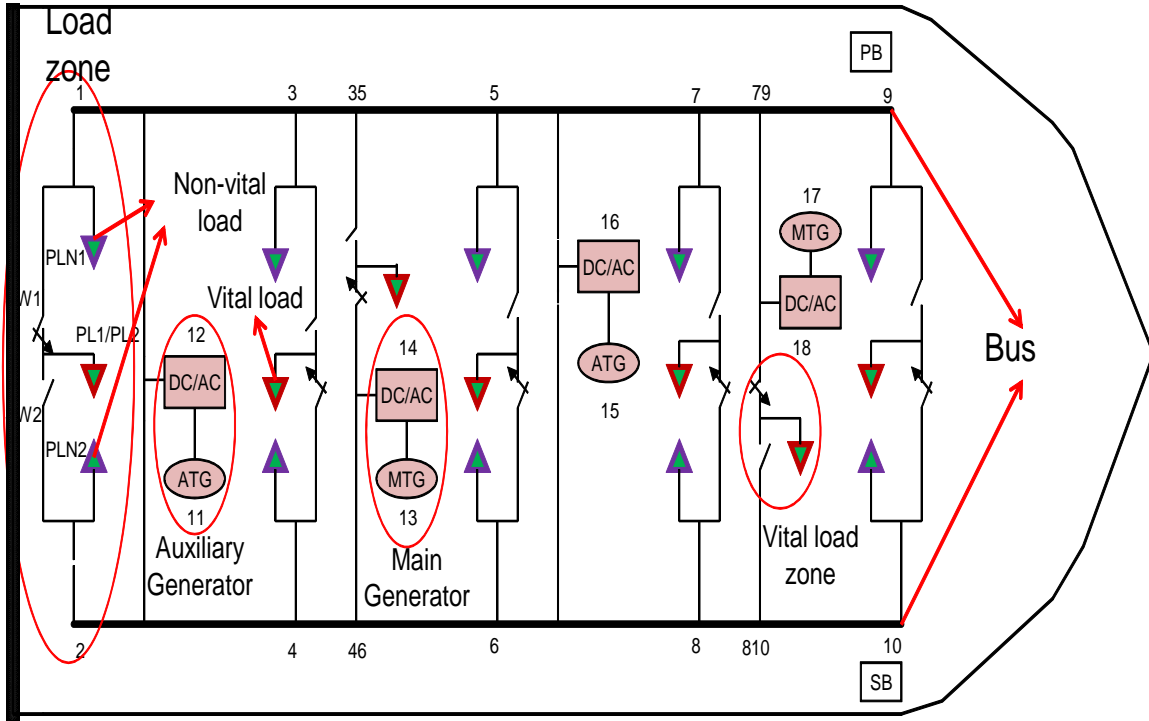


Figure 1.6: Shipboard model [Ref: Model provided to Electric Ship Research and Development Consortium, Keith Corzine, Missouri University of Science and Technology, 2010.]

is first converted into DC and fed into the loads, which may need reconversion to AC. Each zone has two load centers driven by generator switchboards radially from PB and SB. An analytical view of the new notional shipboard smartgrid model in Fig. 1.5 is shown in Fig. 1.6. The faults are assumed to occur in the buses connecting two load zones and switch states are reconfigured to optimally deliver (restore) power to the loads. In a centralized reconfiguration of the microgrid, the centralized controller handles the reconfiguration after receiving the fault location information from the sensors connected to the smartgrid via a *redundant ring* based communication network [18]. In a multi-agent based decentralized SSG reconfiguration, the agents communicate through this network. Shipboard power systems have some inherent characteristics that make them different from typical terrestrial power

distribution systems. Some of the unique characteristics of the SPSs are as follows [19]:

- There is very little rotational inertia relative to load in an SPS;
- SPS is an isolated system with no power supply from outside power system;
- SPS has a wider frequency range compared to the terrestrial power system;
- Shipboard prime movers typically have shorter time constant than prime movers in terrestrial power systems;
- Due to the limited space on shipboard, SPS does not have a transmission system. The electric power in SPS is transmitted through short cables. It leads to less power loss and voltage drop as compared to terrestrial power systems;
- There is a large portion of nonlinear loads relative to the power generation capability;
- In SPS, a large number of electric components are tightly coupled in a small space. A fault happens in one part of the SPS may affect other parts of the SPS;
- A large number of electronic loads, such as combat, control and communication sensors, radiators, and computers are sensitive to power interruptions and power quality;
- Some electrical components, which affect the reconfiguration process, are unique to SPS such as Automatic Bus Transfers (ABT), Manual Bus Transfers (MBT), Low Voltage Protection devices (LVPs), and Low Voltage Release devices (LVRs).

Therefore, reconfiguration methods that are developed for terrestrial power system cannot be applied to SPS. Consequently, a tightly coupled system such as a shipboard CPS, provides unique challenges related to its design for reconfigurability, and guaranteeing quality-of-service (QoS) arising therefrom.

1.3 MVDC Shipboard Reconfiguration

In an MVDC power distribution system, especially when applied to a tightly coupled micro grid, such as a shipboard system, predominantly the challenges are directly related to fault diagnosis and reconfiguration of shipboard power system, while rendering flexibility and survivability in fight-through and battle situations. Automatic reconfiguration is necessary in these cases to ensure continued service to vital loads such as weapon system, propellers, etc. Not only restoring service optimally is important, but also the timeliness with which the service is being restored while maintaining system stability is equally important. Innovative solutions with respect to control and communications of power electronic devices inside a shipboard system have become a necessity. Fig. 1.7 describes various areas of research

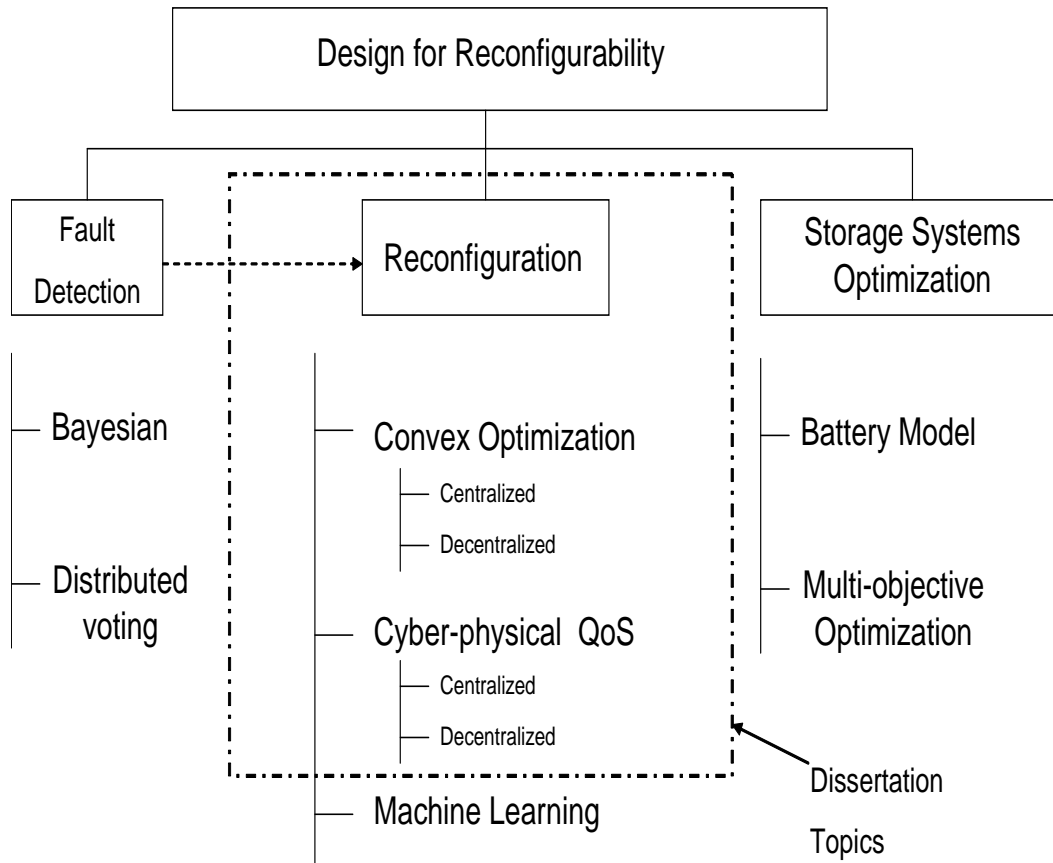


Figure 1.7: Overview of Shipboard Smartgrid Research Areas

related to shipboard smart grid and our focus in this dissertation. The two major objectives we address in this research are as follows:

- Given the location of the faults and isolation of the non-faulted loads that require service, what is the optimal power that can be delivered to the loads by reconfiguring the switch states (ON/OFF) associated with the loads. The reconfiguration can be done either in centralized or in distributed manner. Analysis in terms of global optimality, convergence speed, robustness, and reliability of both approaches are required.
- Provide a quality of service (QoS) guarantee for reaching from to a reconfigured state to a fault state, considering actions of all the physical subsystems and computational components associated with the power system. One major component of the QoS provided in our approach in terms of total delay, or the end-to-end response time (i.e., time taken from the occurrence of faults to restoration of service to the loads after reconfiguration). Another important aspect is the reliability with which the QoS requirement is met, given a system configuration. Both centralized and distributed approaches can be quantified with this QoS.

A detailed body of prior work related to the objectives of our dissertation is given in the next section.

1.4 Prior Work on SSG Reconfiguration

In recent years, many researchers have concentrated on providing suitable solutions for reconfiguration of shipboard smartgrid. The proposed solutions can be broadly divided into centralized and decentralized strategies. Fig. 1.8 provides an overview of the prior work related to shipboard smartgrid reconfiguration in the context of centralized and decentralized solutions. Literature review on related work in the areas of shipboard system reconfiguration is rich in general, with many notable contributions from numerous researchers around the world. For instance, distributed agents based reconfiguration [20, 21, 22, 23], genetic

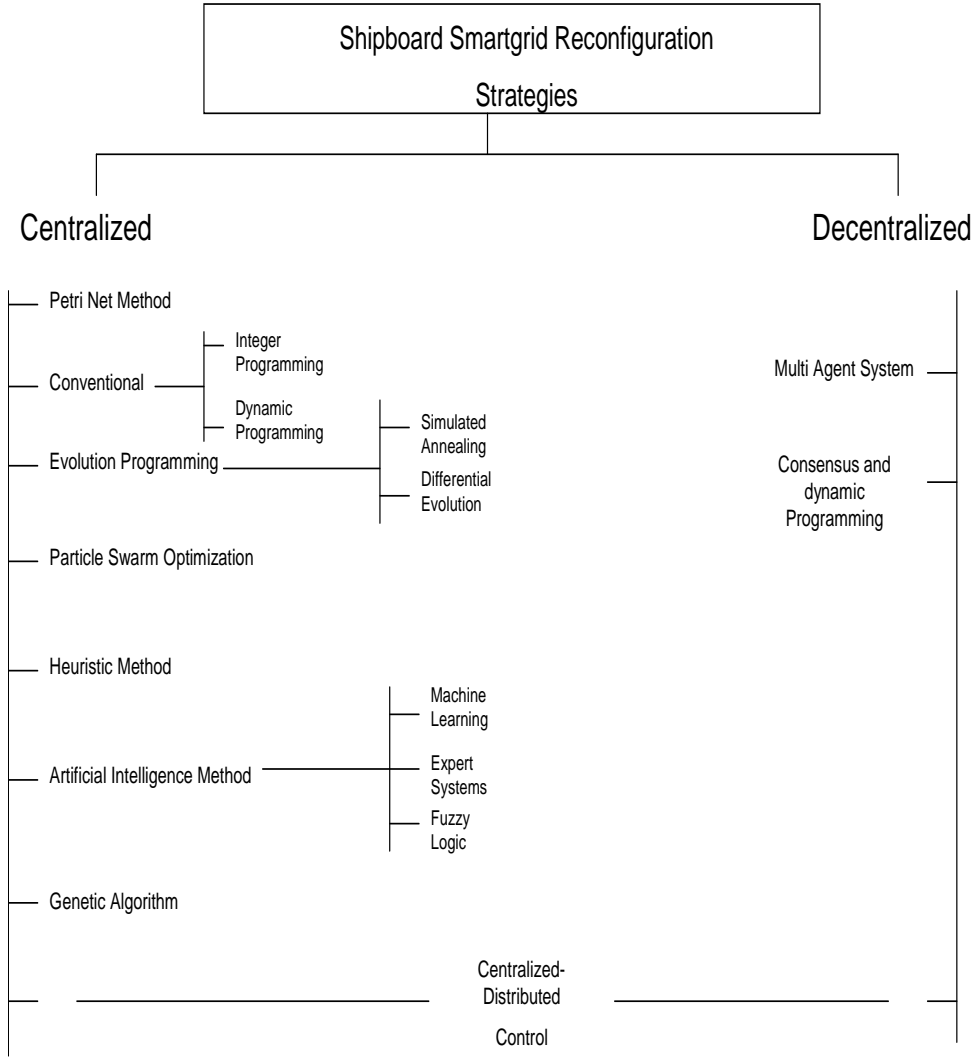


Figure 1.8: *Overview of Shipboard Prior Work on Smartgrid Research*

algorithms based stochastic optimization [24, 25, 26, 27, 28], zonal DC model based SSG reconfiguration, swarm intelligence based modern stochastic approaches [29], [30], and reinforcement learning based dynamic SSG reconfiguration [31] approaches, to name a few. We now categorically mention the prior work related to our proposed SSG reconfiguration methodologies in this dissertation.

1.4.1 Centralized Approaches

This approach is more traditional and has received great attention from researchers over the years. Traditionally, centralized reconfiguration for service restoration for terrestrial systems has been observed as an optimization problem that uses the objective as the sum of power or current delivered to the loads [32]. Mixed integer non-linear programming techniques were employed to solve the problem. Other reconfiguration objectives, such as power loss reduction [33] and stability margins [34], have been considered. Heuristic approaches [35], expert systems [36] based strategies, and mathematical programming [14] approaches have also been proposed. In addition, a combination of genetic algorithm and fuzzy logic [37] is used to solve large terrestrial systems reconfiguration problem. However, these efforts typically require running a complete power flow algorithm after each switching step (to determine if the constraints are satisfied) making the process slow and infeasible in some cases. Hence, better approaches are based on optimizing the objective function while simultaneously satisfying the power flow constraints.

A shipboard power system is non-linear and several methods using optimization for SPS have been proposed. Butler et al. [38] first proposed a novel fixed charge network flow method for reconfiguration for restoration based on maximizing the power delivered to loads while satisfying radiality constraints. The optimization was further improved to satisfy more constraints [39], include heuristic methods [40], and incorporate geographic fault information [41]. Other extensions of these methodologies account for non-radial topologies and mixed AC/DC systems [42], as well as islanding scenarios [43]. For these methods,

however, bi-directional flow of current was not considered which is inadequate for multiple fault scenarios and distributed generators (DG). The formulation for the reconfiguration problem considering both DG and bi-directional power flow results in a non-deterministic polynomial-time (NP) hard problem and was first presented in [44]. A global optimum to this problem can be found by branch and bound [45] methods or exhaustive search.

1.4.2 Centralized Cyber-Physical Modeling and Delay Analysis

The problem of probabilistic QoS guarantees in CPS in recent years has drawn significant attentions. In [46], QoS requirements for CPS is discussed by evaluating IEEE 802.15.4 based networking infrastructure. The theory of network calculus [47] has been used to support probabilistic delay bounds [48]. The network calculus and its probabilistic extensions provide bounds of traffic rate and service time. This essentially helps analyzing the worst case performance bounds. However, determining worst case bounds in shipboard system has limited applicability in most practical scenarios. The relative large variance in the end-to-end delay in shipboard CPS, due to the heterogeneity of several subsystems, results in loose bounds that can not characterize the delay distribution accurately. In [49], a control scheme for data center energy management is provided to optimize the trade-off between maximizing the payoff obtained from the computational services and minimizing energy costs for computation. However, most applications in shipboard systems trade retransmission for a lower delay of higher priority packets for maintaining high efficiency, especially in battle situations. These motivate the need for probabilistic delay analysis rather than worst case bounds. Our approach is based on basic principles of probability theory [50], real-time queuing theory [51], and their application to networks employing various transmission control protocols. We develop a stochastic model for the interaction of the individual level of network for analysis, assuming that each level system action is independent of the others. We differentiate our work from real-time scheduling solutions which are already elaborated in [51] [52] [53] [54], by developing a general analytical framework for analysis and design of

real-time scheduling and communication solutions. The analytical results accurately predict the end-to-end response time in SPS reconfiguration and therefore, can be used to maintain a required QoS on the response time.

In the recent past, some studies about delay distribution of MAC protocols for local area networks have been done [55]. The access delay of several MAC protocols has been investigated including IEEE 802.11b DCF protocol [56]. In these works, the distribution of retransmissions is only obtained, keeping the transmission time the same for each attempt. In other words, random backoff policies of CSMA/CD protocol have not been considered.

1.4.3 Decentralized Reconfiguration

Centralized methods of SSG reconfiguration only consider global optimality of power delivery across the entire shipboard. In SSG, decentralized optimization is typically proposed in a multi-agent architecture, where, power is locally distributed to the loads after the occurrence of faults (to recover temporarily from an interruption in service). The local response can then be complimented by centralized global optimization discussed in [57] to optimally distribute power to the entire system of loads when more reaction time is available [58]. A fully decentralized multi agent system based mesh structured SSG reconfiguration is described in [19] using spanning tree algorithm for local information accumulation and diffusion to achieve global load restoration. Another approach for reaching global state of load restoration using distributed multi-agent optimization for general microgrid system is presented in [59]. In [59], the global information related to load restoration is first discovered based on average consensus of interacting agents, and then dynamic programming is used to solve the global reconfiguration problem. This does not scale well with the size of the smartgrid. None of the prior approaches in [19] [59], however, provide any certificate of the quality of the proposed solutions or study the impact of information exchange between agents via a communication network. Some related work that provides modeling and analysis

of communication under imperfect network condition, such as, packet loss and delay, have been researched in detail in [60]-[61]. None of the prior work, however, provides detailed insights into solving the SSG reconfiguration problem in a decentralized manner.

1.5 Motivation of Research

The reconfiguration methodologies for the shipboard SSG discussed in the previous Section are examples of centralized and decentralized solutions. In a centralized reconfiguration approach for the power system, a central controller is required to make reconfiguration decisions. The central controller collects data from the entire power system, analyzes the collected data, and then makes reconfiguration decisions. All the previous approaches suffer from high complexity due to NP-hard combinatorial optimization and thus have limited use in practical shipboard systems. Reduction in complexity of the methods can therefore greatly improve the effectiveness of the SSG reconfiguration solution with marginal penalty in optimal power restoration. Additionally, guaranteeing robustness to faults for algorithms is not provided in previous related research. A valid way to probabilistically guaranteeing power delivered to the load in the event of fault occurrences is required.

Most communications in shipboard systems trade retransmission for a lower delay of higher priority packets for maintaining high efficiency, especially in battle situations [18]. These motivate the need for probabilistic delay analysis rather than worst case bounds. A stochastic approach is required that models the interaction of the individual network to find the distribution of total delay in reconfiguration. The important aspects of QoS guarantee for SSG reconfiguration, were ignored in the literature before.

In a centralized reconfiguration system without redundancy, if the central controller fails, the entire reconfiguration system fails. This is the single point of failure problem for centralized solutions. A central controller for reconfiguration of a power system performs large number of computations, such as power flow calculations, optimization, stability analysis, etc. When the number of electric components increases, or the topology of the power system

becomes large, the computational burden of central controller increases. It may slow down the reaction time of the central controller and decrease the performance of the reconfiguration system. Also, the central controller of the reconfiguration system gathers data from the sensors located on the underlying power system and sends reconfiguration decisions to the actuators in the power system to switch CBs through a communication infrastructure. Therefore, for a large power system with numerous electrical components and sensors, the amount of communication bandwidth required for operation of a central controller will be very high and costly. The communication requirements of a central controller may become the bottleneck of the central reconfiguration solution for a SSG. In recent years, decentralized methods such as MAS technologies [40],[42] have been increasingly popular for the reconfiguration of SSG. MASs mostly revolve around a facilitator agent that works as a dominant agent that has preset global information for the SSG. Other agents have to refer to the global information in the facilitator agent in order to make reconfiguration decision. If the facilitator agent fails, the reconfiguration system cannot work properly. Consensus and dynamic programming have attractive features for small scale system reconfiguration, but proves to be prohibitively slow when applied to a medium to moderately large SSG reconfiguration. Furthermore, none of the previous work provides insights into communication network impacts on the convergence and quality of the decentralized reconfiguration of SSG.

1.6 Contributions

In view of the discussion on previous research on SSG reconfiguration, in this dissertation, we aim to extend and innovate implementable algorithms of SSG and analyze communication network effects to optimize our algorithms. Specific contribution of this dissertation has been summarized below:

- Low-complexity methods can be effectively applied to the reconfiguration problem to produce solutions that are near-optimal. This is demonstrated with the aid of a

new MVDC ship model. With reduction in complexity, near-optimal solution can be reached in milliseconds, which makes it an attractive option to be used with future real time SPSs. The original problem is converted to a continuous non-convex problem by relaxing the integer constraints on the switches were assumed to be binary variable in earlier research works. Interior-point based methods [62] are applied to find the local optimum solution. Steady-state simulation analysis indicates that the local optimum obtained from integer relaxation followed by rounding, matches closely with the global optimum found by the branch and bound. Next, the non-convex relaxed integer problem is converted to a convex relaxed integer problem through affine transformation of the equality constraints. The global solution to this transformed convex problem is found by applying an interior-point method based solver. Through extensive simulation with various fault cases we demonstrate that the relaxed-integer convex and non-convex approaches provide very good quality suboptimal solution for SSG system reconfiguration.

- Robustness of the system is analyzed by considering the cumulative distribution of the power delivered in the event of K random fault cases (followed by reconfiguration). In this case, all vital and semi-vital loads are served partially or fully within a certain probability. This approach aims at quantifying the system robustness against faults, but adds more information on power delivery to each category of loads under a fault scenario.
- A tradeoff between power delivered and the number of switching operations needed to restore power is captured. Specifically, a bi-objective optimization problem is formulated with a second objective of minimizing the number of switching operations and “scalarize” it with the first objective of maximizing power delivered to loads. Empirical solutions of this combined weighted dual objective is presented against a random 2-fault case. The analysis is easily extendable to any K random fault cases.

Specific discussions and results related these contributions can be found in our papers [63, 64].

- A comprehensive integrated real-time analysis (RTA) framework to characterize total (end-to-end) delay distribution for SPS Reconfiguration. Specifically, each physical/cyber system delay is considered, including sequence of operations, information aggregation delay, queuing delay, transmission delay, communication protocols, and the computational delay associated with fault isolations and reconfiguration of switch status (ON/OFF).
- An analytical upper (worst-case) bound is provided on QoS and empirical validation of the same is done using simulation of the RTA framework.
Specific discussions and results related these contributions can be found in our paper [65].
- A novel time-varying gradient algorithm that includes the impact of practical communication links such as queuing delay, packet loss, and quantization noise is provided and analyzed in the context of decentralized dual decomposition based SSG reconfiguration problem.
- A theoretical lower bound on the convergence of the time-varying gradient algorithm under imperfect network conditions is derived, assuming that the time delay in the network is bounded (no packet loss).
- A new measure called outage convergence rate is introduced. This measure corresponds to the probability that the actual total delay exceeds the expected total delay when there is packet loss in the network.
- A comparison of total delay is presented for centralized and distributed approaches to analyze the effectiveness of the proposed optimization strategy.

Specific discussions and results related these contributions can be found in our papers [66, 67].

All the above contributions are directly related to our case-study on SSG system reconfiguration. However, the approaches introduced and methodologies used in this dissertation can be valuable for analysis of other CPS optimization scenarios. Thus the overall impact of this work extends far beyond the case study presented.

1.7 Organization of the Thesis

The rest of this dissertation is organized as follows:

- Chapter 2 presents centralized SSG reconfiguration formulations and analysis of robustness to faults. A combined objective of maximizing power delivery and minimizing the number of switching actions is included as part of the analysis.
- Chapter 3 demonstrates a Cyber-physical end-to-end delay analysis framework that employs appropriate stochastic models encompassing the heterogeneity of actions viz., the reconfiguration of power systems, data generation by sensor nodes resulting from faults occurring in the power system, processing actions at control center. Validation of the proposed framework is also provided.
- Chapter 4 presents the decentralized method of SSG reconfiguration using dual decomposition, and analyzes convergence of the proposed approach under perfect network conditions (no packet loss, and bounded time delay).
- Chapter 5 presents modeling and analysis of the impact of imperfect network (unbounded delay with packet loss) on decentralized dual decomposition based SSG reconfiguration. A time-varying gradient algorithm is proposed and analyzed under imperfect network that solves the SSG reconfiguration problem in a decentralized manner.

- Chapter 6 presents a comparative analysis of centralized and decentralized strategies of SSG reconfiguration discussed in this dissertation.
- Chapter 7 summarizes the entire dissertation. Concluding remarks and recommendations for future work are presented. A preliminary belief propagation based SSG reconfiguration approach is modeled and analyzed.

Chapter 2

Centralized Reconfiguration of Shipboard Smartgrid

In this chapter, we propose centralized methodologies of optimized SSG reconfiguration. The SSG system under considerations is introduced in Fig. 1.6 with load centers and switches to direct power to loads from the generators. Specifically, during the proposed reconfiguration, the status (ON/OFF) of switches are optimized such that maximum power is delivered to loads after the occurrence of a fault. The optimized reconfiguration is achieved by prioritizing power delivered to vital loads over semi-vital and non-vital loads. Analysis of the non-convex SSG reconfiguration formulation is done by an appropriate non-convex solver and by convex approximation. Unlike the non-convex solution that is based on branch and bound methods, convex approximation significantly reduces complexity.

2.1 Introduction

SSG essentially need automated reconfiguration to maintain continued service to loads after a fault. It is often proved that an integrated power system (IPS) provides a better solution than the manual process of restoration in terms of fight-through and survivability. In this process, multiple generators of various sizes and power generation capabilities are placed throughout the ship. IPS minimizes the amount of service interruption to affected portion of the ship during battle damage or any other sudden faults.

In this chapter, first, we demonstrate that low-complexity methods can be effectively applied to the reconfiguration problem to produce solutions that are near-optimal, with the aid of a new MVDC ship model. With reduction in complexity, near-optimal solution can be reached in milliseconds, which makes it an attractive option to be used with future real time SPSs. In [68], an analytical view of the methods to solve the reconfiguration problem is presented for the first time in the literature, and are applied to solve the reconfiguration problem for the new MVDC ship model in this paper. Fig. 2.1 summarizes the approaches. With a new notional shipboard model in [64], the effectiveness of the solution approaches is demonstrated. To accomplish this, the same process as described in [68] is followed. Specifically, the branch and bound based exhaustive search is applied to the original non-convex mixed integer problem $P1$ to find a global optimum switch configuration. Next, the original problem $P1$ is converted to a continuous non-convex problem $P2$ by relaxing the integer constraints on the switches such that $X \in [0, 1]$ where X is any switch variable. Interior-point based methods [62] are applied to find the local optimum solution. Steady-state simulation analysis indicates that the local optimum obtained from integer relaxation followed by rounding, matches closely with the global optimum found by the branch and bound. Next, the non-convex relaxed integer problem $P2$ is converted to a convex relaxed integer problem $P3$ through affine transformation of the equality constraints. The global solution to this transformed convex problem is found by applying an interior-point method based solver. Extensive simulation with various fault cases reveal that the global optimum for $P3$, and the local optimum for $P2$ closely match with the optimal reconfiguration solution of the original non-convex mixed integer problem $P1$ with high regularity. This may be possible as the non convexity of the original problem is in fact, limited to a few non-linear equality constraints in the AC power flow section of the generator while the majority of the formulation is convex.

Second, robustness of the system is analyzed by considering the cumulative distribution of the power delivered in the event of K random fault cases (followed by reconfiguration).

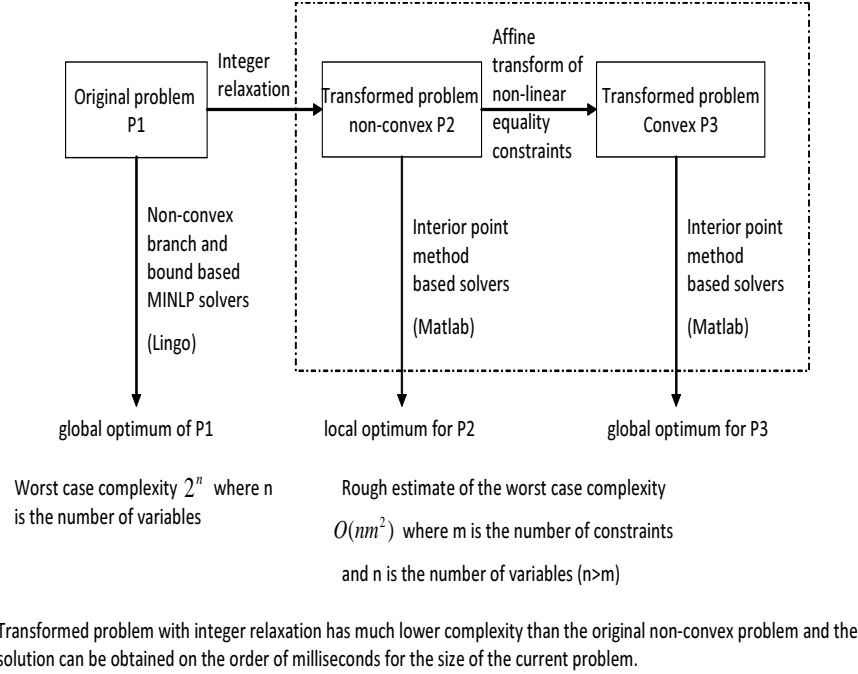


Figure 2.1: *Methods to analyze optimal solutions to SPS reconfiguration problem*

In this case, all vital and semi-vital loads are served partially or fully within a certain probability. This approach aims at quantifying the system robustness against faults as in [64], but adds more information on power delivery to each category of loads under a fault scenario.

Finally, the tradeoff between power delivered and the number of switching operations needed to restore power is captured. Specifically, a bi-objective optimization problem is formulated with a second objective of minimizing the number of switching operations and “scalarize” it with the first objective of maximizing power delivered to loads. Empirical solutions of this combined weighted dual objective is presented against a random 2-fault case. The analysis is easily extendable to any K random fault cases.

This chapter is organized as follows. The shipboard power system model is discussed in Section II. A detailed description of the reconfiguration methods is provided in Section III. Simulation of reconfiguration results on a new notional shipboard model [64] and further analysis with the present model in Fig. 1.4 are presented in Section IV, computational

complexity of the original and proposed methods for reconfiguration are discussed in Section V and finally, conclusions are summarized in Section VI.

2.2 Reconfiguration formulation

In this section, three formulations for SPS reconfiguration are presented. They include the original mixed-integer nonconvex (MINLP), relaxed-integer non-convex, and relaxed integer convex formulations. A description for each formulation is provided in the following subsections. Also, a dual objective formulation is included that attempts to maximize power delivery to loads while minimizing number of switching operations.

2.2.1 Mixed-Integer Non-Convex formulation (P1)

In this formulation the objective function and the constraints are similar to the ones presented in [44, 68]. However, this paper primarily extends the work in [68] to include examples of new balanced SPS systems. Once again, we are interested in determining the optimal switch configuration that maximizes the power delivered to loads. The detailed formulations are presented below: Objective function:

$$Max \sum_{I \in L} W_{VL} S_{VL} + W_{SVL} S_{SVL} + W_{NVL} S_{NVL} \quad (2.1)$$

Subject to AC constraints Equality constraints

$$PG_i - PD_i = \sum_j V_i V_j Y_{ij} Re \{ \angle(\theta_{ij} + \delta_j - \delta_i) \} \quad (2.2)$$

$$QG_i - QD_i = \sum_j V_i V_j Y_{ij} Im \{ \angle(\theta_{ij} + \delta_j - \delta_i) \} \quad (2.3)$$

Inequality constraints

$$PG_i^{min} \leq PG_i \leq PG_i^{max} \quad (2.4)$$

$$QG_i^{min} \leq QG_i \leq QG_i^{max} \quad (2.5)$$

$$I_{ij} \leq I_{ij}^{max} \quad (2.6)$$

$$V_i^{min} \leq V_i \leq V_i^{max} \quad (2.7)$$

$$\delta_i^{min} \leq \delta_i \leq \delta_i^{max} \quad (2.8)$$

DC constraints Equality constraints

$$\sum_i I_{in_i} = \sum_i I_{out_i} + IL_i \quad i \in FB, j \in TB \quad (2.9)$$

$$V_i = V_j + I_{ij} \times Z_{ij} \quad (2.10)$$

Inequality constraints

$$PL_i \leq PL_i^{max} \times SW_i \quad \text{for variable load} \quad (2.11)$$

$$PL_i = B_i \times PL_i^{max} \times SW_i \quad \text{for fixed load} \quad (2.12)$$

$$I_{ij} \leq I_{ij}^{max} \quad (2.13)$$

$$V_i^{min} \leq V_i \leq V_i^{max} \quad (2.14)$$

Switching constraints

$$SW_i + SW_j = 1 \quad \text{where } SW \in \{0, 1\} \quad (2.15)$$

Several important observations can be drawn from equations (4.1),..., (4.2) which are discussed below:

1. Weight are associated to prioritize service to different types of load as discussed in 2.1. We assign $W'_{NVL} = 1$ and assume that $W'_{VL} > W'_{SVL} > W'_{NVL}$ where NVL , VL and SVL are non-vital, vital and semi-vital loads respectively. Specifically, $W'_{VL} = 100$ and $W'_{SVL} = 10$ are picked for our analysis. L represents the set of loads in the power system.

2. Several constraints involving power flow, generator power limits, load limits, bus current and voltage limits are imposed. PG and QG are the active and reactive power, respectively, generated from the AC generator. PD and QD are the active and reactive power demanded, V_i is the voltage at bus i , δ_i is the angle associated with the voltage at bus i , Y_{ij} is the magnitude of the complex admittance from bus i to j , and θ_{ij} is the angle of the admittance from bus i to j , PL_i is the power delivered to loads connected at bus i , B_i is a binary variable that connects a fixed load to PB or SB and can be predetermined. IL_i is the load current at bus i , I_{ij} is the current flow from bus i to bus j , I_{in_i} and I_{out_i} are the currents entering and leaving bus i , FB is the set of “from (source)” buses, TB is the set of “To (destination)” buses, Z_{ij} is the branch impedance of branch i and j . $(.)^{max}$ and $(.)^{min}$ are used to indicate the maximum and minimum value of each variable, respectively. Unless explicitly mentioned, all variables indicate their magnitudes.

3. Switches are formulated as binary variables. The mutual exclusivity constraints on the switches determine if the power delivered to the higher priority loads is from port side or starboard side.

2.2.2 Relaxed-Integer Non-convex Formulation ($P2$)

In order to reduce complexity of the original MINLP problem, the binary switch variables are relaxed to have any value between 0 and 1, i.e., $SW \in [0, 1]$, while the mutual exclusivity constraint shown in (4.2) still holds good. This problem can be solved by interior point based non-linear solvers.

2.2.3 Relaxed-Integer Convex Formulation ($P3$)

A convex form of the previous relaxed integer formulation is obtained by affine transformation of the non-linear equality constraints using Newton’s power flow method [69]. In this,

the power flow equations (2.2) and (2.3) are rewritten as follows:

$$PG_i - PD_i = V_i \sum_{j \neq i} V_j Y_{ij} \cos(\theta_{ij} + \delta_i - \delta_j) + V_i^2 Y_{ij} \cos(\theta_{ij}) \quad (2.16)$$

$$QG_i - QD_i = V_i \sum_{j \neq i} V_j Y_{ij} \sin(\theta_{ij} + \delta_i - \delta_j) + V_i^2 Y_{ij} \sin(\theta_{ij}) \quad (2.17)$$

Using (2.16) and (2.17), the Jacobian \mathcal{J} is calculated and the incremental change in voltages and angles at every step of iteration from initial values of the angles δ_i and voltages V_i is obtained. So the constraints take linear forms as

$$\begin{bmatrix} \Delta PG_i \\ \Delta QG_i \end{bmatrix} = [\mathcal{J}_i] \begin{bmatrix} \Delta \delta_i \\ \Delta V_i \end{bmatrix} \quad (2.18)$$

It is easy to show that, for a finite range of δ_i and V_i the constraints given in (2.18) are affine. Therefore, this problem is a relaxed-integer convex problem and the global optimum for this problem can be found using an interior point method based solver.

It is shown subsequently that the optimal solutions provided by the low-complexity solvers discussed above provide close match with the global solution. This is a crucial feature for a “good quality” sub-optimal solution in general.

2.2.4 Dual-objective Formulation

Another objective of minimizing the number of switching operations while maximizing the power delivered to the loads is now introduced. The purpose of introducing this objective is to provide a trade-off between power delivered and switching operations performed as each switching operation incurs power loss and could result in undesirable transients in the system. To describe the formulation, first, the minimum “Hamming” distance from pre-fault switch state to the current switch state is taken into account. This distance is given as: $T(X) = SW_{pre\,fault_i} - SW_i$ where $i \in 1, \dots, N$. With MINLP formulation, the two objective functions are given as follows:

$$F_1 = Max \sum_{I \in L} W_{VL} S_{VL} + W_{SVL} S_{SVL_I} + W_{NVL} S_{NVL} \quad (2.19)$$

$$F_2 = \text{Min} \sum_N^{X=1} T(X) \quad (2.20)$$

With the relaxed-integer cases, the ‘‘Hamming’’ distance in (2.20) is changed to the ‘‘Euclidian’’ distance which is given by $E(X) = (SW_{prefault_i} - SW_i)^2$ so that it becomes

$$F_2 = \text{Min} \sum_N^{X=1} E(X) \quad (2.21)$$

The optimization problem defined above has two objective functions, F_1 and F_2 , that work against each other. That is, as each switching operation in F_1 attempts to increase power in order to maximize power delivered, the constraints in (2.2),..., (4.2) become difficult to satisfy unless more switching operations are performed. Therefore, F_2 will increase if F_1 is increased and vice versa. The domains of objective F_1 and F_2 are the same, and in particular are convex, as they both are functions of switch variables. The multi-objective domain is therefore, convex. It is common to combine such mutually conflicting objectives into a single objective function using the ‘‘weighted sum’’ approach [70] and look at pareto optimal solutions. The combined single objective optimization problem can be formulated as below:

$$F = w \times F_1 - (1 - w) \times F_2 \quad (2.22)$$

The parameters w and $(1 - w)$ in the combined objective function reflect ‘‘importance’’ of the corresponding objective function and may vary from 0 to 1. If the the two functions have comparable values the w parameter in (2.22) can meaningfully capture the trade-off between F_1 and F_2 . In this case, since F_1 is a function of power and F_2 depends on switching operations, different ranges for F_1 and F_2 are possible. Therefore, in order to bring F_1 and F_2 to a comparable scale, the ‘‘upper-lower-bound’’ transformation technique suggested for multi-objective optimization problem in [71] is used. In this approach, the transformed objectives F_1^{tf} and F_2^{tf} are obtained such that the weighted dual objective becomes

$$F = w \times F_1^{tf} - (1 - w) \times F_2^{tf} \quad (2.23)$$

subject to constraints (2.2), ..., (4.2). F_1^{tf} and F_2^{tf} , formulated as functions of the optimization variable x are as follows:

$$F_n^{tf}(x) = \frac{F_n(x) - F_n^0(x)}{F_n^{max}(x) - F_n^0(x)}, \quad n = 1, 2. \quad (2.24)$$

$F_n^{max}(x)$ and $F_n^0(x)$ are given by

$$F_n^{max}(x) = \underset{1 \leq l \leq n}{Max} F_n(x_l^*), \quad n = 1, 2. \quad (2.25)$$

$$F_n^0(x) = \underset{x \in X}{Min} (F_n(x)), \quad n = 1, 2. \quad (2.26)$$

Here, X is the design space, x_l^* is the point that maximizes the 1st objective function and n is the number of objective functions. With this transformation, F_1^{tf} and F_2^{tf} now typically range between 0 and 1.

2.3 Analysis Of Results

In this section, first, solutions to the reconfiguration problem from the three different formulations are compared. The original non-convex reconfiguration problem is solved using ‘‘LINGO’’ software package, while the other two formulations are solved using interior point methods in MATLAB. Second, a power flow CDF is presented to analyze the robustness of the system under study, and finally, the tradeoff between power delivered and number of switching operations is analyzed based on the dual objective formulation. To obtain the power flow CDF and to analyze the tradeoff, the transformed relaxed-integer convex formulation is used.

The new MVDC ship model presented in Fig. 1.6 is used for validation and analysis of the formulations $P1$, $P2$, and $P3$. Seven DC load zones are fed power from two main

generators (MTG) and two auxiliary generators (ATG), with each MTG of 6 *MW* and ATG of 2 *MW* generation capacities. Five load zones have vital, semi-vital, and non-vital loads while two load zones have vital loads only. Asynchronous bus transfer (ABT) is used to switch between *PB* and *SB*, and is characterized by mutually exclusive switches as shown in Fig. 2.2. Another well known notional ship model depicted in Fig. 1.4 is used for the rest of this analytical study. This model has seven load zones with two ship service converter module serving loads in each zone. A distributed generator (DG) along with the main generator (G) is used to enhance the overall service capability. The main generator generates a maximum power of 16 *MW* while the DG can generate up to 4 *MW*.

For each system discussed, it is assumed that (1) the vital loads require 0.5 *MW*, semi-vital loads require 1 *MW*, and non-vital loads require 0.5 *MW* for operating in their respective full capacity. (2) The non-vital loads are directly serviced through the buses, while the vital and the semi-vital loads are serviced through the ABTs. (3) The combined power of the generators is sufficient to drive all the loads under normal operating condition. (4) All distributions are radial, as it provides advantages such as lower short-circuit current, easy switching, and less complex installation and functioning of sensor equipment.

The optimization methods described in Section 2.2 are applied to reconfigure the SPS after occurrence of one or more faults. Only steady-state reconfiguration status is considered in this paper. Table 6.1 shows the constrained parameters used in the simulations and their respective maximum and minimum values. First, an optimal pre-fault configuration for system model in [64] is presented, where all the loads are serviced to their full capacities. The total capacity of loads that are served under normal condition is 13.5 *MW*. It is assumed that, under steady-state, a component is unavailable whenever there is a fault; so the current through that component is forced to a very low value. This is achieved by increasing the branch resistance in the simulation. It is obvious that some loads are left without power after the fault. The reconfiguration formulations *P1*, *P2*, and *P3* ensure that the power is restored in a manner such that those loads are serviced optimally and according

Table 2.1: *Simulation parameters*

Constrained parameters	max.	min.
PG_i (MTG)	6 MW	0 MW
PG_i (ATG)	2 MW	0 MW
I_{ij}	500 A	-500 A
V_i	95 V	105 V
δ_i	1°	-1°
PL_i (VL)	0.5 MW	0 MW
PL_i (SVL)	1 MW	0 MW
PL_i (NVL)	0.5 MW	0 MW
SW_i	1	0
B_i	1	0

to their priority. This means that vital and semi-vital loads are restored before non-vital loads. Fig. 2.2 shows a pre-fault condition where all the loads are serviced for a particu-

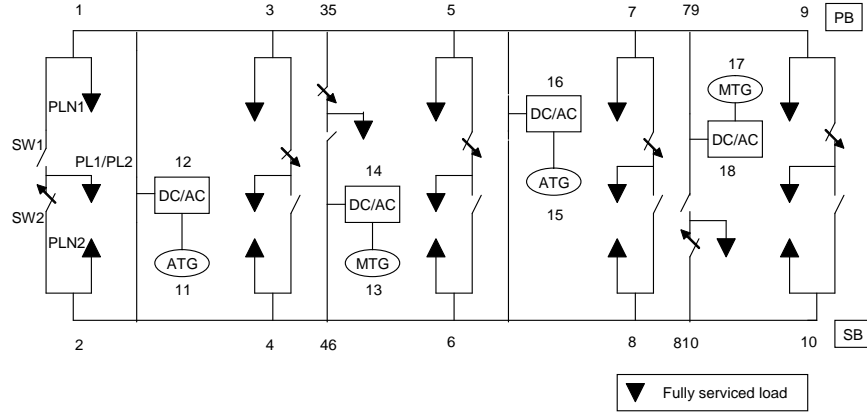


Figure 2.2: *Schematic view of SPS under normal condition (pre-fault)*

lar switch configuration. Reconfiguration algorithms are applied for MINLP ($P1$), relaxed integer non-convex ($P2$) and relaxed-integer convex ($P3$) cases from this initial (pre-fault) configuration. Now a fault scenario is considered where faults occur between branches 1 – 3, 3 – 35, and 35 – 5. The portion of the PB between 1 and 5 is thus left without power and the switches need to change so that the loads can be serviced based to their priority mainly through the SB. The optimal reconfiguration, as it turns out in this case requires the opening of $SW2$, $SW35$, $SW5$, $SW7$, $SW810$, $SW10$, and closing of $SW1$, $SW4$, $SW6$,

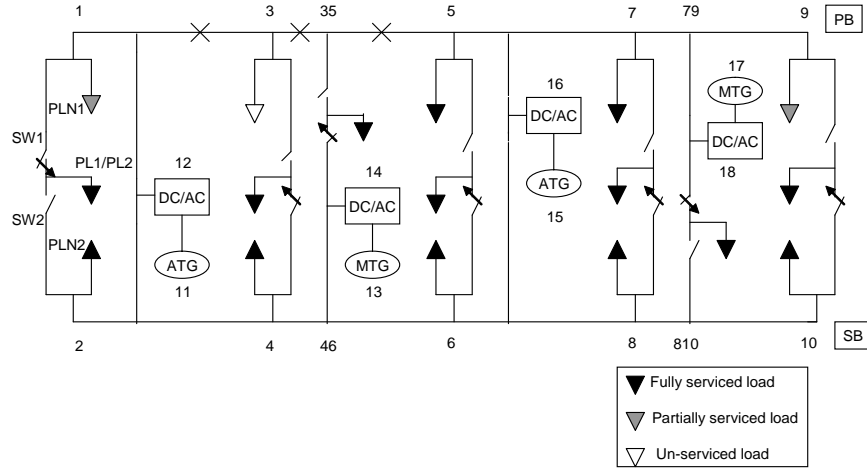


Figure 2.3: Schematic view of SPS under faults occurring at 1 – 3, 3 – 35, and 35 – 5

Table 2.2: Power delivered to loads under faults occurring at 1 – 3, 3 – 35, and 35 – 5

Load positions	Vital (MW)	Semi-vital (MW)	Non-vital (MW)	SW positions (closed)	MTG (Total) (MW)	ATG (Total) (MW)	Solver
Load 1/2 Load 3/4 Load 35 Load 5/6 Load 7/8 Load 810 Load 9/10	0.5000 0.5000 0.5000 0.5000 0.5000 0.5000 0.5000	1.0000 1.0000 1.0000 1.0000 1.0000 1.0000 1.0000	0.6319 0.5000 1.0000 1.0000 1.0000 0.6590	SW1 SW4 SW46 SW6 SW8 SW810 SW10	8.5590	4.0000	Global Non-convex with mixed integer (LINGO)
Load 1/2 Load 3/4 Load 35 Load 5/6 Load 7/8 Load 810 Load 9/10	0.5000 0.5000 0.5000 0.5000 0.5000 0.5000 0.5000	1.0000 1.0000 1.0000 1.0000 1.0000 1.0000 1.0000	0.6319 0.5000 1.0000 1.0000 1.0000 0.6590	SW1 SW4 SW46 SW6 SW8 SW810 SW10	8.5590	4.0000	Local Non-convex with integer relaxation (MATLAB)
Load 1/2 Load 3/4 Load 35 Load 5/6 Load 7/8 Load 810 Load 9/10	0.5000 0.5000 0.5000 0.5000 0.5000 0.5000 0.5000	1.0000 1.0000 1.0000 1.0000 1.0000 1.0000 1.0000	0.6319 0.5000 1.0000 1.0000 1.0000 0.6590	SW1 SW4 SW46 SW6 SW8 SW810 SW10	8.5590	4.0000	Global Convex with integer relaxation (MATLAB)

SW_8 , SW_{79} , and SW_9 to ensure maximum power supply to the vital and semi-vital loads. The non-vital loads attached to the PB at nodes 1 and 9 are partially serviced due to insufficient power left in the generators, and the non-vital load attached to PB at node 3 is left unserved. The power drawn from the main generators drops to 8.56 MW and the ATGs have to service to their full capacity. As seen from Table 2.2, the optimal MINLP

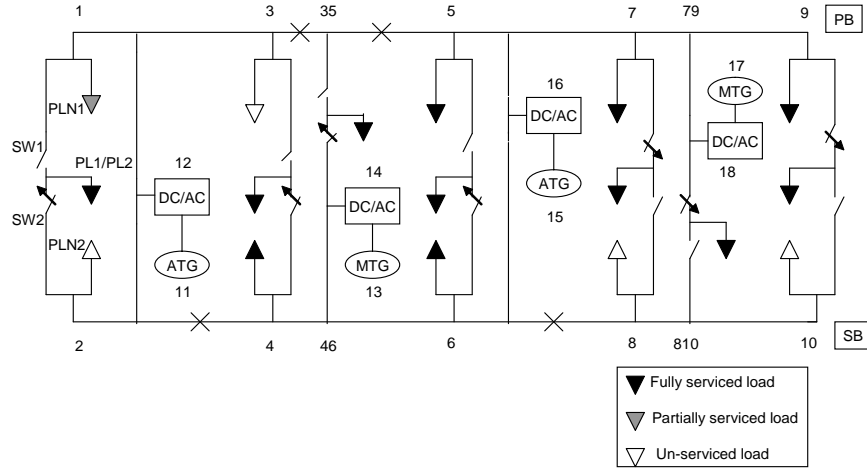


Figure 2.4: Schematic view of SPS under faults occurring at 3 – 35, 35 – 5, 2 – 4 and 6 – 8

Table 2.3: Power delivered to loads under faults occurring at 3 – 35, 35 – 5, 2 – 4 and 6 – 8

Load positions	Vital (MW)	Semi-vital (MW)	Non-vital (MW)	SW positions (closed)	MTG (Total) (MW)	ATG (Total) (MW)	Solver
Load 1/2	0.5000	1.0000	0.4786	SW2	8.5949	4.0000	Global Non-convex with mixed integer (LINGO)
Load 3/4	0.5000	1.0000	0.5000	SW4			
Load 35	0.5000	1.0000	1.0000	SW46			
Load 5/6	0.5000	1.0000	0.5000	SW6			
Load 7/8	0.5000	1.0000	0.5000	SW7			
Load 8/10	0.5000	1.0000	0.5000	SW79			
Load 9/10	0.5000	1.0000	0.5000	SW9			
Load 1/2	0.5000	1.0000	0.3212	SW1	8.6131	4.0000	Local Non-convex with integer relaxation (MATLAB)
Load 3/4	0.5000	1.0000	0.6506	SW4			
Load 35	0.5000	1.0000	1.0000	SW46			
Load 5/6	0.5000	1.0000	0.5000	SW6			
Load 7/8	0.5000	1.0000	0.5000	SW7			
Load 8/10	0.5000	1.0000	0.5000	SW79			
Load 9/10	0.5000	1.0000	0.5000	SW9			
Load 1/2	0.5000	1.0000	0.3421	SW2	8.6004	4.0000	Global Convex with integer relaxation (MATLAB)
Load 3/4	0.5000	1.0000	0.6364	SW4			
Load 35	0.5000	1.0000	1.0000	SW46			
Load 5/6	0.5000	1.0000	0.5000	SW6			
Load 7/8	0.5000	1.0000	0.5000	SW7			
Load 8/10	0.5000	1.0000	0.5000	SW79			
Load 9/10	0.5000	1.0000	0.5000	SW9			

solver and near-optimal interior-point method based solvers produce the same switch status in this case. Fig. 2.3 also shows the switch status after reconfiguration.

Another fault scenario is considered, where 4 faults occur between branch 3 – 35, 35 – 5, 2 – 4 and 6 – 8. This creates an islanding scenario where loads on the left side of the fault locations between 3 – 35 and between 2 – 4 have no alternative paths from the generators.

The ATGs again ramp up to their maximum power to service the priority loads; non-vital loads at nodes 2, 3, 8 and 10 are shed, while the non-vital load at node 1 is partially serviced due to insufficient power from the ATG node 11. However, all the vital and the semi-vital loads are fully serviced. In the global optimum solution shown in Fig. 6.1, $SW3$, $SW35$, $SW5$ and $SW810$ are open and $SW4$, $SW46$, $SW6$ and $SW79$ are closed. Table 2.3 shows that the global optimum solution for $P3$ produces the same switch configuration as the global optimum solution for $P1$. Also, the total power delivered to the loads are almost the same in both cases. The local optimum solution for $P2$ is however, different in one switch position ($SW2$ closed instead of $SW1$) and marginally less total power is delivered to the loads. Further extensive simulations are performed with various fault scenarios to compare solutions provided by $P1$, $P2$ and $P3$. No significant difference in the total power delivered is observed after reconfiguration, even though switch status for the three solutions may differ for a small number of cases.

Next, an analytical study of the robustness of the system is provided using the model in Fig. 1.4. CDF of the power delivered to the loads is used to analyze the robustness against several random faults and is defined as $CDF = Prob. \{Power\ delivered\ to\ loads \leq P_D\}$, where P_D is the desired power. As shown in Fig. 2.6, the CDF of the power delivered to the loads is plotted for all possible random locations for 2, 3, and 4 faults. The pre-fault

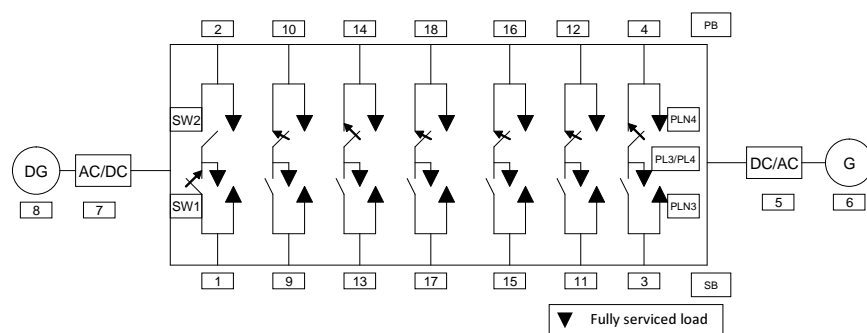


Figure 2.5: Schematic view of SPS under normal condition (pre-fault)

configuration for this system is shown in Fig. 2.5. There are several observations that can be drawn from the CDF analysis of the system which are summarized below:

1. The total load that are serviced is 17.5 *MW* of which the total power required to serve the vital loads is 3.5 *MW*, total power required for the serving the semi-vital loads is 7 *MW* and the rest 7 *MW* is used to serve the non-vital loads. Table 2.4 shows the percentage of the total load served for various random fault cases.
2. For all possible 2-fault cases, the system is able to sustain power delivered to about 16.47 *MW* in 50% of the cases. For random 3-fault cases, the power delivered dips to 15.16 *MW* whereas for random 4-fault cases, the power delivered to loads further reduces to 14 *MW* 50% of the cases. Therefore, Fig. 2.6 and Table 2.4 confirm that 100% of the vital loads are served for these fault cases 50% of the time, 100% of the semi-vital loads are served 50% of the time. The non-vital loads are, however shed to maintain power delivered to the higher priority loads.
3. For random 2-fault cases, the system is able to serve 100% of the vital loads and 100% of the semi-vital loads for 90% of the cases. For random 3-fault cases, vital loads are not served only about 10% of the time, while for 4-fault cases vital loads are not served 15% of the time. These are cases where faults occur at the generator buses.

Table 2.4: *Power delivered as a function of faults*

Percentage	2-faults	3-faults	4-faults
50	16.47 MW	15.16 MW	14 MW
10	13.2 MW	4.09 MW	0 MW

Therefore, the CDF tool based robustness study of the shipboard power system reconfiguration incorporates a probabilistic view of the robustness of the system to various random faults.

Finally, the results of the dual-objective formulation in (2.22) of the optimization problem is presented. The weight w (2.22) is varied from 0 to 1 to investigate the combined objective of the power delivered to the loads (F_1) and the number of switching operations (F_2). In Fig. 2.7 and Fig. 2.8, a case with 2 faults occurring between 12 – 4 and 7 – 1

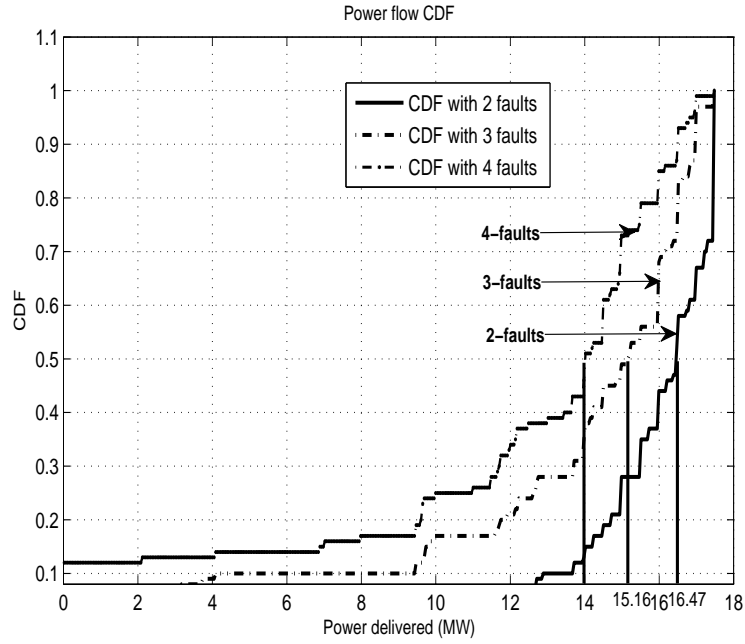


Figure 2.6: CDF of power delivered (MW)

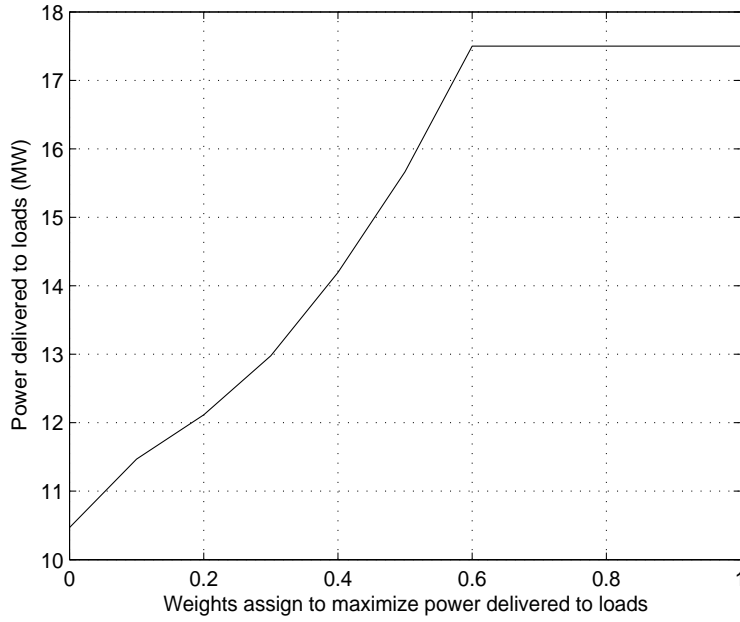


Figure 2.7: Power delivered for faults between 12 – 4 and 7 – 1

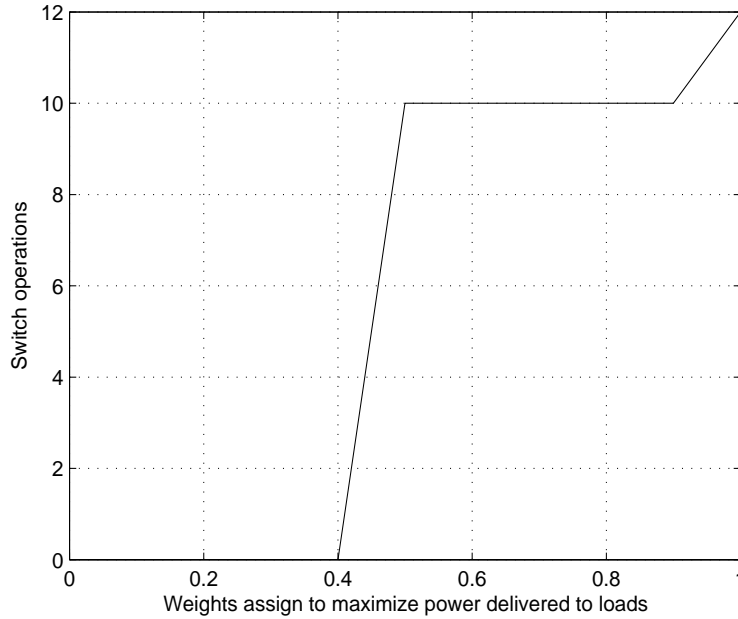


Figure 2.8: *Number of switching performed for faults between 12 – 4 and 7 – 1*

with model in Fig. 2.5 is presented which shows power delivered to the loads and number of switch operations performed respectively. As the weight w is increased from 0 to 1, Fig. 2.8 shows an increase in the number of switch operations. When w increases from 0.4 to 0.5 the number of switch pair operations increases from 0 to 5. This is due to the fact that the switching surface allows more number of switches to change suddenly and accounts for a more stable locally optimal state. With the weighted objective function, when relatively more importance is given to power delivery, the number of switch operations also increases, which is expected as more switching is needed to deliver more power to the loads. As seen in Fig. 2.7 and Fig. 2.8, more than 5 switch pair changes, however, do not increase the amount of power delivered to the loads in this particular example. Therefore, 5 switch pair changes are sufficient to deliver maximum power to the loads, corresponding to the best trade-off between the power delivered and number of switching operations.

In a separate analysis, a step by step study of the reconfiguration solution with the assumption that only one pair of switches is allowed to change at each step of reconfiguration

Table 2.5: *Power delivered and switch transition to faults occurring at 2 – 10 and 12 – 4*

Power delivered to loads	12.3652	13.8652	15.3653	16.8653	17.1503	17.5000
SW1	1	1	1	1	1	1
SW2	0	0	0	0	0	0
SW3	0	0	0	0	0	1
SW4	1	1	1	1	1	0
SW9	1	1	1	1	0	0
SW10	0	0	0	0	1	1
SW11	1	1	1	1	1	1
SW12	0	0	0	0	0	0
SW13	0	0	0	1	1	1
SW14	1	1	1	0	0	0
SW15	0	1	1	1	1	1
SW16	1	0	0	0	0	0
SW17	0	0	1	1	1	1
SW18	1	1	0	0	0	0

is shown in Table 2.5. The first column indicates the initial switch state; final state when the reconfiguration is complete is shown in the last column, and all the other columns in between represent the intermediate switch states resulting in maximum incremental power delivery to loads from a previous column. Each switch state deliver power to loads incrementally from 12.36 MW to 17.5 MW. The analysis is particularly useful when cost associated with switch operations becomes significant; thereby only a limited number of switch operations have to be performed in restoring power to the loads after reconfiguration. Obviously, the solution may not be globally optimal when the number of switch pair changes is restricted to less than 5, but will ensure maximum power delivery for a fixed number of switch operations.

2.4 Computational Complexity

In this section, first, the complexity of the solutions provided to optimally reconfigure the SPS is analyzed. “LINGO” software is used to solve the original non-convex mixed integer problem. It uses “branch-and-bound” method to maintain a provable upper and lower bound on the objective value which is ϵ -suboptimal to the global optimum. First, assuming convexity, the algorithm finds an upper and a lower bound on the optimal objective value p^* . If the difference between any upper and lower bounds satisfies $U_k - L_k \leq \epsilon$, it terminates or otherwise, creates branches for any index $k \in 1, \dots, n$ on the switch variables to form two subproblems. Using convex relaxations on the switches other than the k -th switch, it

Table 2.6: Execution time efficiency (ETE) for original nonconvex and transformed convex methods. Reference execution time for original nonconvex method = 1 second

Number of variables (n)	Constraints(m)	ETE
8	6	1.125
14	12	0.123
30	28	0.002

produces and upper and lower bound on the optimal value of each subproblem. The optimal value p^* of the original problem is the smaller of the two subproblems. This eventually forms a binary tree with each leaf node created by fixing a variable that is not fixed in the parent node. So, a node at depth i in the tree corresponds to a subproblem with i switch variables have fixed values. The upper and lower bound on p^* are obtained by the minimum of upper and lower bounds over all the leaf nodes. The algorithm terminates when $U_i - L_i \leq \epsilon$. Therefore, in the worst case, a complete binary tree is developed to depth n which makes the complexity as 2^n where n is the number of switch variables. For our problem with $n = 14$ the worst-case complexity is 2^{14} which is relatively large for this reconfiguration problem.

The worst-case complexity for interior-point based method is $O(nm^2)$ where n is the number of variables and m is the number of constraints and $n > m$. The complexity of this method is thus polynomial in time but in worst-case much less than the “branch and bound” based method. The Interior-point method solves the reconfiguration problem by applying Newton’s method to a sequence of equality constrained problems. Results show that local optimum found by interior-point based solvers match global optima by “branch and bound” method for this reconfiguration problem. This is due to the fact that the problem is highly convex with some non-convexity in the generator constraints. Our convex formulation of the relaxed-integer non-convex problem reinforce this claim. The complexity of this relaxed-integer convex problem, is however, same as the relaxed-integer non-convex problem although a global optimum of this problem can be found for the former as any local optimum for a convex problem is the global optimum solution. In this case sequential

convex programming [62] is applied by maintaining estimate of solution $x^{(k)}$ and a trust region $T^{(k)} \subset R^n$ such that (2.18) is affine. With relaxed-integer convex formulation we are able to convincingly state that our reduced-complexity solution provide exactly the same result as the “LINGO” based global optimum solution presented in [44]. In Table 2.6 the ETE - percentage efficiency in execution - is defined as

$$ETE = \frac{\text{Execution time for transformed convex}}{\text{Execution time for original nonconvex}} \quad (2.27)$$

This shows that assuming platform independence, if the execution time for original non-convex method with $n = 14$ and $m = 12$ is 1 second, the proposed convex method will provide the same result in 123 milliseconds. For low values of n and m exhaustive search is easy to perform. Therefore, there is no gain in transforming the non-convex problem. As Table 2.6 shows, for $n = 8$ and $m = 6$ branch and bound performs better. As the number of switches increases a very high execution time efficiency is possible.

2.5 Summary

In this chapter, two centralized optimization solutions are evaluated that deliver near-optimal power to loads in shipboard power system. The complexity of proposed solutions is polynomial in time and much lower than the complexity of the global solver that uses a “branch and bound” based approach. Local optimum for relaxed-integer non-convex formulation and global optimum for relaxed integer convex formulation match the global optimum for original MINLP non-convex formulation with high regularity. Further, cumulative distribution of power flow is used to show that in 50% of the fault cases (up to 4 random faults) the vital and semi-vital loads are serviced. Analysis of the tradeoff between power delivery and number of switching operations performed during reconfiguration is also provided. As expected, it is observed that an increase in switching is necessary to deliver more power to loads. Furthermore, change of switch states is tracked from pre-fault state to final state, while (1) changing one switch pair at a time; and (2) maximizing power delivery at each

state. The tradeoff between number of switch operations and power delivered is also quantified.

In the next chapter, we investigate centralized SSG reconfiguration involving interaction between sensors, power systems and communication network. We adopt a cyber-physical approach to understand and quantify the delay in SSG reconfiguration from the occurrence of faults.

Chapter 3

Centralized Reconfiguration-Response Time Analysis

In this Chapter, the distribution of end-to-end delay associated with fault diagnosis and reconfiguration in an all electric shipboard smartgrid system (SSG) is investigated from a cyber-physical system (CPS) perspective. Specifically, a multi-layer end-to-end delay analysis framework is presented.

3.1 Introduction

As we discussed, next generation all electric navy shipboard smartgrid system (SSG) is envisioned to have the ability to be reconfigured to route power to loads after the occurrence of faults to maintain continued service to loads. The analysis of the response time from the occurrence of a fault to restoration of service to loads is of primary concern. It is important to estimate the SSG reconfiguration delay, especially for mission critical applications. This guarantees the ship's survivability against battle damages. The delay involved in SSG reconfigurations can be evaluated by modeling the process flow through the physical power systems, communication and sensor networks, and computing components in the command and control center. The challenges with reliable cyber-physical modeling has been discussed in detail in [72]. Communication networks (wired and wireless) are essentially used to provide both connectivity infrastructure and data aggregation [73] in CPS. Depending on the nature

of the generated traffic, SSG reconfiguration requires, like many other networked applications, real-time quality of service (QoS) guarantees [74]. Such QoS requirements has been traditionally related to two main transport parameters: information loss (reliability) and delay (timing). Additionally, in an SSG, the number of switch operations for reconfiguration of the power system and the delay associated with it play a critical role in determining QoS guarantees. The random nature of data transmission and distribution, and the number of switch operations hinder the development of deterministic QoS guarantees in the shipboard CPS. Therefore, QoS guarantees on the end-to-end response time for SSG reconfiguration can be given in a probabilistic manner to address both timing and stability requirements. In this work, the end-to-end delay distribution for real-time power system reconfiguration after the occurrence of faults is characterized. Cumulative distribution function (cdf) of the delay for a desired response time is used as the QoS metric. Several centralized topologies of the sensor network and their impacts on the delay distribution are analyzed using a real-time analysis (RTA) framework. Real-time QoS guarantee on SSG reconfiguration with current and potential communication technology (FDDI/Ethernet/Gigabit Ethernet) implementations for shipboard are also compared. Specific contributions of this chapter are summarized below:

- A comprehensive integrated RTA framework to characterize end-to-end delay distribution for SSG Reconfiguration. Specifically, each physical/cyber system delay is considered, including sequence of operations, information aggregation delay, queuing delay, transmission delay, communication protocols, and the computational delay associated with fault isolations and reconfiguration of switch status (ON/OFF).
- Provide an analytical upper (worst-case) bound on QoS and empirical validation of the same using simulation of the RTA framework.

We base our results on communication network delay distribution suggested in [75], but we extend it further to combine heterogeneity of independent physical subsystems and architectures of sensor network to characterize the end-to-end delay distribution. Furthermore,

we provide a tight lower bound using the Hoeffding’s inequality [76] on the sensor and communication network delay distribution. This lower bound provides the worst case sensor and communication network QoS guarantee. Finally, it is important to mention that accurate characterization of integrated end-to-end delay in CPS is still an open problem and much work is foreseeable in the areas of abstraction and architectures, distributed network control, and verification and validation as mentioned in [77]. Our proposed approach for integrated delay analysis framework provides important insights that improve future real-time scheduling of shipboard system applications.

3.2 Problem Statement

The QoS requirement in SSG reconfiguration varies based on the priorities assigned to the loads. An analytical model for the actual physical system in Fig. 1.5 under normal (no-fault) condition [63] is shown in Fig. ???. For example, when there is an interruption in power delivery due to faults, system reconfiguration must be done so that power is first delivered to vital loads. Sensor nodes that are distributed across the SSG, collect information from underlying power system network and send their measurements to a sink through a multi-hop route in the network. Every sensor node is characterized by its input traffic rate λ , maximum number of retransmission attempts, R_{max} , and a MAC protocol. In general for our analysis, Poisson point traffic at each sensor node or fusion center and packets of exponential length with a fixed mean are assumed. The approach presented in Section 3.4 can be extended to other traffic models. Given the parameters of the node and a chosen transmission control protocol, we obtain first, the delay distribution between two nodes i and j for a new arriving packet. Second, we combine the delay distribution by factoring in the architecture (arrangements of nodes), to find the aggregated delay distribution of conveying the collected information from sensor nodes to a processing center. Third, we consider the delay from the computing device (command and control center) and the delay for control decisions to pass to actuators. We then combine the delay from each physical system and

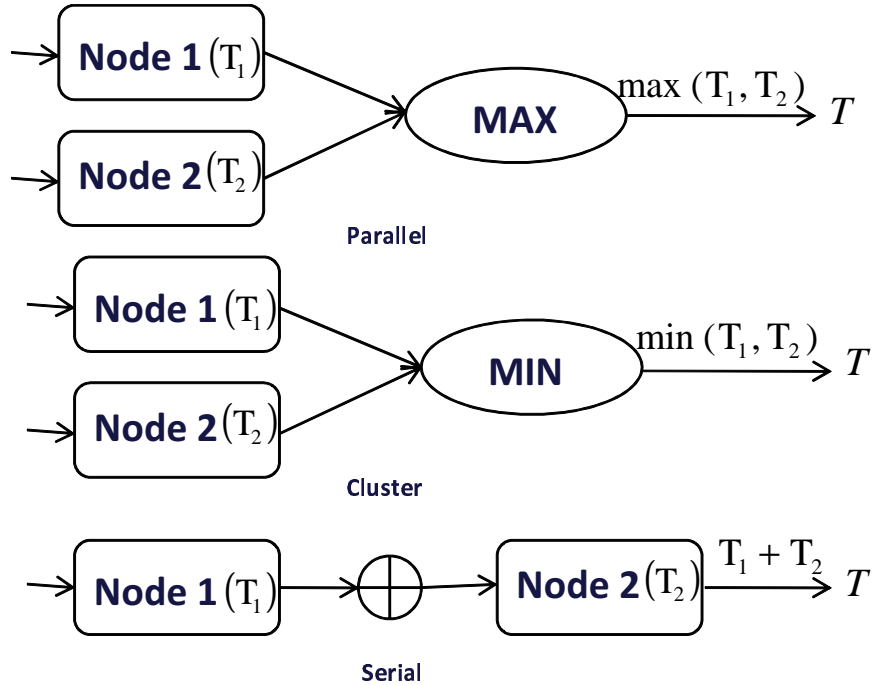


Figure 3.1: *General Framework for End-to-end Response Time*

computing device with appropriate stochastic models for suitably characterizing the end-to-end response time. In the next section, we discuss a general approach for end-to-end delay characterization in SSG reconfiguration.

3.3 General Framework for End-to-end Response Time Distribution

As indicated, the response time of the SSG reconfiguration is essentially the aggregate time taken by the power system, sensors, command and control, and communications systems in response to an initial event causing faults in the power system. The time to complete each involved subsystem functionality (delay) can be viewed as random variables having probability density functions. In Fig. 3.1, the response time analysis (RTA) framework is designed to compute the overall reaction time distribution of the system, i.e., the cumulative probability that a response can be formulated and initiated in a time period that is less than or equal to some arbitrary time. This is achieved by combining the densities assigned to

each event in accordance with the appropriate laws of probability. The subsystems are composed of a combination of serial, parallel, and cluster nodes. The traffic from each node is generated following a stochastic process and is assigned a probability distribution (or fixed-time delay). Three types of nodal configurations are possible. The serial or “chain” arrangement of nodes denotes that an event, occurring at each node, does not commence until the previous node is completed. The total time taken is therefore, the sum of the time taken by the nodes. The parallel arrangement of nodes implies that all events must occur at the nodes before a new is begun. So, the total time taken is the maximum of the time taken by any node in that arrangement. The cluster arrangement of nodes suggests that the occurrence of any one event in the node is sufficient for the flow in the network to continue. Therefore, the total time taken is the minimum time taken by any node in this arrangement. Each of the arrangements are illustrated with two nodes in Fig. 3.1. Let T_1 and T_2 be the random variables associated with time in completing the task for node 1 and node 2, and T is the aggregated time. Assuming independence of variables T_1 and T_2 , the cumulative distribution $F(t)$ and probability density functions $f(t)$ can be computed as in [78] for each arrangement. In general, with M nodes in the arrangement the distribution and density functions can be formulated as follows:

- Parallel:

$$F(t) = \prod_{i \in M} F_i(t) \text{ and } f(t) = \sum_{i \in M} f_i(t) \prod_{j \neq i \in M} F_j(t) \quad (3.1)$$

- Cluster:

$$F(t) = \sum_{i \in M} F_i(t) - \prod_{i \in M} F_i(t)$$

$$\text{and } f(t) = \sum_{i \in M} f_i(t) \prod_{j \neq i \in M} [1 - F_j(t)] \quad (3.2)$$

- Serial:

$$f(t) = f_i(t) * f_j(t) \quad \forall j \neq i \in M \quad (3.3)$$

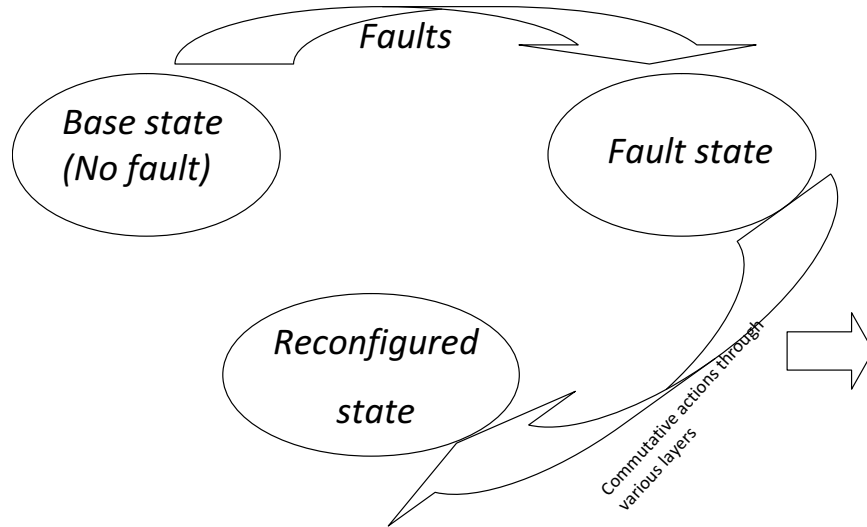


Figure 3.2: *Process Overview of Shipboard Power System Reconfiguration*

where $'*'$ denotes convolution operation. In this work, a centralized analysis framework is considered. The sensors collect data from the the underlying subnetwork after initiation of an event and send the information to a centralized fusion center for the resolution of the fault locations and reconfiguration status.

3.4 End-to-end response time for SSG reconfiguration

To find the end-to-end response time distribution, the individual distributions are combined in sequential, parallel, or clustered manner, corresponding to their sequence of operations. The framework in Section 3.3 is applied to characterize the response time. The end-to-end response time is computed for the power system to recover from a fault state to a normal (active) state, as shown in Fig. 3.2. The sequence of operations of the networks can be logically viewed as interactions among self-contained power system, sensor and communications network, and command and control network.

3.4.1 Delay distribution of power electronics network

The time required for restoration of service to the vital loads after the occurrence of faults is considered. A change of switch status (ON/OFF) is required to redirect power optimally to the vital loads. Therefore, the delay distribution is dependent on switch operations and hence discrete. *Lemma 1* has the main result.

Lemma 1. *The probability mass function (pmf) of the response time for servicing the vital loads after reconfiguration of the power network is given by:*

$$P_{pw}(x) = \sum_{j=0}^{N_{max}} c_{ij}(x)q_j(x) \quad (3.4)$$

where, $c_{ij}(x) = P(\text{VL in } i \text{ switching} | \text{system in } j \text{ switching})$ and $q_j(x) = P(\text{system in } j \text{ switching})$. c_{ij} occurs within every switch-pair change after the system is serviced. x is the delay variable.

Proof. The pmf of the response time for servicing the vital loads of the power network is given by:

$$P(\text{VL served in } i \text{ switching} \leq t) = \sum_{i \in \{0, \lfloor \frac{t}{iT_s} \rfloor\}} P_i, \quad (3.5)$$

where, P_i is $P(\text{VL served in } i \text{ switching})$. If N_{max} is the time required for the entire system to be reconfigured from the initial fault state, then P_i in (3.5) can be viewed as the marginal form of the following conditional and prior distributions;

$$\begin{aligned} P(\text{VL in } i \text{ switching} \leq t) &= \sum_{j=0}^{N_{max}} P(\text{VL in } i \text{ switching} \\ &\quad | \text{system in } j(\geq i) \text{ switching}) \\ &\quad \cdot P(\text{system in } j(\geq i) \text{ switching}). \end{aligned} \quad (3.6)$$

By introducing the delay variable x in (3.6), $P_{pw}(x)$ in (3.4) is obtained. Notice that, the marginal distribution of the service time for VL , i.e., $P_{pw}(x)$ will depend on the choice of the conditional model c_{ij} . \square

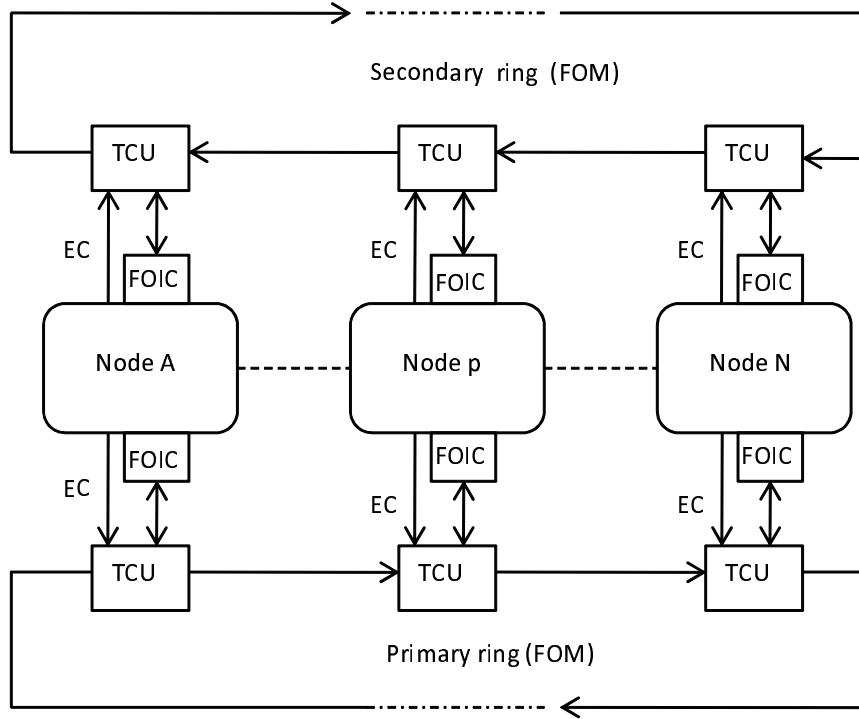


Figure 3.3: *Communication Network Infrastructure for Shipboard LAN*

3.4.2 Delay distribution of communications network

Communication network introduces delay due to shared medium access for information flow. The operation of the communication network carries the fault information between sensor network and the centralized resolution center. The navy shipboard system presently uses IEEE 802.5 Token ring standard (data rate 16 Mbps) for SAFENET I, and ANSI $x3T9.5$ token ring standard (data rate 100 Mbps) for SAFENET II [18], both based on FDDI dual ring topology, forming a ship-wide network backbone infrastructure. As shown in Fig. 3.3, the nodes act as sensors that collect variations in voltages and currents whenever a fault occurs and communicates the information to the central processor via the ring. The total delay T_n in successfully transmitting a packet is the sum of a number of random delays associated with queuing (T_w), access (T_a), transmission (T_s), and propagation (τ_p). Specifically, $T_n = T_w + T_s + T_a + \tau_p$. T_s is equal to the mean message length per line bandwidth. *Lemma 2* and *3* have the final results of delay distribution for Ethernet and FDDI token

ring backbone network respectively.

Lemma 2. *The density function for total delay (T_n) with for Ethernet (IEEE 802.3) as MAC protocol is given by:*

$$\begin{aligned}
f_{T_n}(x) &= \lambda(1 - \rho) \int_0^x e^{-\mu(1-\rho)(x-z)} \frac{P\{R=0\}}{T_s} \\
&+ \left[\frac{z}{aT} - \left\lfloor \frac{x}{aT} \right\rfloor \right] \sum_{r=1}^{r_2} \sum_{k=0}^r \frac{a_r(\lfloor \frac{z}{aT} \rfloor - \eta)}{w^r} \binom{r}{k} \\
&\cdot p_b^k p^{r-k} p_s \left[\frac{z}{aT} \right] \frac{1}{aT} + \sum_{r=1}^{r_2} \sum_{k=0}^r \frac{a_r(\lfloor \frac{z}{aT} \rfloor - \eta) - \eta}{w^r} \\
&\cdot \binom{r}{k} p_b^k p^{r-k} p_s \left[\frac{1}{aT} - \left\lfloor \frac{z}{aT} \right\rfloor \frac{1}{aT} \right]. \tag{3.7}
\end{aligned}$$

Here, $\rho = \frac{\lambda}{\mu}$ is the utilization of the single server system. λ is the arrival rate at the queue input. μ is the average number of message served/milliseconds. A slotted non-persistent CSMA protocol under Poisson point traffic with retransmission is typically used in Ethernet, with uniform backoff (UB) [75] of large range $w (> 20$ packets). $a = \frac{\tau_p}{T_s}$. The maximum round-trip delay is smaller than the packet transmission time, i.e., $2\tau_p \leq T_s$. R is the number of retransmissions allowed. $P\{R=r, K=k\} = \binom{r}{k} p_b^k p^{r-k} p_s$, $0 \leq k \leq r$; $r, r_2 \leq R$; p_b is the probability that the channel is sensed as busy; p_c is the probability that a collision occurs, and p_s is the success probability of accessing the channel. $p_s \geq 0.5$ is needed for finite average delay. Under UB, the distribution of X_r is simply $P\{X_r = kn\} = \frac{a_r(kn)}{w^r}$, $k = r, r+1, \dots, rw$.

Proof. The density function for T_w can be computed directly from $M/M/1$ queue analysis [50] as

$$f_{T_w}(x) = (1 - \rho)\delta(x) + \lambda(1 - \rho)e^{-\mu(1-\rho)x}, \quad x > 0. \tag{3.8}$$

The derivative of equation(22) in [75] gives the pdf of combined T_a, T_s, τ_p . Finally, linear convolution with (3.8) results in (3.7). \square

Lemma 3. *The density function of the backbone network delay T_{FDDI} with ANSI x3T9.5 token ring as MAC protocol is given by:*

$$f_{T_{FDDI}}(x) = \frac{uC_b p}{\lambda_b} \delta(x) + (1-p)uC_b \exp\{-uC_b x\} \quad (3.9)$$

where, λ_b is the message arrival rate at backbone, p is the probability that the backbone is busy, C_b is the bandwidth of FDDI link, and u is the mean transmission frequency of a packet through the FDDI link.

Proof. See Appendix I. □

3.4.3 Delay distribution of sensor network

Sensors are placed as nodes in the dual ring based communication network. The placements of the nodes/sensors determine the delay distribution of the network. For clarity, we only limit our discussions on the top ring, and assume that under communication network faults, a part or the entire bottom ring will become active. It is always assumed that the sensors act only as measuring devices; the data fusion occurs at the command and control center (CCC).

Architecture I: Centralized Network Control

In this case, all the sensor nodes are connected directly to a single ring. This architecture is feasible in small-sized ships where all the load centers are closely located. Fig. 3.4 shows this architecture. This effectively creates a parallel arrangement of sensor nodes as in Fig. 3.1. The aggregation time from all the active sensors to the CCC is obtained as $T_{SensorNet \rightarrow CCC} = \max_{i \in n_s} (T_{w_i} + T_{a_i})$, where, n_s is the number of active sensors in the sensor network. The corresponding distributions can therefore be easily obtained from (3.1) as $F_{SensorNet \rightarrow CCC}(x) = \prod_{i \in n_s} F_i(x)$, and $f_{SensorNet \rightarrow CCC}(x) = \sum_{i \in n_s} f_i(x) \prod_{j \neq i \in n_s} F_j(x)$. The response time for the communication and sensor network $T_{SensorNet}$ captures of the time taken for (1) all the sensor node data to reach CCC, (2) the decision containing the switching information from CCC to reach actuators and (3) change the switch status on the

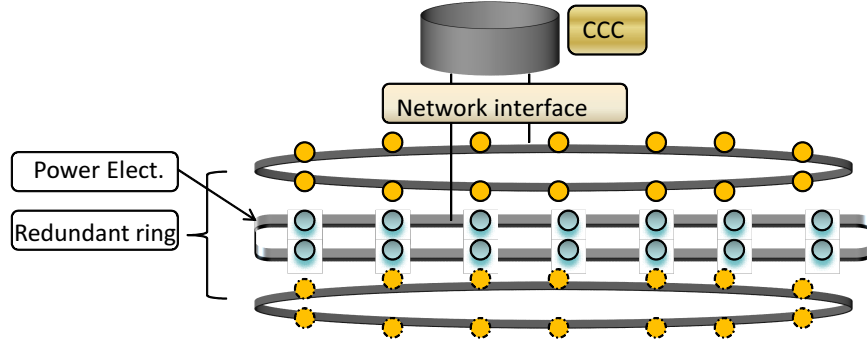


Figure 3.4: *Centralized Network Control for Shipboard LAN*

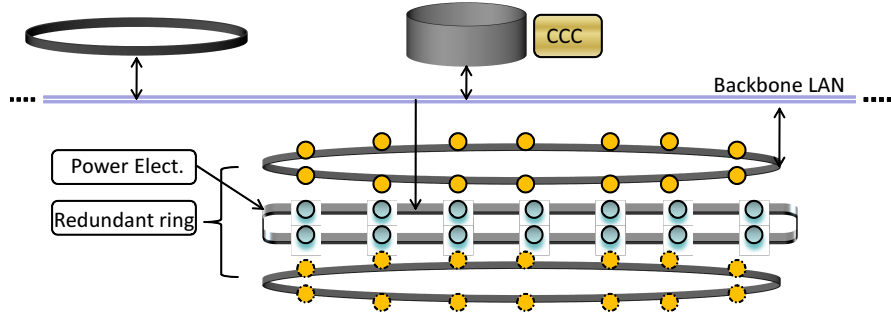


Figure 3.5: *Centralized Network Control with Backbone for Shipboard LAN*

power network. The last operation can be assumed to have a minimal constant time delay and is ignored. Also note that the first two operations have similar delays. Therefore, the sensor network response time $T_{SensorNet} = T_{SensorNet \rightarrow CCC} + T_{CCC \rightarrow SensorNet}$.

Architecture II: Centralized Network Control with Backbone

In this, the backbone ring network across the ship connects several networks as shown in Fig. 3.5. The CCC is also connected to the backbone network. This architecture is employed in larger shipboard systems where communication between several operational subsystems in the ship is necessary. For example, subsystems related to operations and management, navigation and weapon control etc., may all be connected to the same backbone network. Therefore, reconfiguring the power system using this architecture introduces additional queuing and channel access delay at the backbone router. Assuming Poisson arrival of traffic at the backbone router, the aggregated time to reach fusion center at the CCC can be for-

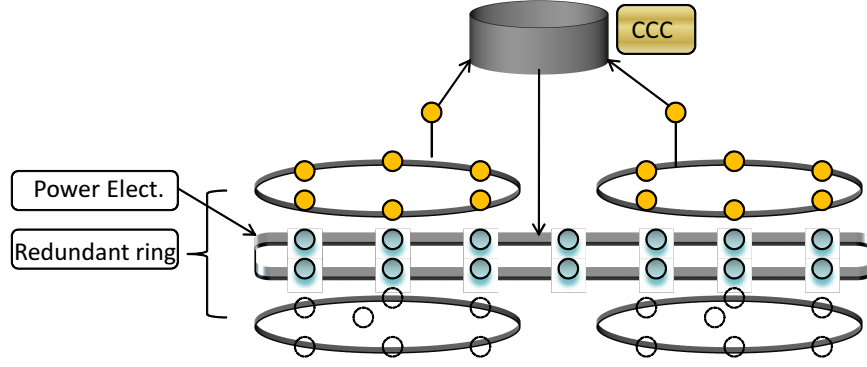


Figure 3.6: *Centralized-Cluster Network Control for Shipboard LAN*

mulated as $T_{SensorNet \rightarrow CCC}(x) = \max_{i \in n_s} \{(T_{w_i} + T_{a_i})_{SensorNet} + (T_{w_b} + T_{a_b})_{BackboneNet}\}$. The corresponding distributions $T_{SensorNet \rightarrow CCC}(x)$ of can be obtained as $F_{SensorNet \rightarrow CCC}(x) = \prod_{i \in n_s} F_{Sensor+Backbone_i}(x)$ and $f_{SensorNet \rightarrow CCC}(x) = \sum_{i \in n_s} f_{Sensor+Backbone_i}(x) \prod_{j \neq i \in n_s} F_{Sensor+Backbone_j}(x)$, where, $f_{Sensor+Backbone_i}$ can further be computed as $f_{Sensor+Backbone_i}(x) = (f_{w_i}(x) * f_{a_i}(x))_{SensorNet} * (f_{w_b}(x) * f_{a_b}(x))_{BackboneNet}$

Architecture III: Centralized-Cluster Network Control

In this case, sensors are placed as nodes in a subnet LAN system (also termed as a cluster). Sensors act only as measuring devices in the cluster. Fig. 3.6 shows such an architecture. The cluster heads acts as semi-agents that perform preprocessing and passing of data to the CCC. No lateral coordination between cluster heads is assumed. The aggregated time to reach the CCC using clusters of multiple sensor network is two fold; first, data aggregation are done in the cluster-heads from the underlying sensor nodes, and second, from cluster heads to the CCC; the return paths from the CCC incurs similar delays: $T_{ClusterNet \rightarrow CCC} = \min_{i \in n_s} (T_{cluster_{w_i}} + T_{cluster_{a_i}})$, where, $T_{cluster_{w_i}}$ and $T_{cluster_{a_i}}$ are queuing and access delays for cluster-heads, respectively. Each of the cluster-heads has an effective parallel arrangement of sensor nodes. So, this aggregation time $T_{SensorNet \rightarrow ClusterNet}$ is found similarly as $T_{SensorNet \rightarrow CCC}$. The total sensor network response time can therefore be computed in this case as $T_{SensorNet \rightarrow CCC} = T_{SensorNet \rightarrow ClusterNet} + T_{ClusterNet \rightarrow CCC}$, assuming a negligible preprocessing time at each cluster-head. Accordingly, the distribution

function is $f_{SensorNet \rightarrow CCC}(x) = \left[\sum_{i \in n_s} f_i(x) \prod_{j \neq i \in n_s} F_j(x) \right] * \left[\sum_{l \in n_{cs}} f_l(x) \prod_{j \neq l \in n_{cs}} F_l(x) \right]$, where, each sensor node delay density function $f_i(x)$ and each cluster-head delay density function $f_l(x)$ can straightforwardly be obtained from (3.1).

3.4.4 Delay distribution for fault diagnosis

In this case, the CCC resolves the location of the faults from either decision fusion (Centralized-Cluster) or data fusion (Centralized and Centralized with Backbone). In all such cases, it is reasonable to assume that the distribution of resolution time (T_c) is uniform between a minimum $T_{c_{min}}$, and a maximum $T_{c_{max}}$. Therefore, it can be simply denoted as $f_c(x) = \frac{x}{T_{c_{max}} - T_{c_{min}}}$, $T_{c_{min}} \leq x \leq T_{c_{max}}$. The final total delay is: $T = T_{pw} + T_{SensorNet \rightarrow CCC} + T_{CCC \rightarrow SensorNet} + T_c$. The corresponding total delay distribution is $f_T(x) = f_{T_{pw}}(x) * f_{SensorNet \leftrightarrow CCC}(x) * f_c(x)$. $f_{SensorNet \leftrightarrow CCC}$ is the total delay density distribution for collecting fault information from sensor network to CCC and decision information from CCC to the actuators. Other variations of this centralized architectures, can be modeled similarly based on the RTA framework. The QoS metric for the end-to-end response time is characterized by the cumulative distribution function as:

$$F_T(x) = P \left\{ f_T(x) < \frac{x_0}{T} \right\} = \int_0^{\frac{x_0}{T}} f_T(x) dx. \quad (3.10)$$

The scope and usability of the RTA framework for real-time SSG reconfiguration is described in the following statement:

Under the assumption of uniform fault occurrence, the RTA framework provides an upper (worst-case) bound on the integrated end-to-end response time for SSG reconfiguration QoS. An empirical validation of the statement is provided in Section 3.5.2.

3.5 Analysis and Validation of Proposed Framework

In this section, first, the analytical delay distribution of (1) power network, and (2) communication network under appropriate stochastic models are obtained. Second, OPNET

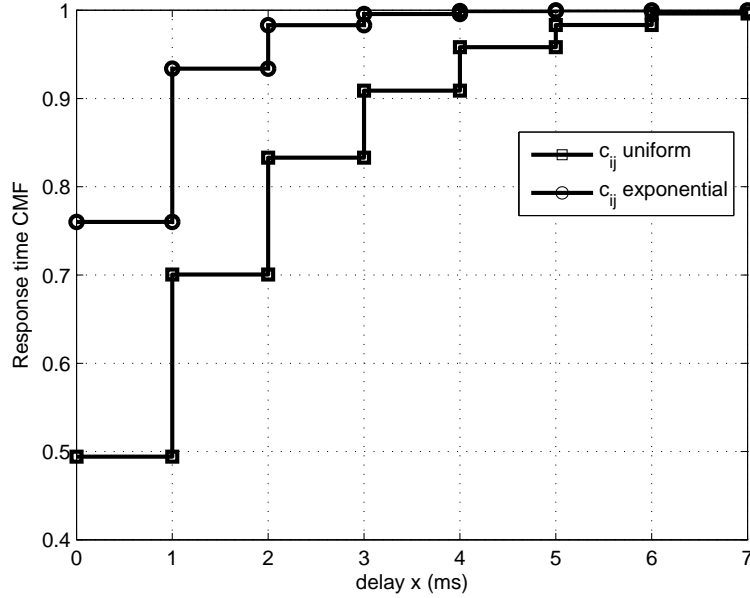


Figure 3.7: Response Time Distribution of Power Network with Uniform Fault Occurrence, and $c_{ij}(x)$ Uniform and Exponential

network modeler and MATLAB are used to simulate the end-to-end delay distribution for Architectures I-III to empirically validate *Proposition 1*.

3.5.1 Analysis Procedure for Proposed Framework

In this analysis, it is considered that the occurrence of faults in the power system is uniform, and that up to 5-fault cases occur with equal probability. Therefore, $q_j(x)$ is found by calculating the number of switch-pair changes from an initial no-fault stage for all possible fault occurrences. Typically, one switch-pair change at a time is assumed. Uniform and exponential model for the conditional distribution $c_{ij}(x)$ is considered. The response time distribution for power network reconfiguration is given in Fig. 3.7. As mentioned before, the conditional model for $c_{ij}(x)$ impacts the delay distribution for reconfiguration. The exponential model for $c_{ij}(x)$ produces lower delay than the uniform model.

Next, analytical results of the communication network delay distribution in (3.7) are provided. For CSMA/CD, network delay grows if packets are dropped due to collision re-

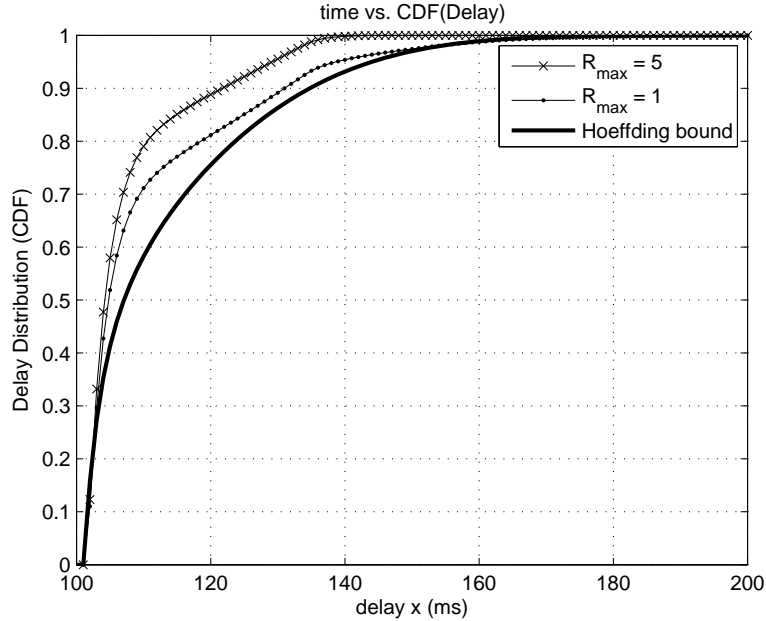


Figure 3.8: *Response Time Distribution of Communication Network with Slotted Non-persistent CSMA, $w = 32$, $p_s = 0.7$*

quiring retransmission. Fig. 3.8 shows the CDF of network delay as a function of maximum number of retransmission R . R is normally set to ensure a reasonable trade off between efficiency and reliability. Switched Ethernet provides negligible access delay for the channel [79]. So queuing delay determines the mostly delay in the communications network. An upper bound based on Hoeffding’s inequality [76] provides an estimate of the minimum delay possible in the network. The difference between the actual response time from its worst-case bound is the figure of merit for shipboard system designers.

3.5.2 Validation of RTA Framework

The simulation procedure shown in Fig. 3.9 to validate the RTA framework follows a test procedure in [80]. The virtual testbed (VTB) developed in MATLAB is used to simulate power systems, and command and control networks while OPNET (IT GURU ACADEMIC) is used to simulate the sensor and communication networks. The intermediate data exchange

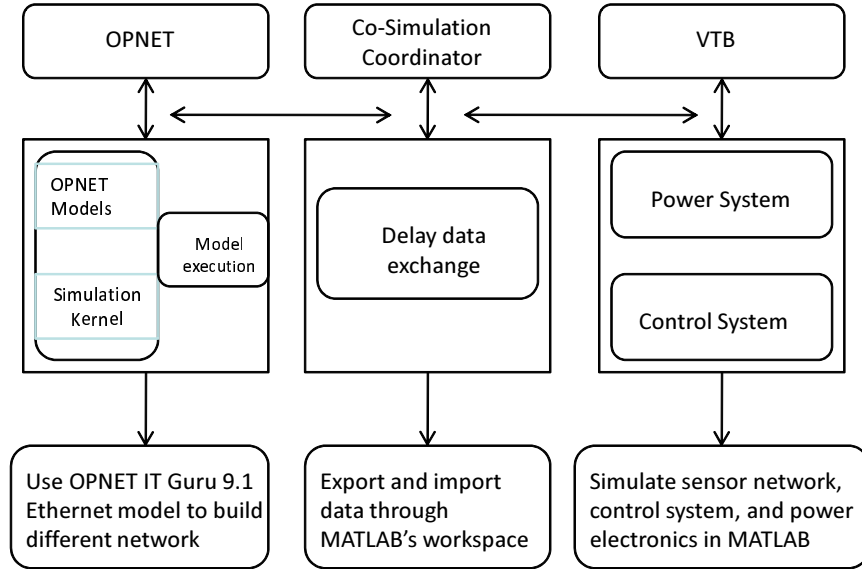


Figure 3.9: *Simulation process for validation of the proposed framework. The validation uses shipboard system reconfiguration as the VTB process*

between OPNET and MATLAB is done thorough MATLAB's workspace that acts as a co-simulation co-ordinator. The time elapse to import OPNET data files to the co-simulation co-ordinator interface is ignored. The delay in fault location resolution using standard sensor data fusion algorithms [81] is assumed to be distributed uniformly. The reconfiguration algorithm [63] is run in the VTB and finally all the delays are accumulated to obtain the end-to-end delay (response time). A total of 14 sensors are used in centralized, centralized backbone, and centralized-cluster fashion. In the centralized-cluster, 3 cluster heads each communicates with 5, 5, and 4 sensors, respectively. In the centralized backbone, two additional networks (not related to SSG reconfiguration) are connected to the CCC. In the simulations, each sensor node is denoted by an Ethernet workstation and an Ethernet server denotes the CCC. Each sensor node is connected to the ring network via an Ethernet switch; so, no collision of data in the primary shared medium occurs. Fig. 3.10 shows the sensor and communication network for Architecture-I. For simplicity, we show a single sensor node connected through a switch to the ring network. In practice, this can be a combination of multiple voltage, and current measuring sensor nodes. Fig. 3.11 shows the sensor and com-

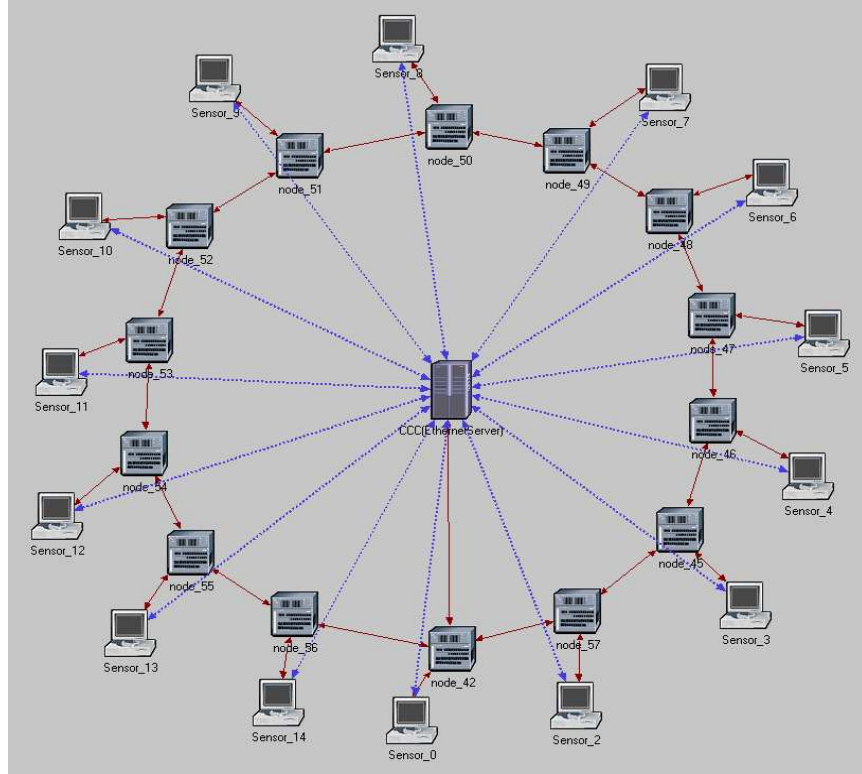


Figure 3.10: *OPNET model for Architecture-I with 14 sensor nodes connected by Ethernet 100-BASE-T Duplex links in a switched LAN topology*

munication network for Architecture-II. The Ethernet workstations are now connected via a shared backbone LAN to the central Ethernet server unit. Several closely located sensor nodes form subnetworks, each connecting to a ship-wide backbone network. Other Ethernet LANs or subnetworks are also connected to the backbone LAN network. Fig. 3.12 shows the sensor and communication network for Architecture-III. First, the maximum delay from each sensor node to the cluster head within a subnetwork $T_{SensorNet \rightarrow ClusterNet}$ is computed; then the minimum delay from the cluster heads to the CCC is added as $T_{ClusterNet \rightarrow CCC}$.

A comparative study of delay distributions for various centralized architectures (Architecture I-III) is now provided. Only the end-to-end delay distribution for reconfiguring the vital loads optimally under uniform $c_{ij}(x)$ assumption is presented. Similar analysis for various conditional probabilities of $c_{ij}(x)$ and $q_j(x)$, and for serving other category of loads (semi-vital, non-vital) or the entire power system can be straightforwardly obtained follow-

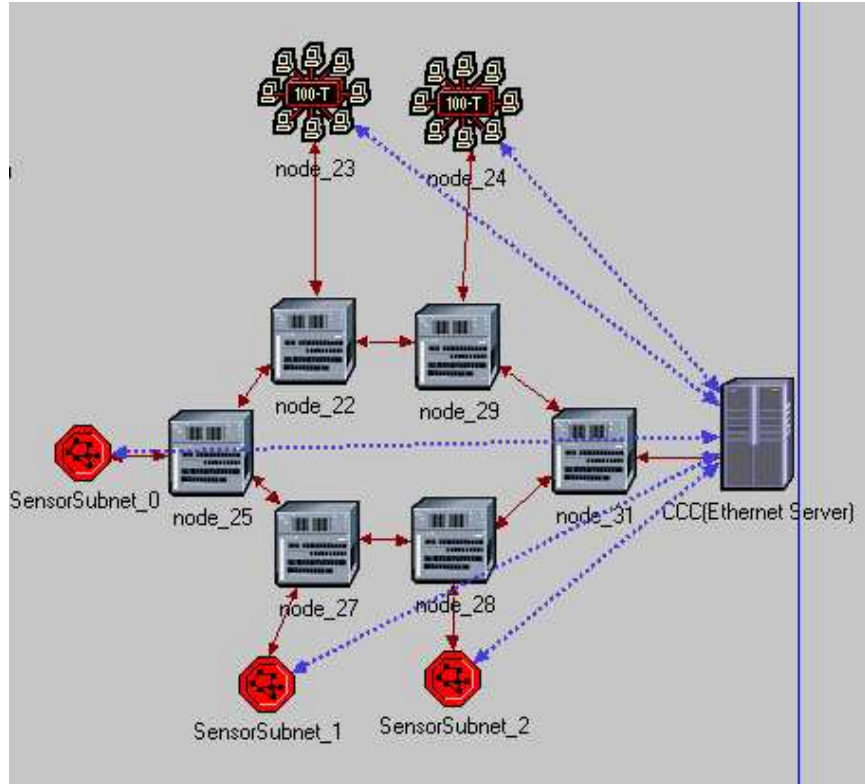


Figure 3.11: *OPNET model for Architecture-II with total 14 sensor nodes in 3 subnets connected by Ethernet 100-BASE-T Duplex Backbone in a switched LAN topology*

ing the RTA framework. Fig. 3.13 shows results of end-to-end delay distribution for architectures I-III for validating our framework. The centralized-cluster (Architecture-III) produces lower delay than other two (viz. probability of 0.94 with which service can be restored within 80 milliseconds). Architecture-II with backbone has the highest delay. The RTA framework tightly lower bound the actual system response time. This also confirms the statement in Section 3.4.4 regarding the scope and usability of the RTA framework. RTA framework suggests that, Architecture-III must be used for faster response time on SSG reconfiguration. Additionally, it provides redundancy in sensor subnetwork that helps in resolving fault locations. However, this also require more connections to the server than the backbone network. The navy shipboard uses FDDI dual ring topology for the network backbone architecture to compromise among delay, reliability. On the other hand, Ethernet provides low-cost solution for shared medium access, with slower response time. The end-to-

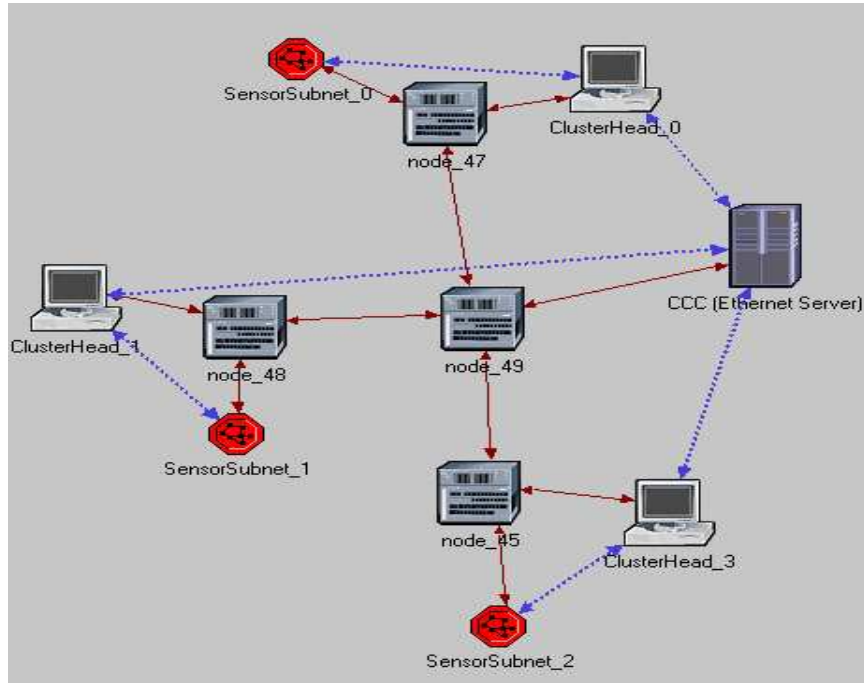


Figure 3.12: *OPNET model for Architecture-III with 14 sensor nodes in 3 subnets with 3 cluster heads connected by Ethernet 100-BASE-T Duplex links in a switched LAN topology*

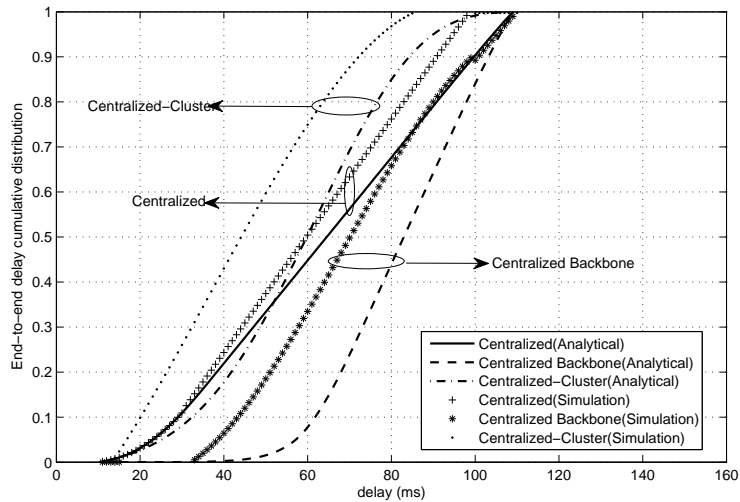


Figure 3.13: *Comparison of End-to-end Response Time Distribution for Different Architectures with Switched Ethernet, and 14 Sensors*

end response time employing backbone network topologies (Architecture-II) with Ethernet, FDDI and Gigabit Ethernet as the network backbone are now compared. The number of

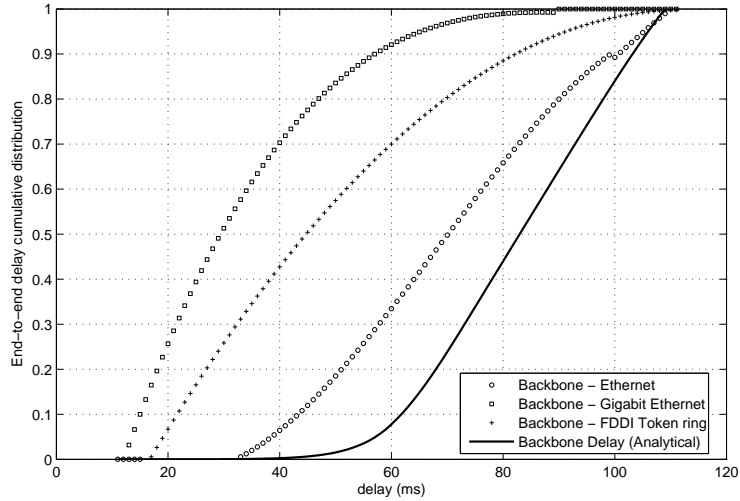


Figure 3.14: Comparison of End-to-end Response Time Distribution for Architecture-II With Ethernet, Gigabit Ethernet, and FDDI Token Ring Backbone

sensor nodes and traffic generation rate at each node remains the same. Fig. 3.14 shows that with Gigabit Ethernet as the network backbone, the response time is improved as compared to FDDI token ring based topology presently employed by shipboard systems. The response time with normal Ethernet with 100-Base-T duplex link provides the worst response time. However, Ethernet and Gigabit Ethernet allow integration of legacy network devices into the backbone topology in an easy and cost effective manner. Therefore, they can be considered in the future as alternative solutions for efficient backbone communications for electric ships.

3.6 Summary

In this Chapter, a framework for real-time end-to-end response-time analysis for centralized SSG reconfiguration is provided. Specifically, reconfiguration time for optimal power delivery to vital loads after the occurrence of faults are considered. The RTA framework is validated by simulation for various centralized topologies. The analysis provides a tight upper (worst-case) bound on the integrated end-to-end delay, considering the heterogeneity

in various physical/cyber subsystems. Based on the RTA framework, various design choices capturing the trade off between delay, number of connection, reliability, and technology can be made. The QoS service guarantee of the end to end system response time for SSG reconfiguration can address various system design issues for future shipboard system.

In the next two chapters we investigate decentralized reconfiguration of SSG. We decompose the SSG reconfiguration problem into smaller separable subproblems and study the convergence of the proposed reconfiguration solution under perfect and imperfect network conditions.

Chapter 4

Decentralized Reconfiguration of Shipboard SmartGrid

In this chapter, we seek to investigate the quality of the SSG reconfiguration solution without complete knowledge of the overall system state. This can be achieved via a number of decentralized methods. We propose and analyze a dual decomposition based decentralized optimization method for shipboard smartgrid system. This chapter is organized as follows:

4.1 Introduction

Shipboard smartgrid (SSG) has unique characteristics when compared with terrestrial systems due to their small size, tight coupling between components, load sensitivity to power interruptions and power quality. Several control strategies relative to the ones emphasized in terrestrial smart grids are required for maintaining power quality and survivability of the SSG as we have already discussed in the previous chapters.

In particular, we discussed several centralized methods of SSG reconfiguration that find a globally near-optimal switch status (ON/OFF) to reroute power to loads after the occurrence of one or more faults. Several optimal and near-optimal centralized methodologies related to SSG reconfiguration have been proposed in [44] and in our earlier work [57], respectively. In this chapter, we focus on decentralized reconfiguration of SSG. To this end, one of the key questions of interest in this chapter is the following: *Is it possible to*

quickly restore faults locally and further reach a system-wide power restoration without complete knowledge of the system state? An obvious strategy to address this question is to consider decentralized system optimization. Decentralized approaches are generally more robust than centralized optimization due to the absence of single point failure problem. In SSG, distributed optimization can be very useful in quickly restoring local damages during fight through and battle situations, and therefore has received considerable attention over the past few years.

In SSG, distributed optimization is typically proposed in a multi-agent environment, in which, power is locally distributed to the loads after the occurrence of faults to recover temporarily from an interruption in service. Various related approaches have already been discussed in Chapter 1. In general, the approaches do not scale well with the size of the smartgrid. Further, none of the prior related approaches provide any certificate of the quality of the proposed solutions.

In this chapter, we employ dual decomposition based distributed optimization of SSG reconfiguration. This not only provides a quick local reconfiguration of the SSG, but also indicates how suboptimal the solution is relative to optimal centralized SSG reconfiguration, with or without taking into account communication delay and quantization noise effects. Specific contributions of this work include:

- Using dual decomposition [82], we conveniently decompose the SSG model into several agent subsystems, optimize each subsystems locally, and interact with other neighbor agent subsystems via coupling constraints to reach a global state of system-wide load restoration. A dual decomposition framework in [60] to solve SSG reconfiguration problem using low-complexity gradient algorithm is used.
- By solving the dual of the SSG reconfiguration problem, we provide a strong theoretical basis for the quality of the distributed reconfiguration of SSG relative to the centralized global optimum reconfiguration.

4.2 Dual Decomposition Based Shipboard Smartgrid Reconfiguration

Traditionally, SSG reconfiguration formulation is presented as mixed-integer non-convex optimization problem [44] and stated below for clarity of presentation:

Primal Objective function:

$$Max. \sum_{I \in L} W_{VL} S_{VL} + W_{SVL} S_{SVL} + W_{NVL} S_{NVL} \quad (4.1)$$

C_1 . AC Equality constraints

$$PG_{i_b} - PD_{i_b} = \sum_{j_b} V_{i_b} V_{j_b} Y_{i_b j_b} Re \{ \angle(\theta_{i_b j_b} + \delta_{j_b} - \delta_{i_b}) \},$$

$$QG_{i_b} - QD_{i_b} = \sum_{j_b} V_{i_b} V_{j_b} Y_{i_b j_b} Im \{ \angle(\theta_{i_b j_b} + \delta_{j_b} - \delta_{i_b}) \}$$

C_2 . AC Inequality constraints

$$PG_{i_b}^{min} \leq PG_{i_b} \leq PG_{i_b}^{max}, QG_{i_b}^{min} \leq QG_{i_b} \leq QG_{i_b}^{max}, I_{i_b j_b} \leq I_{i_b j_b}^{max}, V_{i_b}^{min} \leq V_{i_b} \leq V_{i_b}^{max},$$

$$\delta_{i_b}^{min} \leq \delta_{i_b} \leq \delta_{i_b}^{max}$$

C_3 . DC Equality constraints

$$\sum_{i_b} I_{in_{i_b}} = \sum_i I_{out_{i_b}} + IL_{i_b} \quad i_b \in FB, j_b \in TB, V_{i_b} = V_{j_b} + I_{i_b j_b} \times Z_{i_b j_b}$$

C_4 . DC Inequality constraints

$$PL_{i_b} \leq PL_{i_b}^{max} \times SW_{i_b} \text{ (for variable load)}, PL_{i_b} = B_{i_b} \times PL_{i_b}^{max} \text{ (for fixed load)}, I_{i_b j_b} \leq I_{i_b j_b}^{max},$$

$$\text{and } V_{i_b}^{min} \leq V_{i_b} \leq V_{i_b}^{max}$$

C_5 . Switching constraints

$$SW_{i_b} + SW_{j_b} = 1 \text{ where } SW \in (0, 1)$$

The weights w 's are assigned to reflect load priorities as $w_{VL} > w_{SVL} > w_{NVL}$ where NVL , VL and SVL are non-vital, vital and semi-vital loads, respectively. PD and QD are the active and reactive power demanded; V_{i_b} is the voltage at bus i_b ; δ_{i_b} is the angle associated with the voltage at bus i_b ; $Y_{i_b j_b}$ is the magnitude of the complex admittance from bus i_b to j_b ; $\theta_{i_b j_b}$ is the angle of the admittance from bus i_b to j_b ; PL_{i_b} is the power delivered to loads connected at bus i_b ; B_{i_b} is a binary variable that connects a fixed load to PB or SB and can be predetermined. IL_{i_b} is the load current at bus i_b ; $I_{i_b j_b}$ is the current flow

from bus i_b to bus j_b ; $I_{in_{i_b}}$ and $I_{out_{i_b}}$ are the currents entering and leaving bus i_b ; FB is the set of “from (source)” buses; TB is the set of “To (destination)” buses; $Z_{i_b j_b}$ is the branch impedance of branch i_b and j_b . $(\cdot)^{max}$ and $(\cdot)^{min}$ are used to indicate the maximum and minimum value of each variable, respectively. The mutual exclusivity constraints on the switch variables SW ensure that the power delivered to the higher priority loads is from either port side or starboard side (maintains the radial structure of the SSG).

The solution for this optimization problem determines the switch configuration that maximizes the power delivered to loads. In order to implement distributed optimization, we use the relaxed integer form obtained by allowing switch variable SW to take any value between 0 and 1. Furthermore, linearizing the AC equality constraints results in a relaxed-integer convex form. In chapter 2, we quantified the impact of integer relaxation and convex approximation of the original reconfiguration problem. We demonstrated that the relaxed-integer convex form provides a way to achieve near optimal reconfiguration. As a result, in this chapter, we confine ourselves to only the relaxed-integer convex form for the distributed optimization of SSG.

In our multi-agent framework, the SSG is first decomposed into K subsystems, each managed by local agents. We assume that the local agents have estimates of load power demand and switch status within their subsystem. Fig. 4.1 shows the subsystems partition with $K = 6$, and Fig. 4.2 shows an equivalent representation of the decomposed models with private and public variables. Agents are arranged using overlapping ring based structure with each subsystems sharing information with at least one neighbor agent subsystem via public variables acting as coupling constraints. We let $\mathbf{x}_k \in \mathbf{R}^{n_k}$ and $\mathbf{y}_k \in \mathbf{R}^{p_k}$ denote private and public variables, respectively, for subsystem k . Here, n_k and p_k are number of private and public variables, respectively. Each subsystem has a local objective function to

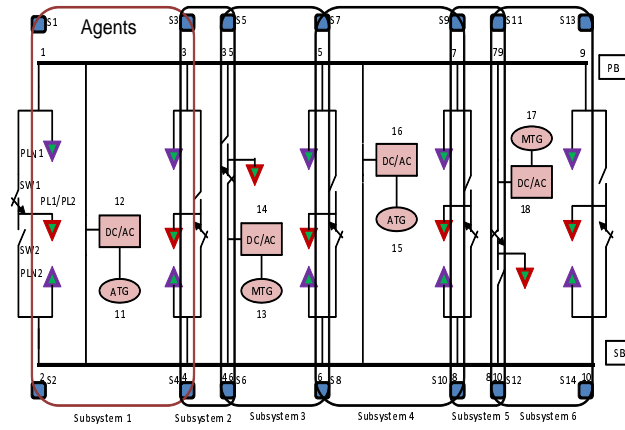


Figure 4.1: *Subsystem formation for dual decomposition. Agents are represented by S_1, S_2, \dots, S_{15}*

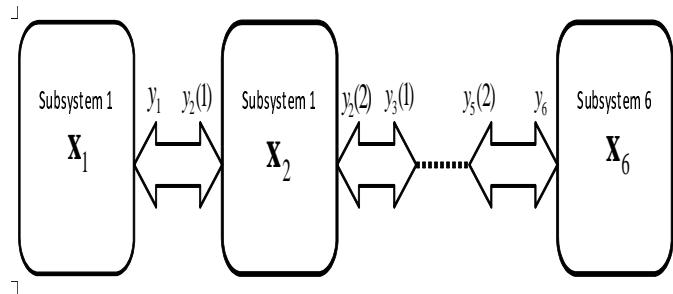


Figure 4.2: *Equivalent model for decomposed subsystems with private variable \mathbf{x}_k and public variables \mathbf{y}_k for all $k \in K$*

optimize that is defined as:

$$\begin{aligned}
l_k(\mathbf{x}_k, \mathbf{y}_k) = & \min_{s \in \mathbf{x}_k} - \sum_{I \in L_k} W_{VL} S_{VL_k} \\
& + W_{SVL} S_{SVL_k} + W_{NVL} S_{NVL_k} \\
s.t. (\mathbf{x}_k, \mathbf{y}_k) \in & C_{rk} \quad r = \{1, \dots, 5\} \quad k = \{1, \dots, K\}
\end{aligned} \tag{4.2}$$

where, l_k is the set of all loads, and C_{rk} is the r -th constraint set for k -th subsystem, obtained from the original constraint set $C1$ - $C5$ in (4.1). With reference to the subsystem partitions presented in Fig. 4.2 we take all the public variables into a single vector $\mathbf{y} = [\mathbf{y}_1, \dots, \mathbf{y}_K]'$ of length p , and $p = \sum_{k=1}^K p_k$. $(\cdot)'$ denotes transposition operation. Each public vector \mathbf{y}_k can be represented by $\left[\sum I_{in_{i_b}}^k, \sum I_{in_{j_b}}^k, v_{i_b}^{dc^k}, v_{j_b}^{dc^k}, \sum I_{out_{i_b}}^k, \sum I_{out_{j_b}}^k \right]'$. $(\cdot)^k$ refers to the voltage and current variables within the k -th subsystem. All other variables in the primal SSG reconfiguration problem are similarly grouped as private vector \mathbf{x}_k for the k -th subsystem. We have $N = \max(p_1, \dots, p_k)$ consistency constraints. They have a common value between each net of any interacting subsystems. The common values of each consistency constraints are contained in a length- N vector \mathbf{z} . We express the constraints as $\mathbf{y} = \mathbf{Ez}$ where, a connection mapping matrix $\mathbf{E} \in \mathbf{R}^{p \times N}$ is

$$\mathbf{E}_{mn} = \begin{cases} 1 & \text{if } y_m \in y(n) \\ 0 & \text{otherwise.} \end{cases} \tag{4.3}$$

Rows in \mathbf{E} specify sets of consistency constraints for the given subsystem interaction. We can partition \mathbf{E} into blocks associated with different subsystems, denoted by $\mathbf{E}_k \in \mathbf{R}^{p_k \times N}$. In that case, each component vector of \mathbf{y} can be mapped to \mathbf{z} as $\mathbf{y}_k = \mathbf{E}_k \mathbf{z}$. Therefore, the global optimization problem in (4.1) can be related to the local optimization for each subsystem k as

$$\begin{aligned}
min. & \sum_{k=1}^K l_k(\mathbf{x}_k, \mathbf{y}_k) \\
s.t. & (\mathbf{x}_k, \mathbf{y}_k) \in C_{rk} \\
& \mathbf{y}_k = \mathbf{E}_k \mathbf{z}.
\end{aligned} \tag{4.4}$$

To implement a decentralized solution of the optimization problem in (4.1), we use dual decomposition method to solve (4.4). The partial Lagrangian is formed by using Lagrange multipliers for the coupling constraint as

$$L(\mathbf{x}, \mathbf{y}, \mathbf{z}, \lambda) = \sum_{k=1}^K (l_k(\mathbf{x}_k, \mathbf{y}_k) - \lambda'_k \mathbf{y}_k) + \lambda' \mathbf{E} \mathbf{z}. \quad (4.5)$$

Here $\lambda \in \mathbf{R}^p$ is the Lagrange multiplier associated with $\mathbf{y} = \mathbf{E} \mathbf{z}$, and λ_k is the sub vector of λ for k -the subsystem. The dual function $q(\lambda)$ is obtained by maximizing over \mathbf{z} . This results in the condition $\mathbf{E}' \lambda = 0$. for $q(\lambda) \leq \infty$. Let $q_k^*(\lambda_k)$ denote the optimal value of each of the subproblem $l_k(\mathbf{x}_k, \mathbf{y}_k) - \lambda'_k \mathbf{y}_k$ subject to local constraint C_{ik} . Then the dual of the original problem (4.4) can be written in terms of the dual variable λ as

$$\begin{aligned} \max. \quad q(\lambda) &= \sum_{k=1}^K q_k^*(\lambda_k) \\ \text{s.t.} \quad \mathbf{E}' \lambda &= 0. \end{aligned} \quad (4.6)$$

Since the problem (4.6) is differentiable, it is solved by standard gradient method similar to one illustrated in [60]. Here, $\|\mathbf{y} - \mathbf{E} \mathbf{z}\|$ is called the consistency constraint residual. It vanishes when the local copies of public variables for each interacting subsystem becomes equal, i.e., global state of reconfiguration is achieved. We subsequently round off the final switch states to 0 or 1 and run the power flow to obtain the power delivered to the all loads of the K subsystems.

As suggested by (4.6), the original reconfiguration solution can be achieved by solving K subproblems in parallel, and exchanging information of the public variables over a communication network. In this chapter, we consider a perfect communication network to evaluate the convergence of the proposed gradient algorithm based SSG reconfiguration. A summary of the proposed decentralized solution of SSG reconfiguration is given in Alg. 1.

In the next section, we provide simulation results of the proposed decentralized SSG reconfiguration under the assumption that no packet loss or delay in information exchange occur over the network.

Alg. 1 Gradient Method for Decentralized SSG Reconfiguration

Input: Dual decomposition problem (4.6)**Output:** $\hat{\mathbf{x}}$

```
1   begin
2       Initialize  $\lambda = 0$ 
3       Optimize  $q_k(\lambda)$  for  $k = 1, \dots, K$ -subsystems
4       Obtain solution for subproblem (4.6) as  $\mathbf{x}_{opt}, \mathbf{y}_{opt}$ 
5       Compute average of public variables over each communication link
6        $\hat{\mathbf{z}} := (E' E)^{-1} E' \mathbf{y}$ 
7       Update the dual variables
       $\lambda := \lambda - \alpha(-\mathbf{y}' + \mathbf{E}\hat{\mathbf{z}})$ .
8       if ( $\|\mathbf{y}^{opt}(t) - \mathbf{E}\hat{\mathbf{z}}(t)\| \leq \eta$ )
9           Break;
10      end if
11  end
```

4.3 Simulation Results

We now provide simulation results of the optimal reconfiguration problem of the shipboard smartgrid system using dual decomposition method under perfect network condition; i.e., no routing delay, quantization noise and packet loss is considered. We use the same simulation parameters for each subsystem from our work in chapter 2. We provide the reconfiguration results of SSG under multiple faults. We assume that (1) all loads are operating at maximum rated power condition before fault occurrence, and (2) all faults occurring at random locations in the smartgrid are identified and isolated before the optimization algorithm is executed. Fig. 6.1 shows a scenario with 4 faults occurring between bus numbers 3 – 35, 35 – 5, 2 – 4, and 6 – 8 on the smartgrid. We show global optimization results only and compare the distributed dual decomposition reconfiguration results with existing centralized optimizations methods [57]. Switch states after reconfiguration are pointed by arrow marks. These switch states mark the absolute global optimization result obtained by using branch and bound based exhaustive search for original centralized mixed-integer non-linear

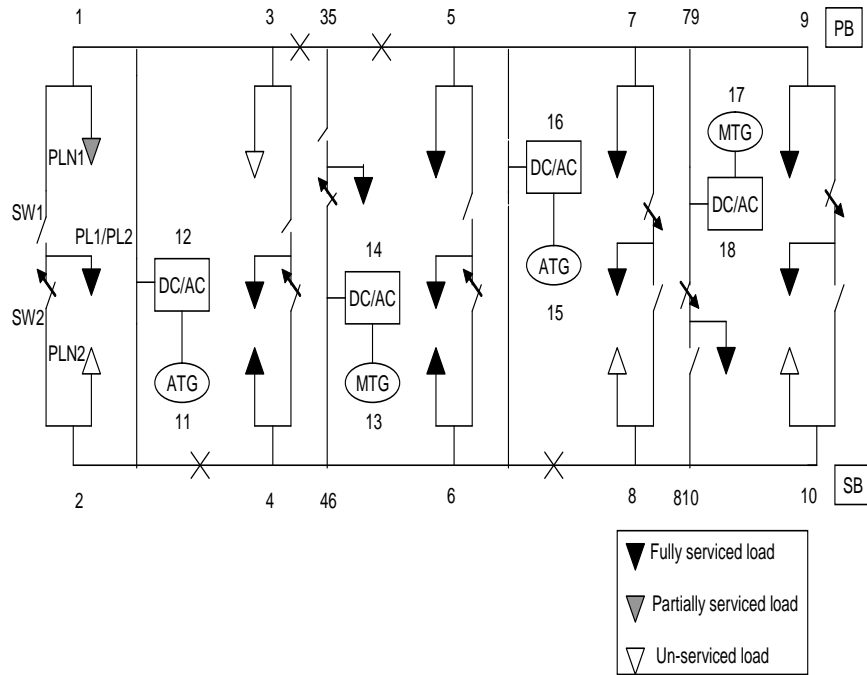


Figure 4.3: Shipboard microgrid with 4 simultaneous faults

Table 4.1: Shipboard smartgrid reconfiguration with 4 faults

Load positions	Vital (MW)	Semi-vital (MW)	Non-vital (MW)	SW positions (closed)	Solver
Load 1/2	0.5000	1.0000	0.4786	SW2	Global Non-convex with mixed integer (LINGO)
Load 3/4	0.5000	1.0000	0.5000	SW4	
Load 35	0.5000			SW46	
Load 5/6	0.5000	1.0000	1.0000	SW6	
Load 7/8	0.5000	1.0000	0.5000	SW7	
Load 810	0.5000			SW79	
Load 9/10	0.5000	1.0000	0.5000	SW9	
Load 1/2	0.5000	1.0000	0.4621	SW2	Distributed Dual Decomposition with integer relaxation (MATLAB)
Load 3/4	0.5000	1.0000	0.5000	SW4	
Load 35	0.5000			SW46	
Load 5/6	0.5000	1.0000	1.0000	SW6	
Load 7/8	0.5000	1.0000	0.5000	SW7	
Load 810	0.5000			SW79	
Load 9/10	0.5000	1.0000	0.5000	SW9	

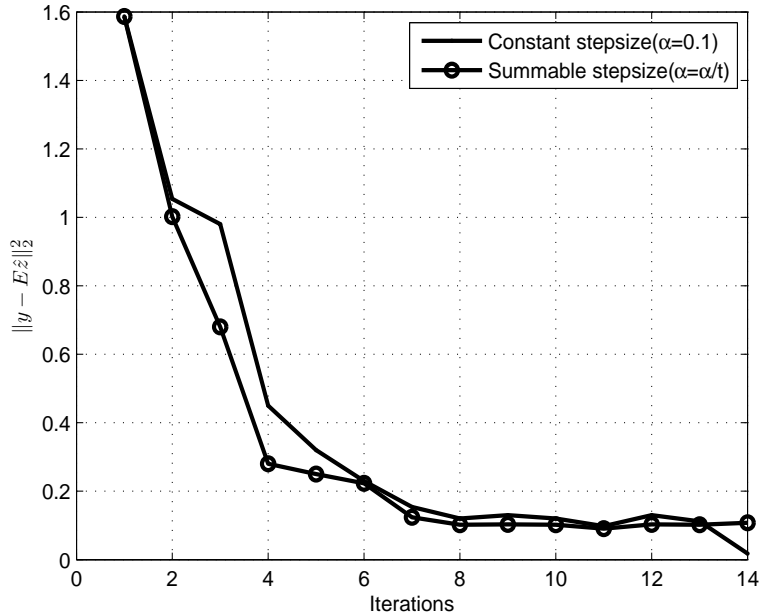


Figure 4.4: *Shipboard microgrid reconfiguration with 4 simultaneous faults*

(MINLP) problem. Distributed dual decomposition produces the same switch state (when rounded off) with global optimum solution and therefore, power delivered to the loads is same the centralized global optimal solution. This is possible as the non convexity of the original problem is in fact, limited to a few non-linear equality constraints in the AC power flow section of the generator while the majority of the formulation is convex.

We now consider the convergence of the distributed gradient method to reconfigure the smartgrid under perfect network condition (no delay). Fig. 5.1 shows that, with constant step size between iterations, the dual decomposition reaches the desired accuracy η within 8 iterations. With diminishing summable step size of α_t/t the algorithm stabilizes with a smoother slope around the optimal point.

Finally, we compare the scalability of our proposed distributed optimization of SSG with consensus based load restoration approach in [59]. In the consensus based approach, the information is exchanged with total number of agents N_a in the system. Contrary to that, in dual decomposition approach only requires N_G neighboring agents to communicate with

each other. As the network size increases, we expect N_G to remain much smaller than N_a for most topologies and therefore, our proposed approach will scale much better with the size of SSG than consensus based load restoration approach in [59]. Additionally, the total number of bits required to exchange per iteration for dual decomposition approach is $n_b N_G \sum_{k=1}^K p_k$, where n_b denotes the number of bits used to send one packet of information. This is much less than sending the entire information matrix of size $n_b N_a (3N_a)$ to all N_a agents for the consensus based approach.

4.4 Summary

In this chapter, we formulate and analyze a distributed method for optimized reconfiguration of shipboard smartgrid. Specifically we decompose the SSG into multiple smaller subsystems that are coupled to each other by convex coupling constraints. We show that by applying dual decomposition method the optimal reconfiguration in terms of the power delivery to loads in the smartgrid under multiple faults can be efficiently achieved. Simulation results indicate close accuracy compared to with original centralized non-convex formulation for the same problem. With perfect network, the distributed dual decomposition achieves the optimality of the switch states within a few iterations.

In the next chapter, we aim to obtain the feasibility of convergence of the time varying gradient method with finite-length buffer at each agent and communication failure (packet loss).

Chapter 5

Decentralized Reconfiguration Under Imperfect Communications

In this chapter, we investigate the impact of communication network on the quality (optimality) of the decentralized reconfiguration solution presented in the Chapter 4.

5.1 Introduction

As we have discussed in the previous chapters so far, predominantly, the challenges related to fault diagnosis and reconfiguration of shipboard smart grid to ensure survivability and flight through are time critical. Therefore, the timeliness and accuracy with which the optimal service restoration is performed is absolutely essential. In this chapter, we seek answers to the following set of fundamental questions related to decentralized SSG reconfiguration discussed in Chapter 4:

(1): *How is the convergence rate of distributed SSG reconfiguration affected by communication network delay, quantization noise, and loss of packets?*

(2): *What are the essential benefits / drawbacks of decentralized SSG reconfiguration when compared with centralized approaches [44],[57], in terms of delay and optimality?*

In chapter 4, we propose dual decomposition based decentralized optimization of SSG reconfiguration, in which, the shipboard system is decomposed into multiple separable subsystems with agents. Specifically, each agent solves a local concave dual function of the original objec-

tive while neighboring agents exchange information over a communication network and fuse the local optimizations into a global solution. The convergence of the proposed approach under varying network delays and quantization noise is therefore an important aspect to model and analyze. The key contributions of this chapter are summarized below:

- A novel time-varying gradient algorithm that includes the impact of practical communication links such as queuing delay, packet loss, and quantization noise is provided and analyzed in the context of dual decomposition based SSG reconfiguration problem.
- A theoretical lower bound on the convergence of the time-varying gradient algorithm under imperfect network conditions is derived, assuming that the time delay in the network is bounded (no packet loss).
- A new measure called outage convergence rate is introduced. This measure corresponds to the probability that the actual total delay exceeds the expected total delay when there is packet loss in the network.
- A comparison of total delay is presented for centralized and distributed approaches to analyze the effectiveness of the proposed optimization strategy.

5.2 Impact of Communication Network

The gradient algorithm presented in [60] and used here considers a perfect network and therefore achieves the optimum value of q^* . However, exchanges of \mathbf{y} are susceptible to communications delay, packet loss, and noise that prevent the algorithm from converging to q^{opt} .

5.2.1 Convergence Rate With No Packet Loss:

We consider (1) delays encountered by sensor nodes due to routing, and (2) noise due to quantization of the real gradient values. First, note that the exchange of public variables between neighboring agents encounter varying time delays. That is, each public variable

sent from agent i to agent j at time \hat{t} may arrive at time $\hat{t} + \delta_{ij}(\hat{t})$, where $\delta_{ij}(\hat{t})$ is the time-varying delay in sending a packet from agent i to j . We assume that the public variables transmitted by agent i may not reach agent j in the same order and that the roundtrip delay $c_{ij}(\hat{t}) = \delta_{ij}(\hat{t}) + \delta_{ji}(\hat{t}) \leq D$, where D is the delay bound. The delay bound implies that there is no packet loss in the network, and all updates complete their roundtrip delays within D . We further assume that the gradient value is bounded to G , implying no abrupt change in the network condition. All the above assumptions are reasonable since a small-size SSG network is not heavily loaded with traffic. Additionally, we assume that the quantization noise is bounded by E . Assuming Gaussian distribution, E is obtained from the known capacity R_c of the information bearing channel, i.e., $R_c(E) = 0.5 \log_2(S/E)$, where S is the signal power [83]. The distributed time-varying algorithm is presented in a concise manner in Alg. 2. Here, agent j computes the gradient update $g(\hat{t})$ for the l^{th} component of \mathbf{y}_k as $g(\hat{t}) = \alpha(y_i^l(\hat{t}) - z_j^l(\hat{t}))$ and sends it to agent i which performs dual update as in line 11 of Alg. 2. We redefine the projection vector in [84] to $P_{t-c_{ij}(\hat{t})}(\cdot)$ that has a time-varying component. This implies that $P_{t-c_{ij}(\hat{t})}(\cdot)$ only selects gradient updates that completes their round trip at time step t , and therefore are sent $\hat{t} = t - c_{ij}(\hat{t})$ time step ago. The time varying dual variable update for the entire state vector $\lambda(t)$ at time step $t + 1$ can now be adequately expressed as

$$\lambda(t + 1) = \lambda(t) + \alpha \sum_{c_{ij}(\hat{t})=0}^D P_{t-c_{ij}(\hat{t})}(\mathbf{g}_q(t - c_{ij}(\hat{t}))) \quad (5.1)$$

where, $\mathbf{g}_q(t - c_{ij}(\hat{t})) \in \mathbf{R}^{pk}$ is the quantized vector gradient update suitable for sending over the network, and α is a constant step size. We now state the lower bound on the convergence rate of Alg. 2 in the following theorem.

Theorem 1. *Let T denote the number of iterations. Assuming the existence of the minimizer q^{opt} , bounded time-delay D , and bounded error due to quantization E , the maximum*

Alg. 2 Time-varying Gradient Method

Input: Dual decomposition problem (4.6)

Output: $\hat{\mathbf{x}}$

```

1   begin
2       Initialize  $\lambda = 0$ 
3       repeat for each agent  $i \in N_G$ (neighboring agent set)
4           Optimize  $q_i(\lambda(t))$ 
5           Obtain solution for subproblem (4.6) as  $\mathbf{x}_i, \mathbf{y}_i$ 
6           Transmit each component of public variable  $y_i^l(t)$  to neighboring agent  $j$ ,
7           where  $l = 1, \dots, p_k$ 
8               repeat for each received  $y_j^l(\hat{t})$ 
9                   Compute average of public variables over subsystem links:
10                       $\hat{z}_{ij}^l(\hat{t}) := (y_j^l(\hat{t}) + y_i^l(\hat{t}))/2$ 
11                      Compute and quantize gradient update  $g_q(\hat{t}) = \alpha(\hat{t})(y_j^l(\hat{t}) - \hat{z}_{ij}^l(\hat{t}))$ 
12                      Transmit the quantized update  $g_q(\hat{t})$  to agent  $j$ 
13          Compute dual variables from gradient updates:
14           $\lambda_{ij}(t+1) := \lambda_{ij}(t) + \begin{cases} g_q(\hat{t}) & \text{if } \hat{t} + c_{ij}(\hat{t}) = t, \\ 0 & \text{otherwise} \end{cases}$ 
15          if ( $\|\mathbf{y}^{opt}(t) - \mathbf{E}\hat{\mathbf{z}}(t)\| \leq \eta$ )
16              Break;
17          end if
18   end

```

value of the dual function $q(\lambda(\mathbf{t}))$ satisfies the following lower bound:

$$\begin{aligned}
 \max_{t=0,1,\dots,T} q(\lambda(t)) &\geq q^{opt} - \frac{1}{2\alpha(T+1)}. \\
 &L_p + \alpha^2(T+1)(D+1)(G+E) \cdot \\
 &[3GD + DE + G + E]
 \end{aligned} \tag{5.2}$$

Where $L_p = \|\lambda_{opt} - \lambda(0)\|_2^2$ is the distance from the initial point, $\lambda(0)$, to the optimal set λ_{opt} .

Proof. As illustrated in [84], assuming the existence of the optimum value λ^{opt} , we know

that $\|\lambda(T+1) - \lambda^{opt}\|_2^2 \geq 0$. This implies

$$\|\lambda(T) + \alpha \sum_{c_{ij}(\hat{t})=0}^D P_{t-c_{ij}(\hat{t})}(\mathbf{g}_q(t - c_{ij}(\hat{t}))) - \lambda^{opt}\| \geq 0 \quad (5.3)$$

Equation (5.3) can be expanded as

$$\begin{aligned} & \|\lambda(0) - \lambda^{opt}\|_2^2 \\ & + 2\alpha \sum_{t=0}^T \sum_{c_{ij}(\hat{t})=0}^D P_{t-c_{ij}(\hat{t})}(\mathbf{g}_q(t - c_{ij}(\hat{t})))' (\lambda - \lambda^{opt}) \\ & + \alpha^2 \sum_{t=0}^T \left\| \sum_{c_{ij}(\hat{t})=0}^D P_{t-c_{ij}(\hat{t})}(\mathbf{g}_q(t - c_{ij}(\hat{t}))) \right\|_2^2 \geq 0 \end{aligned} \quad (5.4)$$

where, a recursion of the term $\|\lambda(t) - \lambda^{opt}\|_2^2$ until $t = 0$ is used. Assuming initial condition of $\lambda(0) = 0$ we get $\|\lambda^{opt}\|_2^2 = L_p$. Bounds for the individual terms of (5.4) are derived in Appendix A and are combined as follows:

$$\begin{aligned} 0 \leq & L_p + 2\alpha \sum_{t=0}^T (\alpha G D (G + E)(D + 1) + q(\lambda(t)) - q^{opt}) \\ & (T + 1)\alpha^2 (D + 1)^2 (G + E)^2 \end{aligned} \quad (5.5)$$

Rearranging the terms in (5.5), we arrive at the upper bound in (5.2) of Theorem 1. \square

For a constant step size α with no error and delay, i.e., with $D = 0$, $E = 0$, the convergence result in (5.2) reduces to $\max_{t=0,1,\dots,T} q((\lambda(t))) \geq q^{opt} - \frac{L_p + G^2 \alpha^2 (T+1)}{2\alpha(T+1)}$. This is similar to the convergence result of ordinary gradient method. Theorem 5.2 shows that in the presence of delays and quantization error, the algorithm still converges, but only to a greater neighborhood around the optimal point.

5.2.2 Convergence Rate With Packet Loss:

Next, we aim to study the convergence of the time varying gradient method with finite-length buffer at each agent resulting in communication failure i.e., packet loss. Using the packet loss model in [85], we integrate effect of packet loss into the convergence rate in

Theorem 5.2. We assume that each packet consists of a gradient update $g_q(\hat{t})$ and with a probability \wp , a packet is dropped. For analysis we further assume that, such failure has independent occurrences and can be modeled as

$$\mathcal{P}\{F_{ij}(t) = m\} = (1 - \wp_{ij})\wp_{ij}^m, \quad m \in \{0, I^+\}, \quad (5.6)$$

where $F_{ij}(t)$ is the number of dropped packets in a given interval t , \wp_{ij} is the probability that packet loss occurs during one transmission from agent i to j , and $I^+ = \{1, 2, \dots\}$. For our analysis, we assume $\wp_{ij} = \wp$, $\forall i, j \in N_a$ hereafter, where N_a is the number of agents. We further define packet drop instance for any agent i as the set of maximum packet drops before a gradient update can be performed, i.e., $X_i = \{F_i^l\}_{l=1}^{P_k}$, where F_i^l denotes the maximum number of failure for the l^{th} element for i^{th} gradient update. Therefore, X_i can have many combinations of failure. We next define A_i as the set of all possible combination of X_i . It is worth noting that, if the maximum roundtrip delay is not fixed, $|A_i|$ can increase indefinitely. We now associate X_i to K_p packet drops and define the drop set as $A_i(K_p) = \{X_i | M(X_i) \leq K_p, X_i \in A_i\}$, where $M(X_i) = \sum_{r=1}^{|X_i|} X_i^r$, represents the maximum number of concurrent drops, i.e., for a given packet drop instance X_i , all gradient updates experience drop $F_i^l \in X_i$. Therefore, the probability of K_p drops occurring is given by $\mathcal{P}\{A_i(K_p)\} = \sum_{X_i \in A_i(K_p)} \mathcal{P}\{X_i\}$, where the probability that X_i can occur is $\mathcal{P}\{X_i\} = \prod_{r=1}^{|X_i|} F_i^r = X_i^r$. Assuming that time delay for update at each node is locally bounded, each agent completes the gradient updates only when the following delay bound holds:

$$\sum_{j \in N_i} (1 + F_i^l(\hat{t}))\delta_{ij}(\hat{t}) + (1 + F_i^l(\hat{t}))\delta_{ji}(\hat{t}) \leq \max_{j \in N_i} D_{ij}(\hat{t}). \quad (5.7)$$

The dual problem in (4.6) can be rewritten including the K_p -packet loss function $G_i(K_p)$ as follows:

$$\begin{aligned} \max_{\nu_i \geq 0} \min_{\lambda \geq 0} q(\lambda, \nu) &= \sum_{i=1}^{K_s} q_i(\lambda_i, \nu_i) \\ \text{subject to: } \mathbf{E}' \lambda &= 0 \end{aligned} \quad (5.8)$$

where, $q_i(\lambda_i, \nu_i)$ is the optimal solution of the following problem:

$$\begin{aligned} & \min_{\lambda} l_i(\mathbf{x}_i, \mathbf{y}_i) - \lambda_i' \mathbf{y}_i \\ & + \nu_i' \left(\max_{j \in N_i} D_{ij} - \sum_{j \in N_i} C_{ij}(\hat{t}) - G_i(K_p) \right) \\ & \text{subject to: } (\mathbf{x}_i, \mathbf{y}_i) \in \mathcal{C}_i \end{aligned} \quad (5.9)$$

where, \mathcal{C}_i is the constraint set for agent i . We now state an important theorem to account for the packet loss model presented in (5.6) to the convergence rate. We are interested in a probabilistic measure to characterize the convergence rate under a fixed maximum number of packet loss. Specifically, we characterize the measure of exceeding the convergence rate from the expected convergence rate in the below theorem:

Theorem 2 (Outage convergence rate with packet loss:). *For a given K_p number of packet drops, and an existing minimizer q^{opt} , the probability that the rate of convergence exceeds the expected rate is obtained by the following upper bound:*

$$\begin{aligned} & Pr \left\{ \left| \max_{t=0,1,\dots,T} q((\lambda(t))) - q^{opt} \right| \geq \epsilon_d \right\} \leq \left[\frac{e^\delta}{(1+\delta)(1+\delta)} \right]^{D_u} \\ & \cdot \frac{1}{2\alpha(T+1)} L_p + \alpha^2(T+1)(D_u + \delta + 1)(G + E) \\ & [3G(D_u + \delta) + (D_u + \delta)E + G + E], \end{aligned} \quad (5.10)$$

where $\delta(> 0)$ is the value by which the convergence rate exceeds the expected value D_u , given by the highest order statistics of a local delay function $G_i(K_p) = K_p \max_{j \in N_i} C_{ij}(\hat{t})$ for each agent node i . N_i is the set of neighbor agents and $C_{ij}(\hat{t})$ is the time-varying roundtrip delay at each connecting link between agents i to j .

Proof. We outline a generalized proof of this theorem. We first assume that the local total delays to and from the neighboring nodes $\{c_{ij}(\hat{t})\}_{i=1, j \in N_i}^{N_i}$ are taken from a continuous population with cumulative distribution $F_{c_{ij}}(x)$ and probability density $f_{c_{ij}}(x)$, where x is

a delay variable. The N_i^{th} order statistics, or the sample maximum, $f_{c_{ij}}^{N_i}$ has the following PDF:

$$f_{c_{ij}}^{N_i}(x) = N_i [F_{c_{ij}}(x)]^{N_i-1} f_{c_{ij}}(x). \quad (5.11)$$

The PDF of the delay with K_p packet drops $F_{G_i(K_p)}$ can be obtained from a $(K_p - 1)$ -fold convolution of the PDF $f_{c_{ij}}(x)$. All $G_i(K_p)$, are take as a vector of random variables \mathbf{X} such that, $\mathbf{X} = [\mathbf{X}_1, \mathbf{X}_2 \cdots, \mathbf{X}_{N_a}(K_p)]'$ where $\mathbf{X}_i = G_i(K_p)$ and \mathbf{X}_i has any arbitrary PDF with mean μ_i and variance σ_i^2 . A closed form expression on the expected value of the highest-order statistic given $\mathbf{X} \sim P_\theta(\mu, \sigma^2)$ is [86]

$$\begin{aligned} E[\mathbf{X}_i] \leq & \\ \frac{1}{2} \left(\sum_{i=1}^n \left[\mu_i + \left(\left(\mu_i - \max_{1 \leq i \leq N_a} \left\{ \mu_i + \frac{N_a - 2}{2\sqrt{N - a - 1}} \sigma_i \right\} \right)^2 + \sigma_i^2 \right)^{1/2} \right] \right. & \\ \left. + (2 - N_a) \left[\max_{1 \leq i \leq N_a} \left\{ \mu_i + \frac{N_a - 2}{2\sqrt{N - a - 1}} \sigma_i \right\} \right] \right) & = D_u. \quad (5.12) \end{aligned}$$

We now define ‘‘outage probability measure’’ as $\mathcal{P}[\text{delay} > D] \approx \mathcal{P}[X \geq D + \delta] \leq \mathcal{F}(N_a, D, \delta)$. Here the function bound $\mathcal{F}(N_a, D, \delta)$ can be given as follows:

$$\begin{aligned} \mathcal{F}(N_a, D_u, \delta) &= \frac{\left(1 + \frac{D_u \delta}{N_a - D_u(1 + \delta)} \right)^{N_a - D_u(1 + \delta)}}{(1 + \delta)^{D_u(1 + \delta)}} \\ &\leq \left(\frac{\exp(\delta)}{(1 + \delta)^{D_u(1 + \delta)}} \right)^{D_u} \quad (5.13) \end{aligned}$$

□

As direct consequence of the theorems 1 and 2, we obtaine the total end-to-end delay for the proposed decentralized SSG reconfiguration as follows:

Corollary 1. *Let T be the number of iterations. Assuming the existence of the minimizer q^{opt} , and a bounded time delay, the exact distribution of total end-to-end delay $F_T(x)$ for global level SSG reconfiguration is given by:*

$$F_{T_d}(x) = N_a \left[F_{c_{ij}}^{N_i}(x) \right]^{N_a-1} f_{c_{ij}}^{N_i}(x). \quad (5.14)$$

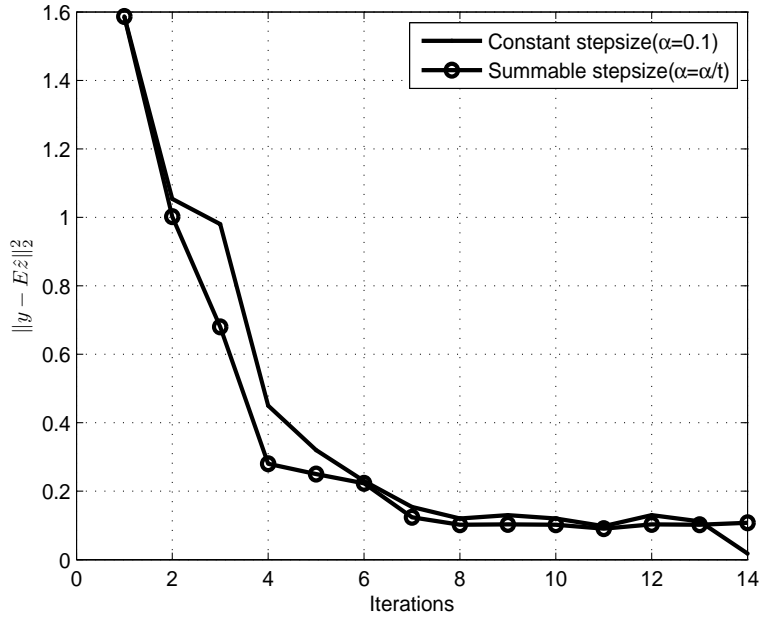


Figure 5.1: *Shipboard microgrid reconfiguration with 4 simultaneous faults*

where, x is the delay variable, $F_{c_{ij}}^{N_i}(x)$ and $f_{c_{ij}}^{N_i}(x)$ are cumulative distribution and probability distributions of total local delay at the i^{th} agent given by (5.11).

Proof. We start with the local delay $C_{ij}(\hat{t})$ between neighboring agents i and j and assume further that all packets reach their destinations. Therefore, the total roundtrip delay for each agent communicating with N_i neighboring agents are captured by the random variable $X_i = \max_{j \in N_i} C_{ij}(\hat{t})$. The total end-to-end delay for T iterations is therefore $T_d = T \cdot \max_{j \in N_a} C_{ij}(\hat{t})$. The cumulative and probability distributions of $\max_{j \in N_i} C_{ij}(\hat{t})$ are found readily from (5.11). We therefore arrive at the final result by finding the N_a^{th} order statistic of each of the local delay variables. \square

5.3 Simulation Results

We consider the convergence of the distributed gradient method used for decentralized SSG reconfiguration. Fig. 5.1 shows that, with constant step size between iterations, the dual de-

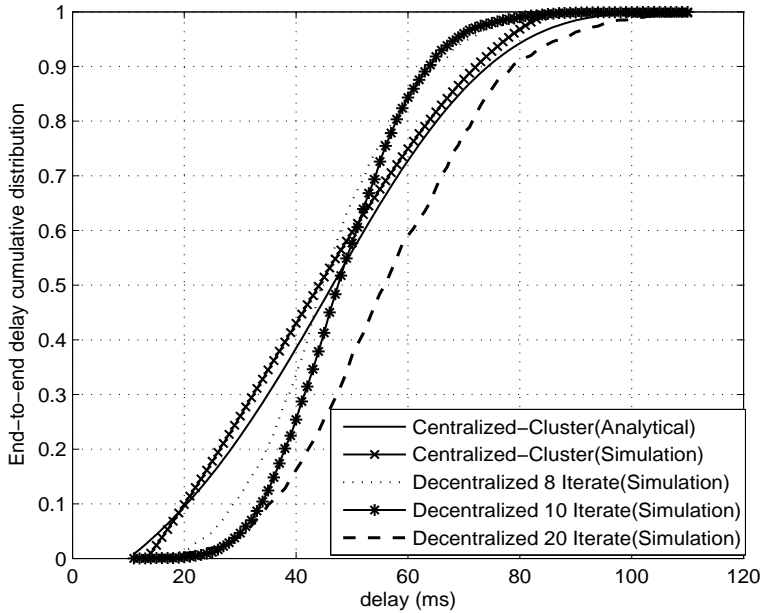


Figure 5.2: Comparison of delay distribution between decentralized and centralized-cluster

composition reaches the desired accuracy η within 8 iterations. With diminishing summable step size of α/t [62], the algorithm stabilizes with a smoother slope around the optimal point. Over a wide range and locations of faults, the decentralized approach has been observed to converge within 8 iterations.

Next, we provide a comparison of total (end-to-end) delay of the proposed decentralized approach for SSG optimization and the corresponding centralized optimization techniques presented in our earlier work [65]. Fig. 6.4 shows the delay distribution of the centralized cluster and decentralized method. As seen in Fig. 6.4, the decentralized approach with 8 iterations provide similar total delay performance with centralized cluster sensor configuration. All networks are subjected to slotted CSMA network with uniform backoff range $w > 32$ and channel access probability $p_s = 0.7$ [65]. We again assume that, perfect network is in place, i.e., no packet loss is encountered. Obviously, the total delay is dependent on the number of iterations required for convergence for decentralized approach. That is, with more iterations, the delay will increase. Fig. 6.3-6.2 show that the proposed approach

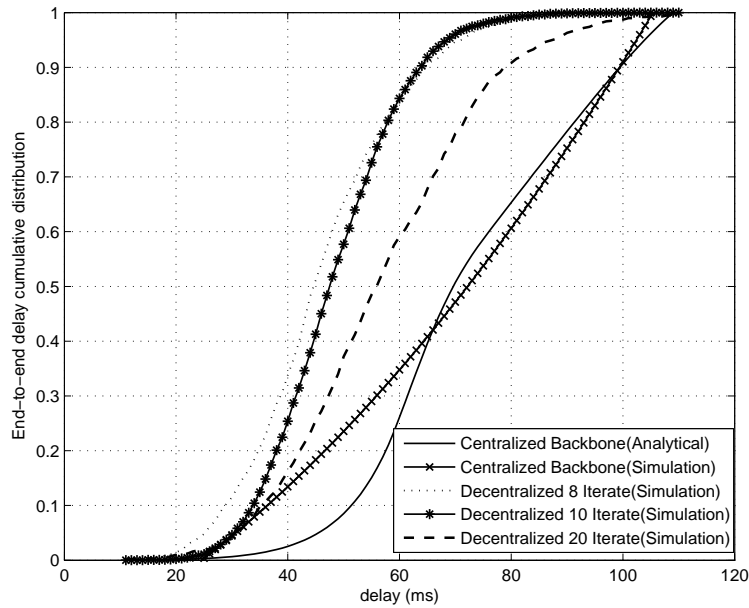


Figure 5.3: Comparison of delay distribution between decentralized and centralized-backbone

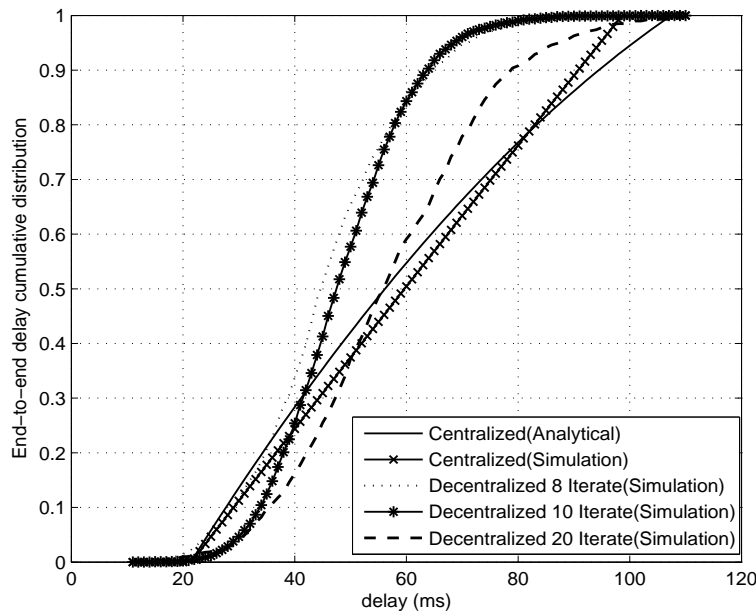


Figure 5.4: Comparison of delay distribution between decentralized and centralized

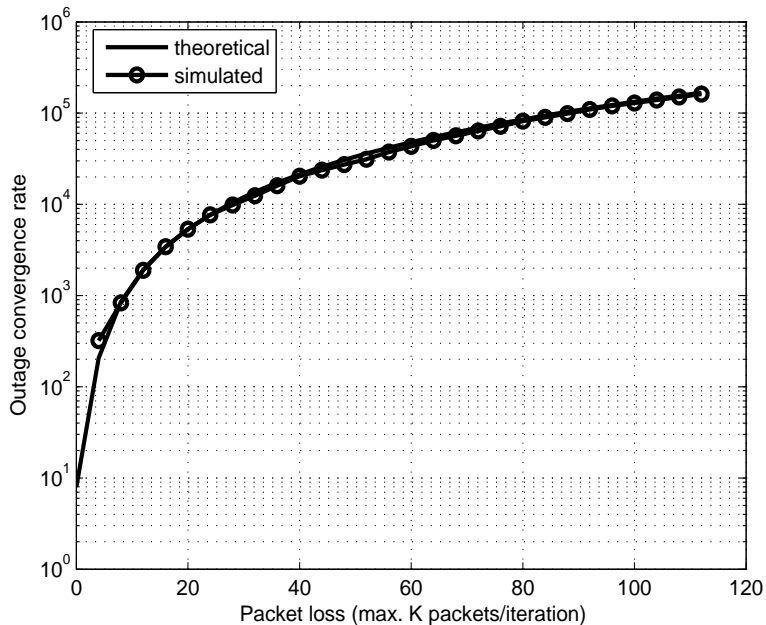


Figure 5.5: *Decentralized dual decomposition convergence rate with K_p packet loss'*

performs better than the centralized-backbone and fully-centralized approaches in terms of the total delay distribution.

The simulation results presented in Figs. 6.4-6.2 demonstrate that the proposed distributed approach produces lower total delay compared to most centralized approaches, which is beneficial for timely power restoration to vital loads in the shipboard.

Next, we verify the convergence rate results in Theorem. 2. Fig. 6.5 shows the theoretical and simulated convergence rate with K_p packet losses per iteration. The theorem provides an upper bound on the convergence rate in terms of per iteration times. We assume each gradient update $g_q(\hat{t})$ involves one packet exchange. Theorem. 2 accurately predicts the convergence rate per iteration times with K_p packet losses per iteration. As expected, when more packets are lost, the convergence rate increases exponentially. We assume an outage probability $\eta_d = 0.1$.

5.4 Summary

In this Chapter, we formulate and analyze the impact of communication network on decentralized method for shipboard smartgrid reconfiguration. We show that by applying dual decomposition method the effective (in terms of the power delivery to loads) reconfiguration under multiple faults can be achieved. We quantify the robustness of the proposed time-varying gradient algorithm by providing a lower bound on the rate of convergence under communication network delay and quantization noise. The analysis reveals that, with bounded time delay and bounded quantization noise and no packet loss in the network, the time varying gradient method to solve the SSG reconfiguration problem still converges, but to a greater neighborhood of the optimal point. We further quantify the effect of packet loss on the convergence rate and propose outage convergence rate as a probabilistic measure of performance. Our proposed outage convergence rate theorem tightly upper bounds the convergence rate with packet loss, for a given outage and a desired accuracy. Therefore, this provides another important probabilistic QoS guarantee for optimization under lossy network. The total end-to-end delay comparison with our earlier work in centralized reconfiguration of shipboard smartgrid shows that distributed approach is effective in reducing the total delay and on does better than centralized strategies for a wide number and location of faults. In the next chapter, we provide comparison of reconfiguration results for both centralized and decentralized solution to effectively demonstrate both approaches. Additionally, we discuss the trade-off of both approaches in relation to SSG reconfiguration.

Chapter 6

Comparative Analysis

In this chapter, we provide a comparative analysis of various reconfiguration strategies of SSG.

6.1 Optimal Centralized Vs. Decentralized Reconfiguration

In this section, we demonstrate the effectiveness of centralized and decentralized strategies to the SSG reconfiguration problem from different formulations in Chapter 2 and in Chapter 3, and compare them. All our proposed solutions are compared with optimal non-convex solution provided by “LINGO” software.

The optimization methods described in Section 2.2 are applied to reconfigure the SSG after occurrence of one or more faults. Only steady-state reconfiguration status is considered in this paper. Table 6.1 shows the constrained parameters used in the simulations and their respective maximum and minimum values. First, an optimal pre-fault configuration for system model in Fig. 2.2 is considered. The centralized and decentralized formulations described in previous chapters ensure that the power is restored in a manner such that those loads are serviced optimally and according to their priority.

For comparison, We assume that (1) all loads are operating with maximum rated power condition before fault occurrence, and (2) all faults occurring at random locations in the smartgrid are identified and isolated before the optimization algorithm is executed. Fig. 6.1

Table 6.1: *Simulation parameters*

Constrained parameters	max.	min.
PG_i (MTG)	6 MW	0 MW
PG_i (ATG)	2 MW	0 MW
I_{ij}	500 A	-500 A
V_i	95 V	105 V
δ_i	1°	-1°
PL_i (VL)	0.5 MW	0 MW
PL_i (SVL)	1 MW	0 MW
PL_i (NVL)	0.5 MW	0 MW
SW_i	1	0
B_i	1	0

Table 6.2: *Shipboard smartgrid reconfiguration with 4 faults*

Load positions	Vital (MW)	Semi-vital (MW)	Non-vital (MW)	SW positions (closed)	Solver
Load 1/2	0.5000	1.0000	0.4786	SW2	Global Non-convex with mixed integer (LINGO)
Load 3/4	0.5000	1.0000	0.5000	SW4	
Load 35	0.5000			SW46	
Load 5/6	0.5000	1.0000	1.0000	SW6	
Load 7/8	0.5000	1.0000	0.5000	SW7	
Load 8/10	0.5000			SW79	
Load 9/10	0.5000	1.0000	0.5000	SW9	
Load 1/2	0.5000	1.0000	0.4621	SW2	
Load 3/4	0.5000	1.0000	0.5000	SW4	
Load 35	0.5000			SW46	
Load 5/6	0.5000	1.0000	1.0000	SW6	
Load 7/8	0.5000	1.0000	0.5000	SW7	
Load 8/10	0.5000			SW79	
Load 9/10	0.5000	1.0000	0.5000	SW9	

shows a scenario with 4 faults occurring between bus numbers 3 – 35, 35 – 5, 2 – 4, and 6 – 8 on the smartgrid. We show global optimization results only and compare the distributed dual decomposition reconfiguration results with existing centralized optimizations methods [57]. Switch states after reconfiguration are pointed by arrow marks. These switch states mark the absolute global optimization result obtained by using branch and bound based exhaustive search for original centralized mixed-integer non-linear (MINLP) problem.

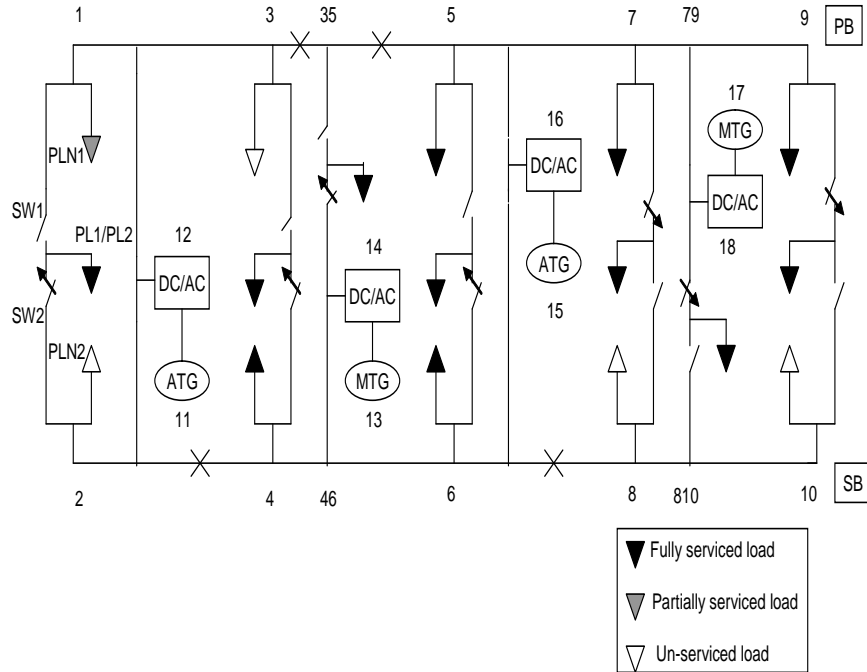


Figure 6.1: Shipboard microgrid with 4 simultaneous faults

As demonstrated by Table 6.2 that they are identical. Fig. 2.2 shows a pre-fault condition where all the loads are serviced for a particular switch configuration. Reconfiguration algorithms are applied for MINLP ($P1$), relaxed integer non-convex ($P2$) and relaxed-integer convex ($P3$) cases from this initial (pre-fault) configuration. Several independent simulation runs show that centralized solutions of $P1$, $P2$, $P3$, and decentralized solution of $P3$ are similar with high regularity.

6.2 Total Delay for Centralized Vs. Decentralized Reconfiguration of SSG

A comparative study of delay distributions for various centralized architectures (Architecture I-III) in ?? with agent based decentralized SSG reconfiguration in ?? under network with no packet loss is now provided. Fig. 3.13 shows results of end-to-end delay distribution for architectures I-III for validating our framework. The centralized-cluster (Architecture-III)

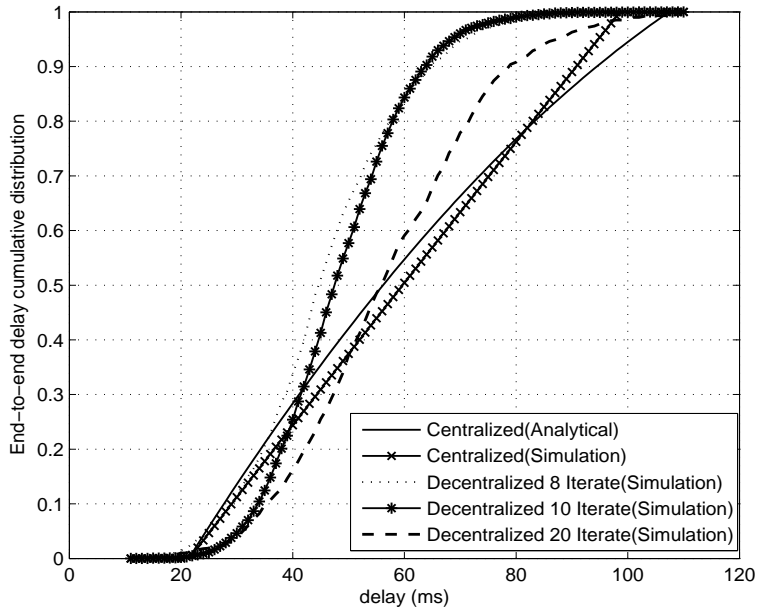


Figure 6.2: Comparison of delay distribution between decentralized and centralized

produces lower delay than other two (viz. probability of 0.94 with which service can be restored within 80 milliseconds). As seen in Fig. 6.4, the decentralized approach with 8 iterations provide better delay performance when compared with centralized configuration. All networks are subjected to slotted CSMA network with uniform backoff range $w > 32$ and channel access probability $p_s = 0.7$ [65].

Fig. 6.3 provides total delay of backbone network in SSG (Architecture-II) that is quite inferior to that of decentralized solution. This can be attributed to the time inherent delay that backbone network topologies suffer from other traffic in the system. We now compare the end-to-end response time employing cluster network topology in SSG (Architecture-III) in chapter 3. the decentralized approach with 8 iterations provide similar total delay performance with centralized cluster sensor configuration. It is important to mention that the total delay is dependent on the number of iterations required for convergence for decentralized approach. That is, with more iterations, the delay will increase. We have used 8 iterations as it was found by simulation that the algorithms converges within 8 iterations

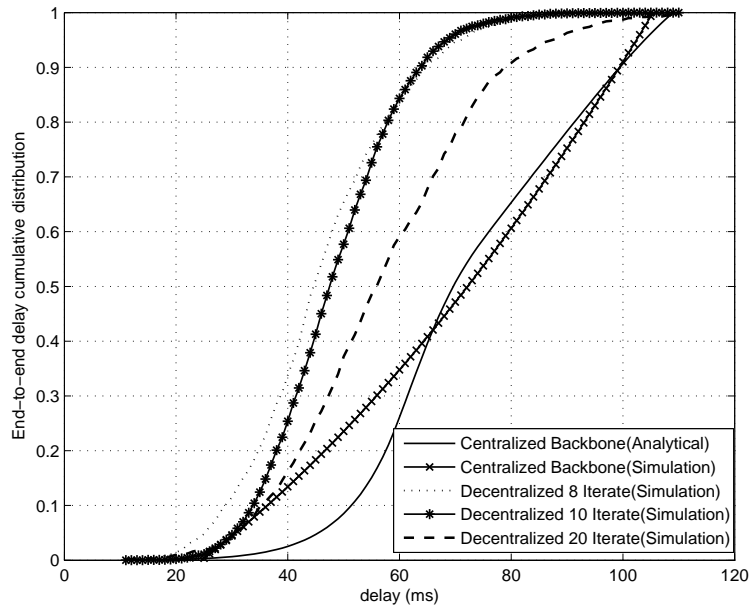


Figure 6.3: Comparison of delay distribution between decentralized and centralized-backbone

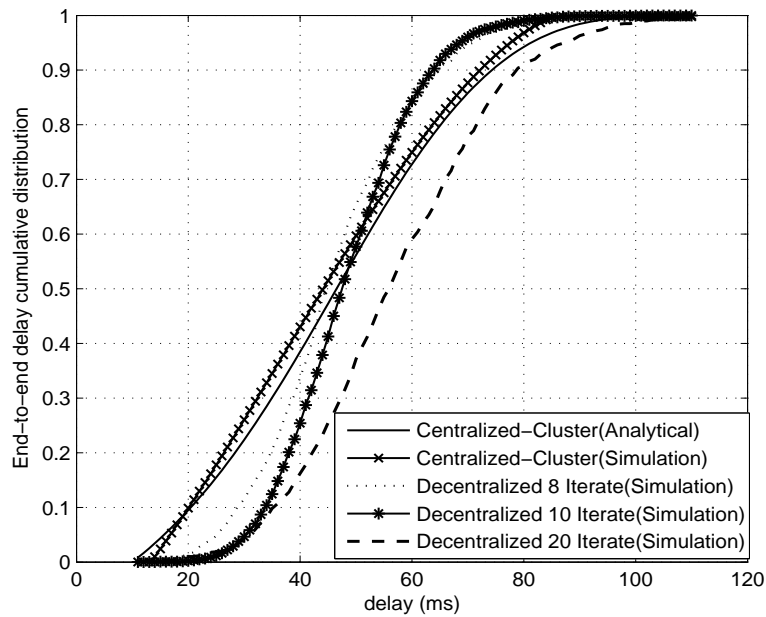


Figure 6.4: Comparison of delay distribution between decentralized and centralized-cluster

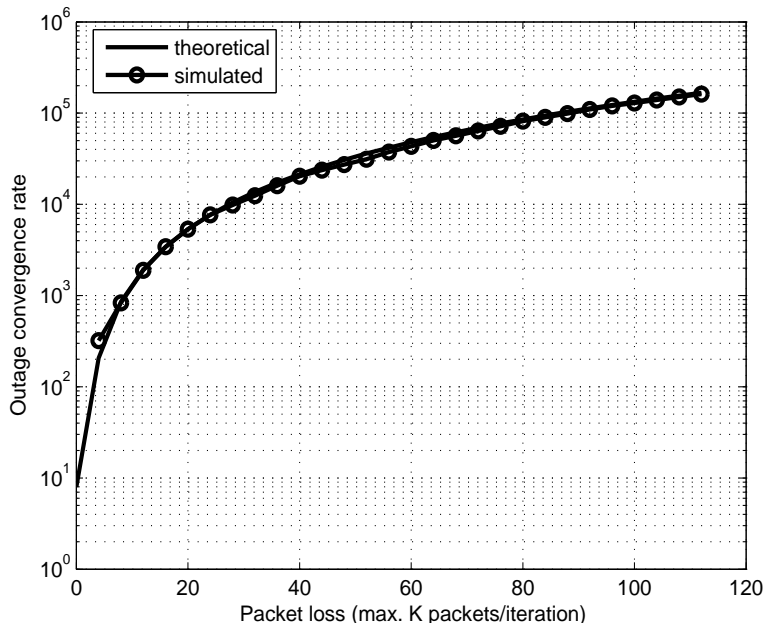


Figure 6.5: *Decentralized dual decomposition convergence rate with K_p packet loss'*

for a wide range of faults and locations. The simulation results presented in Figs. 6.4-6.2 demonstrate that the proposed distributed approach produces lower total delay compared to most centralized approaches, which is beneficial for timely power restoration to vital loads in the shipboard.

6.3 Convergence Under Lossy Network for Decentralized Reconfiguration

We re-iterate the results of convergence rate under packet loss for decentralized reconfiguration for the sake of completeness in our analysis. As demonstrated before, when more packets are lost, the convergence rate increases exponentially. We assume an outage probability $\eta_d = 0.1$. Compared to centralized solution, we note that, the decentralized solution is more robust, i.e., it still is able to converge to a solution within a finite number of packet loss and a finite outage. For centralized strategies, due to single point failure problem, once

packets are lost, the optimal solution can never be reached.

6.4 Summary

In this Chapter, first, comparison between centralized and decentralized optimization solutions for SSG reconfiguration are evaluated that deliver near-optimal power to loads in SSG under faults. The complexity of proposed solutions is polynomial in time and much lower than the complexity of the global solver that uses “branch and bound” based exhaustive search.

Next, we compare the total delay for centralized and decentralized SSG reconfiguration strategies to provide probabilistic QoS involving interaction between sensors, power systems and communication network. We adopt a cyber-physical approach to understand and quantify the delay in SSG reconfiguration from the occurrence of faults. Simulation results demonstrate that decentralized reconfiguration provide overall better performance than centralized reconfiguration in terms of delay.

Under packet loss and variable network delay the decentralized solution provide robust solution to SSG reconfiguration problem.

Chapter 7

Conclusions and Future Work

In this dissertation, centralized and decentralized reconfiguration algorithms are proposed for cyber-physical reconfigurable networks. The proposed reconfiguration methodologies are applied to shipboard smartgrid systems to demonstrate their effectiveness. In this chapter, the main results and conclusions are summarized for centralized and decentralized SSG reconfiguration. Thereafter, possible research directions for future work are suggested.

7.1 Conclusions

Like terrestrial systems, smart grid concepts can be applied to various applications related to shipboard power systems. In this dissertation, one such promising area for application of smart grid technology is the design for reconfigurability for shipboard smartgrid systems is highlighted. ONR has promoted medium-voltage DC (MVDC) distribution in shipboard power systems for future all electric ships. Several proof of concept studies related to design, operation, and control of MVDC shipboard power system have been proposed that encompass new challenges related to flexibility and survivability. In this dissertation, we proposed various methodologies for solutions related to reconfiguration of shipboard smartgrid. Three main contributions of this dissertation are summarized below:

7.1.1 Centralized Reconfiguration

In this dissertation, two centralized optimization solutions are designed and evaluated. These approaches deliver near-optimal power to loads in shipboard power system. The complexity of proposed solutions is polynomial in time and much lower than the complexity of the global solver that uses “branch and bound”. Local optimum for relaxed-integer non-convex formulation and global optimum for relaxed integer convex formulation match the global optimum for original MINLP non-convex formulation with high regularity. Further, cumulative distribution of power flow is used to show that in 50% of the fault cases (up to 4 random faults) the vital and semi-vital loads are serviced. Analysis of the tradeoff between power delivery and number of switching operations performed during reconfiguration is also provided. As expected, it is observed that an increase in switching is necessary to deliver more power to loads. Furthermore, change of switch states is tracked from pre-fault state to final state, while (1) changing one switch pair at a time; and (2) maximizing power delivery at each state. The tradeoff between number of switch operations and power delivered is also quantified.

Next, a general framework for end-to-end response time considering an integrated delay analysis for shipboard CPS is provided. The framework is analyzed through a case study in which power needs to be delivered to vital loads of the shipboard system after occurrence of faults. We consider several sensor network arrangements and evaluate the end-to-end response time. The analysis shows that the developed framework accurately models the distribution of the end-to-end delay while also capturing the heterogeneity in various inter-connecting subsystems. The developed framework can be used to guide the development of QoS-based scheduling and communication solutions for shipboard systems. We validate the proposed model by simulating separate subsystems to compute the delay distributions for various possible centralized architectures. Using our general framework, various design choices capturing the trade off between delay, connection and reliability can be made. Simulation results indicate that our proposed analytical model accurately tracks the end-to-end

delay of the shipboard system reconfiguration which we presented as a case study. The QoS service guarantee of the end to end system response time can be provided by our proposed framework that facilitates addressing various system design issues.

7.1.2 Decentralized Reconfiguration

We formulate and analyze a distributed method for shipboard smartgrid reconfiguration. Specifically, we decompose the SSG into multiple smaller subsystems that are coupled with each other via convex coupling constraints. We show that by applying dual decomposition method the effective (in terms of the power delivery to loads) reconfiguration under multiple faults can be achieved. Extensive simulations indicate that distributed reconfiguration results are closely comparable to the optimal solution of the original non-convex problem. With a perfect communication network to facilitate information exchange among agents, the distributed dual decomposition converges to the solution states within a few iterations. Additionally, we quantify the robustness of the algorithm by providing a lower bound on the rate of convergence under communication network delay and quantization noise. The analysis reveals that, with bounded time delay and bounded quantization noise and no packet loss in the network, the time varying gradient method to solve the SSG reconfiguration problem still converges, but to a greater neighborhood of the optimal point. We further quantify the effect of packet loss on the convergence rate and propose outage convergence rate as a probabilistic measure of performance. Our proposed outage convergence rate theorem tightly upper bounds the convergence rate with packet loss, for a given outage and a desired accuracy. Therefore, this provides another important probabilistic QoS guarantee for optimization under lossy network. The total end-to-end delay comparison with our earlier work in centralized reconfiguration of shipboard smartgrid shows that distributed approach is effective in reducing the total delay and does better than centralized strategies for a wide number and location of faults.

Due to the limitation of the simulation platform, a simplified SSG reconfiguration is not

implemented in hardware. The simulation results confirm that the proposed reconfiguration methodology is effective and promising. No effort is made to demonstrate robustness to a single point of failure and scalability as these are generally accepted characteristics of a completely decentralized reconfiguration of SSG. The use of a reduced order notional SSG prevents a recommendation that reconfiguration strategies can be effectively applied in real-time at this time and motivate a significant recommended future work. Further research is indeed required in understanding the distributed strategies from a probabilistic belief propagation point of view and move towards a completely distributed architecture.

7.2 Future Work

In this section, possible directions for future work related to cyber-physical system optimization are identified. A brief case-study with SSG reconfiguration with an attractive candidate method for distributed reconfiguration is described.

Alternate Distributed Reconfiguration Strategies

Belief propagation based optimization strategies can be very useful in solving a complex SSG reconfiguration problem in a completely distributed manner. In this approach, we introduce Belief Propagation (BP), a prototypical iterative message-passing algorithm that has gained considerable popularity in the recent literature. BP has been applied across disciplines including communications, statistical inferencing, signal processing, machine learning as an attractive, scalable general purpose heuristic for a wide class of optimization and state estimation problem. The main objective of this approach is to identify and model the power system reconfiguration as a state estimation problem that are solvable by BP algorithms. Specifically, we apply min-sum version of BP to find the solution of the constrained relaxed-integer convex optimization problem. We also attempt to resolve conditions under which BP will guarantee convergence to the optimal solution.

Some of the related prior work in BP include solving quadratic optimization, and more

general, convex optimization problem [87], convergence and correctness of min-cost network flow problem [88]. Recently, the message-passing based approach has been applied for optimization and control of power grid [89], power distribution system state estimator [90], and micro-grid state estimation [61].

We essentially follow the Forney style factor graph approach in [91] to model our power system and apply min-sum message passing among variable nodes (represented by agents containing state information of a node) and factor nodes (containing constraints information associated with each state variable). To this end, we first briefly introduce the min-sum BP approach to solve general class of separable convex optimization problem of the form

$$\begin{aligned} \text{Min. } F(\mathbf{x}) &= \sum_{i \in V} f_i(\mathbf{x}_i) + \sum_{C \in \mathcal{C}} f_C(\mathbf{x}_C) \\ \text{s.t. } \mathbf{x}_i &\in \mathfrak{R}, \forall i \in V \end{aligned} \quad (7.1)$$

where, V is a finite set of the decision variables $\mathbf{x} \in R^V$ and C is a finite collection of subsets of V representing constraints. The variable functions $f_i(\cdot)$ and factor functions $f_C(\cdot)$ are convex. In this setting, each \mathbf{x}_i are state vectors that each agent holds. We illustrate the concept of min-sum BP through the well-known maximum-size independent set problem below:

Problem Statement: Select a subset V of maximum cardinality from an undirected graph $G = (V, E)$, so that no two vertices of the chosen subset are neighbors of each other.

The factorized form of the above problem can be formulated as a simple constrained optimization problem

$$\begin{aligned} \text{Min. } \sum_{i \in V} f_i(x_i) + \sum_{(i,j) \in E} f_{ij}(x_i, x_j) \\ \text{s.t. } x_i \in \mathfrak{R}, \forall i, j \in V, \end{aligned} \quad (7.2)$$

where same notations $f_i(x_i)$ and $f_{ij}(x_i, x_j)$ are variable functions and factor functions, respectively. There are further defined as follows:

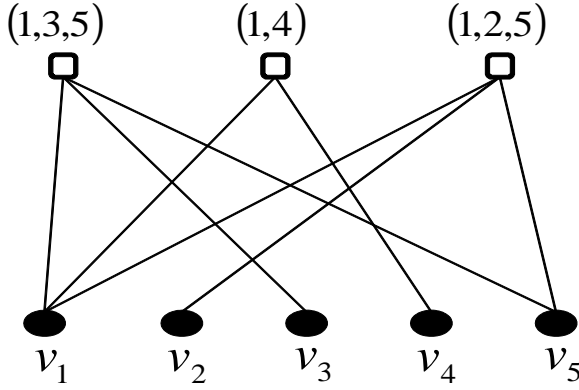


Figure 7.1: An example of a factor graph for (7.5)

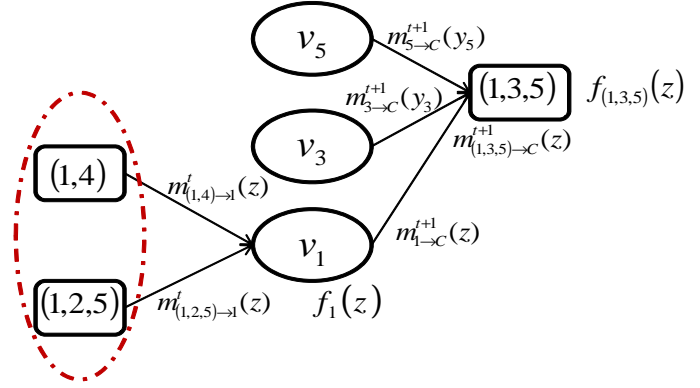


Figure 7.2: Min-sum update for variable node v_1

$$f_i(x_i) = \begin{cases} 0 & \text{if } x_i = 0 \\ -1 & \text{if } x_j = 1 \\ \infty & \text{otherwise.} \end{cases} \quad (7.3)$$

$$f_{ij}(x_i, x_j) = \begin{cases} 0 & \text{if } x_i + x_j \leq 1 \\ \infty & \text{otherwise.} \end{cases} \quad (7.4)$$

We now construct a simple factor graph for the optimization problem (7.2). A factor graph is a bipartite graph with one partition containing variable nodes V and the other partition containing factor nodes representing constraints. There is an edge $e = (V, C) \in V \times C$ iff $v \in C$. Consider that Fig. 7.1 shows the factor graph F_G of the following optimization problem:

$$\begin{aligned} \text{Min.} \quad & \left(\sum_{i=1}^5 f_i(x_i) \right) + f_{1,3,5}(x_1, x_3, x_5) + f_{2,4}(x_2, x_4) + f_{1,2,5}(x_1, x_2, x_5) \\ \text{s.t.} \quad & x_i \in \mathfrak{R}, \forall 1 \leq i \leq 5 \end{aligned} \quad (7.5)$$

The min-sum BP is conceptually quite similar to dynamic programming algorithm that works optimally for tree based factor graphs. The idea is to fix a specific value $z \in R$ of variable x_i corresponding to the variable node v_i . Then compute the cost of optimal assignment for the rest of the problem $b_i(z)$, i.e., $\text{argmin}_{z \in R} b_i(z)$ in a recursive manner. A parallel implementation to this recursive approach leads to the following message updates

for each edge $e = (i, C) \in F_G$:

$$m_{i \rightarrow C}^t(z) = f_i(z) + \sum_{K \in C_i \setminus i} m_{K \rightarrow i}(z) \quad (7.6)$$

$$m_{C \rightarrow i}^t(z) = \min_{y \in R, y_i = z} f_C(z) + \sum_{j \in C \setminus i} m_{j \rightarrow C}(y_j) \quad (7.7)$$

$$(7.8)$$

The message update for node v_1 is demonstrated in Fig. 7.2. The estimate of $b_i(z)$ at the end of iteration for each node $v_i \in V$, and $z \in R$ is obtained as:

$$b_i^t(z) = f_i(z) + \sum_{C \in C_i} m_{C \rightarrow i}^t(z). \quad (7.9)$$

The min-sum algorithm is now formally summarized in Alg. 3. To solve the optimization

Alg. 3 min-sum BP

Input: $G = (V, C)$

Output: $\hat{\mathbf{x}}^N$

```

1   begin
2       Construct factor graph of  $G = (V, C)$ 
3       Set  $N$  as the number of iterations
4       Initialize  $t = 0$ , for each edge  $(i, C) \in G$ , initialize  $m_{C \rightarrow i}^0(\mathbf{x}_i) = m_{i \rightarrow C}^0(\mathbf{x}_i) = 0, \forall \mathbf{x}_i \in \mathfrak{R}$ 
5       for  $t = 1, 2, \dots, N$  do
6           for  $e = (i, C) \in G$  and  $\mathbf{x}_i \in \mathfrak{R}$ , perform following updates
               $m_{i \rightarrow C}^0(\mathbf{x}_i) = f_i(\mathbf{x}_i) + \sum_{C' \in C_i \setminus C} m_{C' \rightarrow i}^{t-1}(\mathbf{x}_i)$ 
               $m_{C \rightarrow i}^0(\mathbf{x}_i) = \min_{y_{C \setminus i}} f_C(\mathbf{x}_i, y_{C \setminus i}) + \sum_{j \in C \setminus i} m_{j \rightarrow C}^{t-1}(\mathbf{y}_j)$ 
7           end for
8            $t := t + 1$ 
9       end for
10      Set belief function as  $b_i^N(\mathbf{x}_i) = f_i(\mathbf{x}_i) + \sum_{C \in C_i} m_{C \rightarrow i}^N(\mathbf{x}_i), \forall 1 \leq i \leq |V|$ 
11      Estimate optimal assignment as  $\hat{\mathbf{x}}^N \in \operatorname{argmin} b_i^N(\mathbf{x}_i), \forall i \in V$ 
12  end

```

problem (4.1) in a distributed manner using the min-sum BP approach, we define various agents and the corresponding state vectors they hold for passing messages as follows:

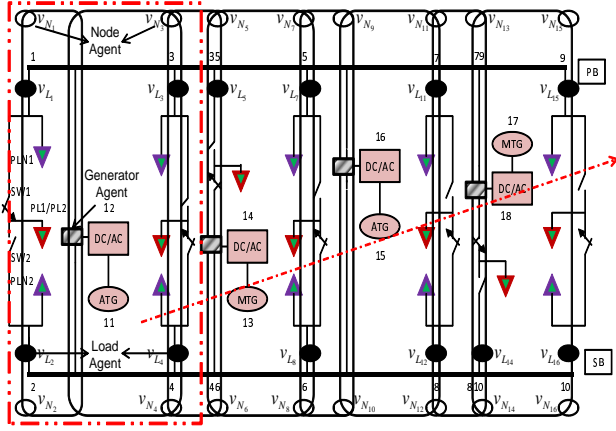


Figure 7.3: Subsystem formation for belief propagation with different types of agents

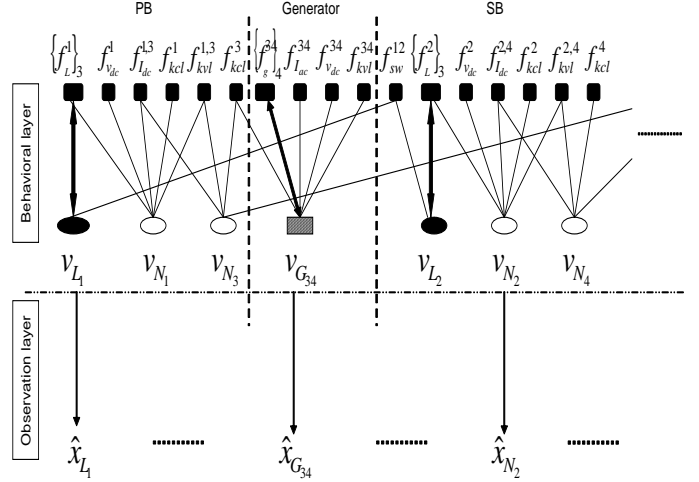


Figure 7.4: Factor graph constructed from the graphical shipboard model $G \in (V, C)$ with variable nodes $v \in V$ as agents and factor nodes $C \in C$ as constraints

- Load agent (Contains load information): $v_{L_i} = \{P_{VL_i}, P_{SVL_i}, P_{NVL_i}, SW_i\}$
- Node agent (Contains node information): $v_{N_i} = \{v_i^{dc}, \sum I_{in_i}, \sum I_{out_i}\}$
- Generator agent (Contains generator information): $v_{G_l} = \{PG_l, QG_l, I_l^{ac}, v_l^{ac}, \delta_l^{ac}\}$

Fig. 7.3 shows placement of the agents in the shipboard system while Fig. 7.4 shows the factor graph generated from the highlighted portion of Fig. 7.3. Therefore, the variable node function and the factor node functions are defined in (7.10) and in (7.11), respectively as

$$f_i(\mathbf{x}_i) = \begin{cases} \sum w_{VL} S_{VL_i} + w_{SVL} S_{SVL_i} + w_{NVL} S_{NVL_i} & \text{if } 0 \leq SW_i \leq 1 \\ \infty & \text{otherwise,} \end{cases} \quad (7.10)$$

$$f_C(\mathbf{x}_i, y_{C \setminus i}) = \begin{cases} 0 & \text{if } C_1, \dots, C_5 \\ \infty & \text{otherwise.} \end{cases} \quad (7.11)$$

As future research, based on the formulation for distributed optimization presented, we can quantify the total delay for reconfiguration similar to the approach presented in the dissertation to show its effectiveness. Furthermore, comparisons between decentralized/distributed strategies are required to understand and implement suitable solution for SSG reconfiguration.

Further research directions related to CPS optimization are presented. Applications are included but not limited to SSG system reconfiguration:

- Next, in the dissertation, we only have considered optimization with constant parameters on the loads. Therefore, further research is needed to understand the sensitivity of our proposed algorithms when the parameters are not fixed. Modifications to the proposed approaches that stochastically model and optimize under load parameter variations and analysis of sensitivity of the solution to change in load parameters will be important extensions to the algorithms proposed in this dissertation.
- Additionally, loads in an SSG dynamically change their priority levels depending on the states of the shipboard, such as, cruise mode, battle mode, etc. Modifications to the proposed approaches can be done to account for change in priority levels of the loads.
- Furthermore, in the dissertation, we only analyzed the effect of imperfect communication network on optimized reconfiguration of SSG, by decoupling the sensor and communication framework from that of the underlying power network. Strategies for joint optimization and control of power and sensor network for enhancing the reconfiguration QoS and robustness can be further explored based on the analysis given in the dissertation.
- Finally, gossip based distributed optimization methodologies involving agents under imperfect communications in the SSG can be proposed and compared with BP based distributed approach. Unlike BP, gossip based approaches guarantees convergence under similar conditions as the proposed shipboard reconfiguration. It is fully distributed, and can be a serious contender for distributed reconfiguration of shipboard as well as

any cyber-physical reconfigurable network, in general, because of its low-complexity implementation compared to the exhaustive search based centralized approaches.

Bibliography

- [1] F. Koushanfar and L. Zhong, “Building an integrated cyber-infrastructure: A micro/macro health services case study,” in *In Proceedings of the 2006 National Science Foundation Workshop On Cyber-Physical Systems*, 2006.
- [2] K. Ravindran, “Cyber-physical systems based modeling of adaptation intelligence in network systems,” in *In Proceedings of the IEEE International Conference on Systems, Man, and Cybernetics(SMC)*, Oct. 2011, pp. 2737–2742.
- [3] P. R. Chester and W. R. Jay, “Zonal electrical distribution systems: an affordable architecture for future,” in *Naval Engineering Journal*, 1993, pp. 45–51.
- [4] R.Rajkumar, L.Insup, S.Lui, and J.Stankovic, “Cyber-physical systems: The next computing revolution,” in *In Proceedings of the ACM/IEEE Design Automation Conference (DAC)*, Jun. 2010, pp. 731–736.
- [5] K. Ravindran, “Nsf workshop on cyber-physical systems,” in *Proceedings available online at <http://varma.ece.cmu.edu/CPS>*, Oct. 2006.
- [6] A. Merlin and H. Back, “Search for a minimal-loss operating spanning tree configuration in urban power distribution systems,” in *5th Power System Computation Conference, Cambridge, England*.
- [7] S. Civanlar, J. J. Grainger, H. Yin, and S. S. H. Lee, “Distribution feeder reconfiguration for loss reduction,” in *IEEE Transactions on Power Delivery*, vol. 3(3), Jul. 1998, pp. 1217–1223.

- [8] M. E. Baran and F. F. Wu, "Network reconfiguration in distribution systems for loss reduction and load balancing," in *IEEE Transactions on Power Delivery*, vol. 4(2), Apr. 1989, pp. 1401–1407.
- [9] K. Nara, A. Shiose, M. Kitagawa, and T. Ishihara, "Implementation of genetic algorithm for distribution systems loss minimum reconfiguration," in *IEEE Transactions on Power Systems*, vol. 7(3), Jul. 1992, pp. 1044–1051.
- [10] S. K. Goswami and S. K. Basu, "A new algorithm for the reconfiguration of distribution feeders for loss minimization," in *IEEE Transactions on Power Delivery*, vol. 7(3), Jul. 1992, p. 14841491.
- [11] D. Shirmohammadi and H. W. Hong, "Reconfiguration of electric distribution networks for resistive line loss reduction," in *IEEE Transactions on Power Delivery*, vol. 4(2), Apr. 1989, p. 14921498.
- [12] H. C. Cheng and C. C. Kou, "Network reconfiguration in distribution systems using simulated annealing," in *Electrical Power System Research*, vol. 29, May 1994, p. 227238.
- [13] V. S. Talukdar, "A multi-agent technique for contingency constrained optimal power flows," in *IEEE Transaction on Power Systems*, vol. 9(2), May 1994, pp. 855–861.
- [14] T. Nagata and H. Sasaki, "An efficient algorithm for distribution network restoration," in *Proceedings of IEEE Power Engineering Society Summer Meeting*, vol. 1, 2001, pp. 54–59.
- [15] J. P. Chiou, C. F. Chang, and C. T. Su, "Variable scaling hybrid differential evolution for solving network reconfiguration of distribution systems," in *IEEE Transactions on Power Systems*, vol. 20(2), May 2005, pp. 668–674.

- [16] J. V. CDR and A. Jr., “Considerations in the design of naval electric power system,” in *Power Engineering Society Summer Meeting*, vol. 1, May 2002, pp. 331–335.
- [17] *IEEE Recommended Practice for 1 kV to 35 kV Medium-Voltage DC Power Systems on Ships*. IEEE Std. 1709, DC Power Systems on Ships Working Group of the IEEE Industry Applications Society Petroleum and Chemical Industry (IAS/PCI) Committee, nov 2010.
- [18] R. J. Kochanski and J. L. Paige, “Safenet: The standard and its application,” in *IEEE LCS*, vol. 2, no. 1, Feb. 1991, pp. 46–51.
- [19] K. Huang, “Models and methods for shipboard power system reconfiguration,” in *Ph.D. thesis, Florida State University*, 2007.
- [20] W. M. Dahalan and H. B. Mokhlis, “Techniques of network reconfiguration for service restoration in shipboard power system: A review,” in *Australian Journal of Basic Applied Science*, vol. 4(11), 2010, p. 55565563.
- [21] H. Lan, Y.-Y. Xiao, and L.-J. Zhang, “Multi-agent system optimized reconfiguration of shipboard power system,” in *Journal of Marine Science Application*, vol. 9, 2010, p. 334339.
- [22] Q. Yu, N. N. Schulz, and A. K. Srivastava, “Multi-agent based reconfiguration of ac-dc shipboard distribution power system,” in *Integrated Computer-Aided Engineering*, vol. 17(4), 2010, p. 347357.
- [23] K. Huang, D. A. Cartes, and A. K. Srivastava, “A multiagent-based algorithm for ring-structured shipboard power system reconfiguration,” in *IEEE Transactions on Systems, Man, and Cybernetics*, vol. 37(5), 2007, p. 10161021.

- [24] S. G. A. Feliachi, K. Schoder and H.-J. Lai, "Distributed control agents approach to energy management in electric shipboard power systems," in *In Proceedings of IEEE Power Engineering Society General Meeting, Montreal, Canada*, Jun. 2006.
- [25] X. Yang and Y. Zhang, "Intelligent real-time fault restoration of the large, shipboard power system based on genetic algorithm," in *International Journal of Information Technology*, vol. 11(12), 2005, p. 129135.
- [26] K. R. Padamati, N. N. Schulz, and A. K. Srivastava, "Application of genetic algorithm for reconfiguration of shipboard power system," in *In Proceedings of 39th North American Power Symposium*, 2007, p. 159163.
- [27] T. Amba, K. L. Butler-Purphy, and M. Falahi, "Genetic algorithm based damage control for shipboard power systems," in *In Proceedings of Electric Ships Technology Symposium (ESTS), Baltimore, MD*, Apr. 2009, p. 242252.
- [28] J. Huang, Y. Chen, and X. Zhang, "Multiobjective optimal service restoration for shipboard power system," in *In Proceedings of IEEE International Conference Intelligent Computing and Intelligent Systems, (ICIS 2009), Shanghai, China*, Nov. 2009, p. 644650.
- [29] N. Kumar, A. K. Srivastava, and N. N. Schulz, "Shipboard power system restoration using binary particle swarm optimization," in *In Proceedings of North American Power Symposium, Las Cruces, NM*, Nov. 2007, p. 164169.
- [30] S. H. K. Vuppalapati and A. K. Srivastava, "Application of ant colony optimization for reconfiguration of shipboard power system," in *International Journal of Engineering, Science, and Technology*, vol. 2(3), 2010, p. 119131.
- [31] S. Das, S. Bose, N. N. S. S. Pal, C. M. Scoglio, and B. Natarajan, "Dynamic reconfiguration of shipboard power systems using reinforcement learning," in *IEEE Transactions on Power Systems (Accepted in Aug 2012)*.

- [32] K. N. Miu, H.-D. Chiang, B. Yuan, and G. Darling, "Fast service restoration for large-scale distribution systems with priority customers and constraints," in *20th International Conference on Power Industry Computer Applications*, vol. 13(3), 1997, pp. 789–795.
- [33] E. R. Ramos, J. L. Martinez-Ramos, A. G. Exposito, and A. J. U. Salado, "Optimal reconfiguration of distribution networks for power loss reduction," in *IEEE Porto Power Tech Proceedings*, vol. 3, 2001, p. 5.
- [34] A. N. Guimaraes, J. F. C. Lorenzetti, and C. A. Castro, "Reconfiguration of distribution systems for stability margin enhancement using tabu search," in *International Conference on Power System Technology*, vol. 2, 2004, pp. 1556–1561.
- [35] A. L. Morelato and A. J. Monticelli, "Heuristic search approach to distribution system restoration," in *IEEE Transactions on Power Delivery*, vol. 4, 1989, pp. 223–241.
- [36] C. S. Chen, C. H. Lin, and H. Y. Tsai, "A rule-based expert system with colored petri net models for distribution system service restoration," in *IEEE Transactions on Power Systems*, vol. 17(4), Nov. 2002, pp. 1073–1080.
- [37] Y. Hsiao and C. Chien, "Enhancement of restoration service in distribution systems using a combination fuzzy-ga method," in *IEEE Transactions on Power Systems*, vol. 15(4), Nov. 2000, pp. 1394–1400.
- [38] K. L. Butler, N. D. R. Sarma, and V. R. Prasad, "A new method of network reconfiguration for service restoration in shipboard power systems," in *Proceedings of the IEEE PES Transmission and Distribution Conference*, vol. 2, 1999, pp. 658–662.
- [39] —, "Network reconfiguration for service restoration in shipboard power distribution systems," in *IEEE Transactions on Power Systems*, vol. 16(4), 2001, pp. 653–661.

- [40] K. L. Butler-Purpy, “Multi-agent technology for self-healing shipboard power systems,” in *Proceedings of the 13th International Conference on Intelligent Systems Application to Power Systems*, 2005, p. 5.
- [41] K. L. Butler-Purpy and N. D. R. Sarma, “Self-healing reconfiguration for restoration of naval shipboard power systems,” in *IEEE Transactions on Power Systems*, vol. 19(2), 2004, pp. 754–762.
- [42] J. Billo, “Shipboard power system reconfiguration using multi agent system,” in *Master’s thesis, University of Texas, Austin*, 2003.
- [43] S. Khushalani and N. N. Schulz, “Restoration optimization with distributed generation considering islanding,” in *Proceedings of the IEEE Power Engineering Society General Meeting*, vol. 3, 2005, pp. 2445–2449.
- [44] S. Khushalani, J. Solanki, and N. N. Schulz, “Optimized restoration of combined ac/dc shipboard power systems including distributed generation and islanding techniques,” in *Electric Power Systems Research*, vol. 78, 2008, pp. 1528–1536.
- [45] V. Balakrishnan, S. Boyd, and S. Balemi, “Branch and bound algorithm for computing the minimum stability degree of parameter-dependent linear systems,” in *International Journal of Robust and Nonlinear Control*, vol. 1(4), 1991, pp. 295–317.
- [46] F. Xia, A. Vinel, R. Gao, L. Wang, and T. Qiu, “Evaluating iee 802.15.4 for cyber-physical systems, eurasip journal on wireless communications and networking,” in *IEEE Transactions on Systems, MAN, and Cybernetics*, vol. 11, 2011.
- [47] R. Cruz, “A calculus for network delay. i. network elements in isolation,” in *IEEE Transactions on Information Theory*, vol. 37, no. 1, Jan. 1991, pp. 114–131.

- [48] A. Burchard, J. Liebeherr, and S. Patek, "A min-plus calculus for end-to-end statistical service guarantees," in *IEEE Transactions on Information Theory*, vol. 52, no. 9, Sep. 2006, pp. 4105–4114.
- [49] L. Paroliniy, N. Toliaz, B. Sinopoliy, and B. H. Kroghy, "A cyber-physical systems approach to energy management in data centers," in *In Proceedings of First International Conference on Cyber-Physical Systems*, Apr. 2010.
- [50] A. Leon-Garcia, *Probability and random processes for electrical engineering*, 2nd ed. Addison-Wesley, 1994.
- [51] J. Lehoczky, "Real-time queueing network theory," in *In Proceedings of IEEE RTSS*, Dec. 1997, pp. 58–67.
- [52] S.-N. Yeung and J. Lehoczky, "End-to-end delay analysis for real-time networks," in *In Proceedings of IEEE RTSS*, Dec. 2001, pp. 299–309.
- [53] Y. Wang, M. C. Vuran, and S. Goddard, "Cross-layer analysis of the end-to-end delay distribution in wireless sensor networks," in *IEEE Real-Time Systems Symposium*, 2009.
- [54] K.-D. Kang and S. H. Son, "Real-time data services for cyber physical systems," in *ICDCS Workshops*, 2008, pp. 483–488.
- [55] R. K. Bansal, V. Gupta, and R. Malhotra, "Performance analysis of wired and wireless lan using soft computing techniques - a review," in *Global Journal of Computer Science and Technology*, vol. 10, no. 8, Sep. 2010, pp. 67–71.
- [56] *IEEE Std 802.11: IEEE standard for wireless LAN medium access control (MAC) and physical layer (PHY) specifications*, Jun. 2007.
- [57] S. Bose, B. Natarajan, C. Scoglio, S. Das, and N. N. Schulz, "Analysis of optimal reconfiguration of shipboard power systems," in *IEEE Transactions on Power Systems*, vol. 27(1), 2011, pp. 189–197.

- [58] T. Nagata and H. Sasaki, “A multi-agent approach to power system restoration,” in *IEEE Transactions on Power Systems*, vol. 17(2), 2002, pp. 457–462.
- [59] Y. Xu and W. Liu, “Novel multiagent based load restoration algorithm for microgrids,” in *IEEE Transactions on Smart Grid*, vol. 2(1), mar 2011, pp. 152–161.
- [60] S. Samar, S. Boyd, and D. Gorinevsky, “Distributed estimation via dual decomposition,” in *In Proceedings of the European Control Conference*, Jul. 2007.
- [61] Y. Hu, A. Kuh, A. Kavcic, and D. Nakafuji, “Micro-grid state estimation using belief propagation on factor graphs,” in *In Proceedings for APSIPA Annual Summit and Conference*, Dec. 2010.
- [62] S. Boyd and L. Vandenberghe, *Convex Optimization*, 2nd ed. Cambridge University Press, 2004.
- [63] S. Bose, S. Pal, B. Natarajan, C. Scoglio, S. Das, and N. N. Schulz, “Analysis of optimal reconfiguration of shipboard power system (accepted 2011),” in *IEEE Transactions on Power Systems*, 2011.
- [64] S. Bose, B. Natarajan, C. Scoglio, S. Das, and N. N. Schulz, “Analysis of robustness for shipboard power system with non-radial power flow,” in *IEEE Electric Ship Technologies Symposium*, Apr. 2011.
- [65] S. Bose, B. Natarajan, C. Scoglio, N. N. Schulz, D. M. Gruenbacher, and S. Das, “Shipboard power systems reconfigurationa cyber-physical framework for response time analysis,” in *IEEE Transactions on Industrial Informatics (submitted)*, 2012.
- [66] S. Bose, B. Natarajan, C. Scoglio, and N. N. Schulz, “Distributed optimization for shipboard smartgrid,” in *In Proceedings of IEEE Latincom*, Nov. 2012.

- [67] S. Bose, B. Natarajan, C. Scoglio, S. Das, and N. N. Schulz, “Distributed optimization of shipboard smart grid: Convergence analysis under imperfect communication,” in *IEEE Transactions on Smart Grid (submitted)*, 2012.
- [68] S. Bose, B. Natarajan, C. Scoglio, S. Das, and N. N. Schulz, “Analysis of optimized reconfiguration of power systems for electric ships,” in *North American Power Symposium*, Sep. 2010, pp. 1–7.
- [69] J. D. Glover, M. S. Sarma, and T. J. Overbye, *Power system analysis and design*, 4th ed. Thomson, 2008.
- [70] L. Akter and B. Natarajan, “Qos constrained resource allocation to secondary users in cognitive radio networks,” in *Computer Communications*, vol. 32, 2009, pp. 1923–1930.
- [71] T. Marler, “A study of multiobjective optimization methods for engineering application,” in *Ph.D. Thesis, The University of Iowa*, 2005.
- [72] R. Cartwright, A. Cheng, P. Hudak, M. OMalley, and W. Taha, “Cyber-physical challenges in transportation system design,” in *National workshop for research on high-confidence transportation cyber-physical systems: automotive, aviation & rail*, Nov. 2008.
- [73] N. D. Potter and T. J. Cowles, “A high-speed, wireless network for ship-to-ship and ship-to-shore data exchange,” in *Journal of Atmospheric and Ocean Technology*, vol. 17, Jul. 2000, pp. 963–970.
- [74] M. Li, H. Zhu, S. Sathyamurthy, I. Chlamtac, and B. Prabhakaran, “End-to-end framework for qos guarantee in heterogeneous wired-cum-wireless networks,” in *First International Conference on Quality of Service in Heterogeneous Wired/Wireless Networks (QSHINE’04)*, 2004, pp. 140–147.

- [75] Y. Yang and T.-S. P. Yum, “Delay distributions of slotted aloha and csma,” in *IEEE Transactions on Communications*, vol. 51, no. 11, Nov. 2003, pp. 1846–1857.
- [76] W. Hoeffding, “Probability inequalities for sum of bounded random variables,” in *Journal of the American Statistical Association*, vol. 58, no. 301, Mar. 1963, pp. 13–30.
- [77] R. Baheti and H. Gill, “Cyber-physical systems,” in *The Impact of Control Technology*, T. Samad and A.M. Annaswamy (eds.), *IEEE Control Systems Society*, available at www.ieeecss.org, 2011.
- [78] J. F. Bard, “An analytical model of the reaction time of a naval platform,” in *IEEE Transactions on Systems, MAN, and Cybernetics*, vol. 11, no. 10, Oct. 1981, pp. 723–726.
- [79] R. Seifert, *The Switch Book - The Complete Guide to LAN Switching Technology*, 1st ed. Wiley, 2000.
- [80] W. Li, A. Monti, M. Luo, and R. A. Dougal, “Vpnet: A co-simulation framework for analyzing communication channel effects on power systems,” in *IEEE Electric Ship Technologies Symposium*, Apr. 2011, pp. 143–149.
- [81] E. L. Waltz and J. Llinas, *Multisensor Data Fusion*, 1st ed. Artech House, 1990.
- [82] S. Boyd, L. Xiao, A. Mutapcic, and J. Mattingley, “Notes on decomposition methods - notes for ee364b, stanford university,” Apr. 2008.
- [83] T. M. Cover and J. A. Thomas, *Elements of Information Theory*, 2nd ed. Wiley-Interscience, 2006.
- [84] H. Terelius, U. Topcu, and R. M. Murray, “Decentralized multi-agent optimization via dual decomposition,” in *In Proceedings of the 18th World Congress of the International Federation of Automatic Control (IFAC)*, Aug. 2011.

- [85] J. Lee, I. Shin, and A. Easwaran, “Online robust optimization framework for qos guarantees in distributed soft real-time systems,” in *Proceedings of the tenth ACM international conference on Embedded software (EMSOFT’10)*, 2010, pp. 98–98.
- [86] D. Bertsimas, K. Natarajan, and C.-P. Teo, “Tight bounds on expected order statistics,” in *Probability in the Engineering and Informational Sciences*, vol. 20, 2006, p. 667686.
- [87] C. C. Moallemi and B. Roy, “Convergence of min-sum message-passing for convex optimization,” in *IEEE Transactions on Information Theory*, vol. 56, no. 4, Apr. 2010, pp. 2041–2050.
- [88] D. Gamarnik, D. Shah, and Y. Wei, “Belief propagation for min-cost network flow: Convergence and correctness,” *CoRR*, vol. abs/1004.1586, 2010.
- [89] L. Zdeborov, A. Decelle, and M. Chertkov, “Message passing for optimization and control of a power grid: Model of a distribution system with redundancy,” vol. 80, no. 4, Oct. 2009.
- [90] Y. Hu, A. Kuh, A. Kavcic, and T. Yang, “A belief propagation based power distribution system state estimator,” in *IEEE Computational Intelligence Magazine*, vol. 11, Aug. 2011, pp. 36–46.
- [91] H.-A. Loeliger, J. Dauwels, J. Hu, S. Korl, L. Ping, and F. R. Kschischang, “The factor graph approach to model-based signal processing,” in *IEEE Transactions on Information Theory*, vol. 95, no. 6, Jun. 2007, pp. 1295–1322.

Appendix A

Proof of Theorem 1

To evaluate the second term in (5.4), we consider no packet loss in the network; therefore all gradient updates complete their roundtrip time within delay D after T time steps. Moving $P_{t-c_{ij}(\hat{t})}(\cdot)$ to the second operand, indexing the sum at $\hat{t} = t - c_{ij}(\hat{t})$, and adding and subtracting $\lambda(\hat{t})$ from $P_{t-c_{ij}(\hat{t})}(\cdot)$ we can rewrite the second term in (5.4) as $\sum_{\hat{t}=0}^T \mathbf{g}_q(\hat{t})' \sum_{c_{ij}(\hat{t})=0}^D (P_{\hat{t}}(\lambda(\hat{t} + c_{ij}(\hat{t})) + \lambda(\hat{t})) + (\lambda(\hat{t}) - \lambda^{opt}))$. The first part of the sum can be bounded as follows:

$$\begin{aligned}
 & \mathbf{g}_q(\hat{t})' \sum_{c_{ij}(\hat{t})=0}^D P_{\hat{t}}(\lambda(\hat{t} + c_{ij}(\hat{t})) + \lambda(\hat{t})) \\
 & \leq (\|\mathbf{g}(\hat{t})\|_2' + \|\epsilon(\hat{t})\|_2') \left\| \sum_{c_{ij}(\hat{t})=0}^D (\lambda(\hat{t} + c_{ij}(\hat{t})) - \lambda(\hat{t})) \right\|_2 \\
 & \leq \alpha G D (G + E) (D + 1)
 \end{aligned} \tag{A.1}$$

The last inequality in (A.1) is obtained by invoking the lemma 3 in [84] and using $\|\epsilon(\hat{t})\|_2' \leq E$. For the second part, we readily obtain the bound as follows:

$$\begin{aligned}
 \mathbf{g}_q(\hat{t})' \sum_{c_{ij}(\hat{t})=0}^D P_{\hat{t}}(\lambda(\hat{t}) - \lambda^{opt}) & \leq \mathbf{g}(\hat{t})' \sum_{c_{ij}(\hat{t})=0}^D P_{\hat{t}}(\lambda(\hat{t}) - \lambda^{opt}) \\
 & = \mathbf{g}(\hat{t})' (\lambda(\hat{t}) - \lambda^{opt}) \\
 & \leq q(\lambda(\hat{t})) - q^{opt}
 \end{aligned} \tag{A.2}$$

The last term in (5.4) can be written as

$$\begin{aligned}
& \alpha^2 \sum_{t=0}^T \left\| \sum_{c_{ij}(\hat{t})=0}^D P_{t-c_{ij}(\hat{t})}(\mathbf{g}_q(t - c_{ij}(\hat{t}))) \right\|_2^2 \\
&= \sum_{t=0}^T \|\lambda(t+1) - \lambda(t)\|_2^2
\end{aligned} \tag{A.3}$$

From (5.1), we can further deduce the following:

$$\begin{aligned}
\|\lambda(t+1) - \lambda(t)\|_2 &= \alpha \left\| \sum_{c_{ij}(\hat{t})=0}^D P_{t-c_{ij}(\hat{t})}(\mathbf{g}_q(t - c_{ij}(\hat{t}))) \right\|_2 \\
&\leq \alpha \sum_{c_{ij}(\hat{t})=0}^D \left\| P_{t-c_{ij}(\hat{t})}(\mathbf{g}_q(t - c_{ij}(\hat{t}))) \right\|_2 \\
&\leq \alpha \sum_{c_{ij}(\hat{t})=0}^D \left\| \mathbf{g}_q(t - c_{ij}(\hat{t})) \right\|_2 \\
&= \alpha \sum_{c_{ij}(\hat{t})=0}^D \left\| \mathbf{g}(t - c_{ij}(\hat{t})) - \epsilon(t - c_{ij}(\hat{t})) \right\|_2 \\
&\leq \alpha \sum_{c_{ij}(\hat{t})=0}^D \left\| \mathbf{g}(t - c_{ij}(\hat{t})) \right\|_2 \\
&+ \alpha \sum_{c_{ij}(\hat{t})=0}^D \left\| \epsilon(t - c_{ij}(\hat{t})) \right\|_2 \\
&\leq \alpha(D+1)(G+E)
\end{aligned} \tag{A.4}$$

Appendix B

FDDI Backbone Network Delay

B.1 Derivation of FDDI Backbone Network Delay Distribution

The message arrival process in the backbone from the Ethernet stations depends on the traffic generation rate, which is assumed to be Poisson with a mean rate λ_e . If n Ethernet stations are sending capable of sending traffic to the backbone queue S_b with probability p , then the arrival rate from any Ethernet station to S_b is

$$\lambda_{ib} = n\lambda_e p \tag{B.1}$$

If L_b is the message lengths in the ring with k queued messages in S_b , then the lengths of the messages are independent and are exponentially distributed with parameter u . The conditional distribution of k messages in the queue of length q_l is given by

$$p(L_b \leq x | q_l = k) = \sum_{i=1}^k a_i (1 - e^{-ux}) \tag{B.2}$$

where, $a_i \geq 0$ and $\sum_{i=1}^k a_i = 1$. x is the time variable. Using (B.2) we obtain the marginal distribution for L_b as

$$\begin{aligned} p(L_b \leq x) &= \sum_{k=1}^{\infty} p(L_b \leq x | q_l = k) p(q_l = k) \\ &= 1 - e^{-ux}. \end{aligned} \tag{B.3}$$

Therefore, message length distribution at S_b is exponential with mean $\mu_L = EL$. The service time X_B is given by $\frac{L_b}{C_b}$. We obtain the density distribution of X_B as

$$f_{X_B}(x) = uC_b \exp\{-uC_b x\} \quad (\text{B.4})$$

Now, if the mean token rotation time in the backbone network is $\mu_T K$, then the total number of message directed from n Ethernet stations to the Ethernet server in one token rotation cycle is $\mu_T K \sum_{j=1}^n \lambda_{e_j b} p$. Hence, the average rate of message arrival at Ethernet server queue is given by

$$\lambda_{bs} = \sum_{j=1}^n \lambda_{e_j b} p \quad (\text{B.5})$$

For derivation of the probability density function of $f_{T_{FDDI}}$, we obtain the final delay density function as the multiplication of the Laplace transforms (LT) of queuing delay density and service delay density functions, specifically,

$$L_{T_{FDDI}}(s) = L_{W_{Q_B}}(s) L_{X_B}(s). \quad (\text{B.6})$$

We consider a message A arrival to the ring. If message A arrives to an empty queue, with probability $(1 - \rho)$; in this case, the queuing delay is zero and message A is serviced immediately. When customer A arrives to a non-empty queue there is an ongoing service where W_0 is the corresponding residual service time. Regardless, $L_{W_{Q_B}}(s)$ can be obtained following the steps illustrated in [22] as

$$L_{W_{Q_B}}(s) = (1 - p) + p \frac{1 - L_{BP}(s)}{(s + \lambda_b - \lambda_b L_{BP}(s)) \bar{X}_B} \quad (\text{B.7})$$

Here, $L_{BP}(s)$ is the LT of the busy period related to the LT of the cumulative distribution function of service time $L_{X_B}(s)$ for message A and is given by

$$L_{BP}(s) = L_{X_B}(s + \lambda_b - \lambda_b L_{BP}(s)) \quad (\text{B.8})$$

From (B.8), $L_{BP}(s)$ can be obtained if $L_{X_B}(s)$ is known. We find the mean service time \bar{X}_B from (B.4) as

$$\bar{X}_B = \frac{1}{uC_b} \quad (\text{B.9})$$

Using LT on (B.8) we can obtain $L_{X_B}(s)$ as

$$L_{X_B}(s) = \frac{uC_b}{s + uC_b} \quad (\text{B.10})$$

Using (B.10) in (B.8) we obtain the following equation to solve in order to find $L_{BP}(s)$,

$$L_{BP}(s) = \frac{uC_b}{(s + \lambda_b - \lambda_b L_{BP}(s) + uC_b)} \quad (\text{B.11})$$

After algebraic manipulation, we obtain $L_{BP}(s)$ as the following roots of the quadratic equation

$$L_{BP}(s) = \frac{s + \lambda_b + uC_b}{2\lambda_b} \left[1 \pm \left(1 + \frac{4\lambda_b uC_b}{(s + \lambda_b + uC_b)^2} \right)^{\frac{1}{2}} \right] \quad (\text{B.12})$$

For a FDDI link with high frequency data rate (1 Gbps) the term $\frac{4\lambda_b uC_b}{(s + \lambda_b + uC_b)^2} \rightarrow 0$. Therefore, the final expression for $L_{BP}(s)$ is given by

$$L_{BP}(s) = \frac{s + \lambda_b + uC_b}{\lambda_b} \quad (\text{B.13})$$

Therefore, from (B.6), using (B.13) and (B.9), and after algebraic simplification, we obtain the $L_{T_{FDDI}}(s)$ as

$$L_{T_{FDDI}}(s) = (1 - p) \frac{uC_b}{s + uC_b} + \frac{puC_b}{\lambda_b} \quad (\text{B.14})$$

Finally, taking inverse LT of (B.14), we obtain probability distribution function of the FDDI token ring backbone network in (17).